

The authors thank the Reviewers for their revision of our manuscript and their helpful comments. In the following the original comments are inserted in *italic face* while our replies are printed in normal face.

**Reviewer 1:**

*Page 3, Line 87: Figures should be referenced in numerical order: the first reference to a figure in the text should be to figure 1. (I would not re-order the figures to correct this, rather, I would remove the reference to figure 3 in this line.)*

**Reply 1:** Agreed and changed.

*Figure 1 and Figure 3: The figures are really too small. They might be just about OK if made the full width of the two columns in the final version, but I am not sure about this. Text on figures should be a similar size to the text in the figure caption. The legends in these figures are particularly hard to read; it would help if they were not on top of the curves.*

**Reply 2:** Agreed. Figure 1 and figure 3 were split up in two individual figures which now span the full width of the page. The text was changed accordingly.

*Figure 2: It is good that the two panels have the same colour scale for easy comparison. But the scale should go down to the lowest values shown in the left panel. As the figure stands, the colour white is used to represent two distinct things: negative values, and areas where there are no data. The “no data” areas should be left white, and the (white free) colour scale should extend so that it applies to the negative areas. The figure title “PAN, 200807” is not needed to distinguish the two panels and tells the reader nothing that is not in the caption. It should be removed. The contour lines should be in a colour (or colours) that allow them to be seen against the colour scale. With these changes made, Page 3 Line 113 will need to be changed (and can possibly be simplified). Many of these comments also apply to figures 4, 5 and 6.*

**Reply 3:** Agreed. The colour scale was changed to cover the whole range of values of both figures. The titles have been removed. We did not change the contour line colour, because the background colours are now much lighter and white contour lines would be harder to see than black ones. The text was changed accordingly to reflect the updated colour scale.

*Page 6 line 118: “setup” should be “set up” because it is a verb. (Note that on page 7 line 140, “setup” is a noun and should be left as it is.)*

**Reply 4:** Agreed and corrected.

*Page 6 line 131: “The spectral region [...] could be narrowed to [values]” Narrowed from what?*

**Reply 5:** The gap could be narrowed down to 791.0 to 792.0  $\text{cm}^{-1}$  from 790.5 to 792.5  $\text{cm}^{-1}$ . Additional information on this is now given in the manuscript.

*Figure 7: This figure is probably OK if shown at the full 8.3cm width of a journal column. The title “Rows of A” on each panel should be removed.*

**Reply 6:** We changed the figures to better reflect the altitude region of interest. The titles were removed and the figures now span the entire width of the page.

*Page 11 sec 5.1.1: It would be nice to add a figure showing the mean ATMOS profiles and a suitably-averaged MIPAS profile for the same time of year.*

**Reply 7:** We now provide the suggested figure in the revised version of the manuscript. Average MIPAS profiles of the respective region and time of year are used. The text was changed accordingly.

*Page 11 line 212: Remove comma after “profile”.*

**Reply 8:** Agreed and removed.

*Page 13 figure 9: It is again marginal whether this figure is large enough. It is probably OK at the full two-column width of the journal page. It would be a great improvement if the five panels were labelled (a) to (e) so that the text could refer to “panel (e)” rather than “second panel to the right”. (I think this means “second panel from the right” but I am not sure; letter labels would remove this kind of confusion.)*

**Reply 9:** Agreed and changed. The text was changed accordingly.

*Figures 10 and 11: I again have concerns about the sizing of the figures. The text in the captions is unreadably small at the size of the review article. The title on Figure 11 is not needed.*

**Reply 10:** Agreed and changed. Fig. 10 was split up into two individual figures. These figures now each span the full width of the document. The text was changed accordingly.

**Reviewer 2:**

**Major comments**

*The last sentence of the abstract should be removed, it states “The decline in  $CCl_4$  abundance during the MIPAS Envisat measurement period (July 2002 to April 2012) is clearly reflected in the retrieved distributions”. I agree that information on (and a proper quotation of) the  $CCl_4$  trend would have been a very valuable addition to this study, BUT only a subset of the observations is presented, the periods shown do not cover the 10-year time interval (09/2003 - 04/2011 instead of 07/2002 - 04/2012) and the reader has no element to gauge the  $CCl_4$  rate of change and to judge about the validity of this assertion*

**Reply 1:** Trends have now been estimated from the full data set and an respective figure was included in the paper. A subsection was added to discuss the results of the trend estimation. The according text states good agreement with the trends estimated by Valeri et al. (2017).

*Figure 2 shows that the PAN product jointly retrieved with  $CCl_4$  is superior to the standard PAN data available thus far from the MIPAS team, it would be equally important to have an idea of the impact of retrieving versus neglecting PAN on the quality of the  $CCl_4$  product! In particular, is there a systematic impact on the  $CCl_4$  mixing ratios, allowing to close the well-known gap between in situ and remote-sensing data (see e.g. Chipperfield et al., ACP, 16, 2016)? This information would be very valuable for the community and I suggest adding two panels to Fig.2 dedicated to  $CCl_4$  with/without*

**Reply 2:** We believe there is a misunderstanding here. None of the two figures show the PAN results for  $CCl_4$  being left out entirely in the retrieval.  $CCl_4$  was accounted for in the MIPAS retrieval before the gas was an actual target of the retrieval itself. However, optimizing the retrieval for  $CCl_4$  led to changes in the PAN distributions. The influence of these changes are reflected in the two panels of Fig. 2. Since both species, PAN and  $CCl_4$ , were accounted for in the original PAN retrieval, we do not see a benefit from showing  $CCl_4$  results without PAN. Fig. 2 is supposed to ensure that changes made to the retrieval to optimize it for  $CCl_4$  did not decrease the

quality of the PAN results. Fig. 2 proves that, on the contrary, these changes also led to improvement of the PAN results.

*Section 4.2: it is somewhat strange that the FR measurements provide a lower DOF (3.5) than the RR observations (4.0). What could be the reason for this? This deserves a comment.*

**Reply 3:** We don't think this is strange, because the RR measurements have a finer altitude sampling. Measurements were taken at 27 instead of 17 tangent altitudes during the RR and FR period, respectively. This easily explains the higher DOF of the RR observations. A sentence was added for clarification.

*Figure 7 is really small and the y-axis unnecessarily goes up to 80 km, I suggest limiting the altitude range to something like 0-50 km to improve readability*

**Reply 4:** Agreed. The altitude range was limited to 0-40 km and the figure is now spanning the full width of the page to improve legibility.

*Section 5.1.1: ATMOS results are used for a qualitative comparison, but still, why did you use profiles retrieved in the mid-1980s by Zander et al, when the CCl<sub>4</sub> spectroscopy was of poor quality? (see Brown et al., Appl. Opt., 35, 1996). Results reported later on by Zander et al. (e.g. GRL, 23, 1996) are very likely more appropriate for a sensible comparison. An alternative would be to use the ATMOS version 3 results available from <http://remus.jpl.nasa.gov/atmos/atmosversion3/atmosversion3.html> and fully described in Irion et al. (Appl. Opt., 41, 2002)*

**Reply 5:** Agreed. A figure regarding the qualitative comparison was added to the manuscript. We are now using results reported by Zander et al. (1996).

*Section 5.2.1: the agreement between ACE and MIPAS is best below 15 km (lines 265-266 on page 13), but this is also mostly where the number of coincidences is the smallest (second left frame of Fig. 9). Could this inconsistent sampling have an impact on the statistics?*

**Reply 6:** Since the comparison is based on coincident measurements, the impact of inconsistent sampling should be negligible.

#### **Minor comments and typos**

*The title is not very informative; it could be edited to inform about the fact that first intercomparisons are included in this work*

**Reply 7:** Agreed. The title was changed to "MIPAS IMK/IAA Carbon Tetrachloride (CCl<sub>4</sub>) Retrieval and first Comparison with other Instruments".

*Page 2, line 22: "in 1987, when it was restricted": this is incorrect, CCl<sub>4</sub> was not among the first species controlled under the Montreal Protocol, it was added to the list in the 1990 London Amendment*

**Reply 8:** Agreed and changed.

*Page 2, line 28: these top-down emissions were evaluated instead of "reported"*

**Reply 9:** Agreed and changed.

*Page 2, line 29, I think a comma is needed after "unreported"*

**Reply 10:** Agreed and changed.

*Page 2, lien 35, here, I suggest replacing “considerably” by “now”*

**Reply 11:** Agreed and changed.

*Page 2, line 37: I would remove the reference to MIPAS here (“besides those of MIPAS...”, it is appropriate to introduce the new measurements later on, after the review of previous works*

**Reply 12:** Agreed and changed.

*Page 3, line 65, “as reduced” instead of “is reduced”*

**Reply 13:** Agreed and corrected.

*Page 3, line 85: the information about the actual spectral range fitted to retrieve CCl<sub>4</sub> is not consistent across the manuscript (see table 1, end of section 3.2...), this should be fixed*

**Reply 14:** Agreed and corrected.

*Caption of Fig.2: I guess that the “Black: measured spectrum, hardly discernible because overplotted by modelled spectra” warning has nothing to do here...*

**Reply 15:** Agreed and removed.

*Page 7, line 152: I would edit to “of CCl<sub>4</sub> for different time periods. All of the..”*

**Reply 16:** Agreed and added.

*Section 5.1.1.: ATMOS also participated to three other shuttle missions, in 1992, 1993 and 1994.*

**Reply 17:** Agreed. This information is now included in the text.

*Section 5.2.: please reword to something like “Since all collocated measurements were retrieved using the spectroscopic data of Nemtchinov and Varanasi (2003) introduced in HITRAN 2000, MIPAS Envisat retrievals based on the same spectroscopic dataset were also used for consistency and in order not to mask possible other discrepancies.”*

**Reply 18:** Agreed and changed.

## References

- Valeri, M., Barbara, F., Boone, C., Ceccherini, S., Gai, M., Maucher, G., Raspollini, P., Ridolfi, M., Sgheri, L., Wetzel, G., and Zoppetti, N. (2017). CCl<sub>4</sub> distribution derived from mipas esa v7 data: validation, trend and lifetime estimation. *Atmospheric Chemistry and Physics Discussions*, 2017:1–31.
- Zander, R., Mahieu, E., Gunson, M. R., Abrams, M. C., Chang, A. Y., Abbas, M. M., Aelig, C., Engel, A., Goldman, A., Irion, F. W., Kämpfer, N., Michelson, H. A., Newchurch, M. J., Rinsland, C. P., Salawitch, R. J., Stiller, G. P., and Toon, G. C. (1996). The 1994 northern midlatitude budget of stratospheric chlorine derived from ATMOS/ATLAS-3 observations. *Geophys. Res. Lett.*, 23(17):2357–2360.

# MIPAS IMK/IAA Carbon Tetrachloride (CCl<sub>4</sub>) Retrieval and first Comparison with other Instruments

E. Eckert<sup>1</sup>, T. von Clarmann<sup>1</sup>, A. Laeng<sup>1</sup>, G. P. Stiller<sup>1</sup>, B. Funke<sup>1</sup>, N. Glatthor<sup>1</sup>, U. Grabowski<sup>1</sup>, S. Kellmann<sup>1</sup>, M. Kiefer<sup>1</sup>, A. Linden<sup>1</sup>, A. Babenhauserheide<sup>1</sup>, G. Wetzel<sup>1</sup>, C. Boone<sup>2</sup>, A. Engel<sup>3</sup>, J. J. Harrison<sup>4,5,6</sup>, P. E. Sheese<sup>7</sup>, K. A. Walker<sup>2,7</sup>, and P. F. Bernath<sup>2,8</sup>

<sup>1</sup>Karlsruhe Institute of Technology, Institute of Meteorology and Climate Research, Karlsruhe, Germany

<sup>2</sup>Department of Chemistry, University of Waterloo, Waterloo, Ontario, Canada

<sup>3</sup>Institut für Atmosphäre und Umwelt, J. W. Goethe Universität, Frankfurt, Germany

<sup>4</sup>Department of Physics, University of Leicester, University Road, Leicester LE1 7RH, United Kingdom

<sup>5</sup>National Centre for Earth Observation, University of Leicester, University Road, Leicester LE1 7RH, United Kingdom

<sup>6</sup>Leicester Institute for Space and Earth Observation, University of Leicester, University Road, Leicester LE1 7RH, United Kingdom

<sup>7</sup>Department of Physics, University of Toronto, Toronto, Ontario, Canada

<sup>8</sup>Department of Chemistry and Biochemistry, Old Dominion University, Norfolk, VA 23529-0126, USA

*Correspondence to:* E. Eckert (ellen.eckert@kit.edu)

**Abstract.** MIPAS thermal limb emission measurements were used to derive vertically resolved profiles of carbon tetrachloride (CCl<sub>4</sub>). Level-1b data versions MIPAS/5.02 to MIPAS/5.06 were converted into volume mixing ratio profiles using the level-2 processor developed at Karlsruhe Institute of Technology (KIT) Institute of Meteorology and Climate Research (IMK) and Consejo Superior de Investigaciones Científicas (CSIC), Instituto de Astrofísica de Andalucía (IAA). Consideration of peroxyacetyl nitrate (PAN) as interfering species, which is jointly retrieved, and CO<sub>2</sub> line mixing is crucial for reliable retrievals. Parts of the CO<sub>2</sub> Q-branch region that overlap with the CCl<sub>4</sub> signature were omitted, since large residuals were still found even though line mixing was considered in the forward model. However, the omitted spectral region could be narrowed noticeably when line mixing was accounted for. A new CCl<sub>4</sub> spectroscopic dataset leads to slightly smaller CCl<sub>4</sub> volume mixing ratios. In general, latitude-altitude cross-section show the expected CCl<sub>4</sub> features with highest values of around 90 pptv at altitudes at and below the tropical tropopause and values decreasing with altitude and latitude due to stratospheric decomposition. Other patterns, such as subsidence in the polar vortex during winter and early spring, are also visible in the distributions. The decline in CCl<sub>4</sub> abundance during the MIPAS Envisat measurement period (July 2002 to April

2012) is clearly reflected in the altitude-latitude cross-section of trends estimated from the entire retrieved data set.

## 1 Introduction

Carbon tetrachloride (CCl<sub>4</sub>) is an anthropogenically produced halogen yielding trace gas and partly responsible for stratospheric ozone depletion. It is also a potent greenhouse gas with a 100-year global warming potential of 1730 (IPCC, 2013; World Meteorological Organization (WMO), 2014). CCl<sub>4</sub> was commonly used in fire extinguishers, as a precursor to refrigerants and in dry cleaning prior to 1990, when it was restricted within the framework of the London Amendment to the Montreal Protocol. Its abundances in the atmosphere increased steadily from the first part of the 20th century. Emissions declined significantly after 1990, as well as the amount of CCl<sub>4</sub> in the atmosphere with a few years delay. 2007-2012 bottom-up emissions of 1 to 4 kilotonnes/year were assessed by combining country-by-country reports to the United Nations Environmental Programme (UNEP) (Liang et al., 2016). This bottom-up estimate differs considerably from the 57(±17) kilotonnes/year top-down emissions which were evaluated in 2014 (World Meteorological Organization (WMO), 2014) using atmospheric measurements and lifetime estimates. Even

when possible  $\text{CCl}_4$  precursors and unreported, inadvertent emissions are accounted for, the gap between reported bottom-up and estimated top-down  $\text{CCl}_4$  emissions cannot be closed, as bottom-up emissions still only add up to 25 kilotonnes/year (SPARC, 2016). Besides a sink in the atmosphere,  $\text{CCl}_4$  is decomposed in the ocean and the soil with different lifetimes for each sink. Reassessment of the different lifetime estimates, which are essential for an adequate top-down assessment of emissions, leads to lower emissions of  $\sim 40(\pm 15)$  kilotonnes/year. While the gap between bottom-up and top-down emissions is now smaller after reassessments, the discrepancy is still not solved entirely. Previous measurements of stratospheric  $\text{CCl}_4$  have also been performed by the Atmospheric Chemistry Experiment Fourier Transform Spectrometer (ACE-FTS), a Cryosampler instrument employed at Frankfurt University and the balloon borne version of MIPAS (MIPAS-B2). The first version of the balloon borne MIPAS instrument (MIPAS-B) and ATMOS (Atmospheric Trace Molecule Spectroscopy) also measured  $\text{CCl}_4$ , but not during the MIPAS Envisat measurement period (Zander et al., 1996; von Clarmann et al., 1995).

Additional measurements, especially vertically well resolved ones with global coverage such as satellite measurements from MIPAS, can help to improve the understanding of the atmospheric  $\text{CCl}_4$  budget and stratospheric lifetime estimate. Furthermore, as a tracer with relatively short stratospheric lifetimes,  $\text{CCl}_4$  measurements can improve the understanding of changes in Brewer-Dobson circulation further constraining the lower boundary, e.g. processes around the tropopause.

In this study, we present the retrieval of  $\text{CCl}_4$  distributions from MIPAS limb emission spectra. First, we characterize the MIPAS instrument (Sec. 2), followed by a detailed description of the retrieval and the specific issues that had to be dealt with to derive  $\text{CCl}_4$  concentration (Sec. 3). We then compare the results of the MIPAS Envisat  $\text{CCl}_4$  retrieval with those of ACE-FTS, those of the second balloon-borne MIPAS instrument (MIPAS-B2) and those of Cryosampler measurements (Sec. 5) and summarize the results in the conclusions (Sec. 6).

## 2 MIPAS

The Michelson Interferometer for Passive Atmospheric Sounding (MIPAS) was one of the instruments aboard the European Environmental Satellite (Envisat). It was launched into a sun-synchronous orbit at an altitude of approximately 800 km on 1 March 2002. On 8 April 2012, all communication with the satellite was lost ending an observation period of more than 10 years. Envisat orbited the earth 14.4 times a day crossing the equator at 10:00 and 22:00 local time. MIPAS measured infrared emissions between  $685 \text{ cm}^{-1}$  and  $2410 \text{ cm}^{-1}$  (14.6 and  $4.15 \mu\text{m}$ ) (Fischer et al., 2008), which

allows for day and night time measurements with global coverage. The initial spectral resolution of the instrument was  $0.025 \text{ cm}^{-1}$  ( $0.0483 \text{ cm}^{-1}$  after a "Norton-Beer strong" apodization (Norton and Beer, 1976)). An instrument failure in March 2004 led to an observation gap until January 2005 when the instrument was successfully restarted. The first period (June 2002 to March 2004) is referred to as full spectral resolution (FR) period, while the period from January 2005 to April 2012 is referred to as reduced spectral resolution (RR) period. Due to a problem with one of the interferometer slides, MIPAS could only be operated with a spectral resolution of  $0.0625 \text{ cm}^{-1}$  ( $0.121 \text{ cm}^{-1}$  apodized) from January 2005 on. In this study, only measurements from the instrument's "nominal operation mode" are used. In this mode, the number of tangent altitudes increased from 17 during the FR period to 27 during the RR period. The vertical coverage ranges from 6 km to around 68 km during the FR period and up to around 70 km during the RR period, respectively. MIPAS initially took around 1000 measurements per day. In 2005, operation was resumed at reduced duty cycle. By the end of 2007, MIPAS was back at full duty cycle which amounts to approximately 1300 RR measurements per day. The horizontal sampling changed from 510 km during the FR period to 410 km during the RR period.

The temperature and various atmospheric trace gases are retrieved from level-1b data using a retrieval processor developed at the Institute of Meteorology and Climate Research at the Karlsruhe Institute of Technology (KIT) in close cooperation with the Instituto de Astrofísica de Andalucía (CSIC) in Granada, Spain. Results shown in this publication cover both the FR and the RR period.

## 3 Retrieval

The MIPAS Envisat retrieval is based on a non-linear least squares approach and employs a first-order Tikhonov-type regularization (von Clarmann et al., 2003, 2009). The radiative transfer is modelled using the Karlsruhe Optimized and Precise Radiative Transfer Algorithm (KOPRA) model (Stiller, 2000).

The spectral regions used for the retrieval of  $\text{CCl}_4$  are  $772.0 - 791.0 \text{ cm}^{-1}$  and  $792.0 - 805.0 \text{ cm}^{-1}$ . The gap from  $791.0$  to  $792.0 \text{ cm}^{-1}$  is necessary, since even when accounting for line mixing, strong effects from the  $\text{CO}_2$  Q-branch still occur in the residuals. Several results from previous steps in the retrieval chain were used to derive  $\text{CCl}_4$  (Table 1) including the spectral shift ( $z_{\text{tangent}}$ ), the temperature ( $T$ ), the horizontal temperature gradient ( $T_{\text{grad}}$ ) and mixing ratio profiles of  $\text{HNO}_3$ ,  $\text{ClO}$ ,  $\text{CFC-11}$ ,  $\text{C}_2\text{H}_6$ ,  $\text{HCN}$ ,  $\text{ClONO}_2$  and  $\text{HNO}_4$ . In addition, several species were found to improve the retrieval whenever their mixing ratio profiles were fitted alongside  $\text{CCl}_4$ . These are peroxyacetyl nitrate (PAN),  $\text{CH}_3\text{CCl}_3$ ,  $\text{HCFC-22}$ ,  $\text{O}_3$ ,  $\text{H}_2\text{O}$ ,  $\text{C}_2\text{H}_2$  and  $\text{COF}_2$ . Although for most of these species results from preceding retrieval steps are avail-

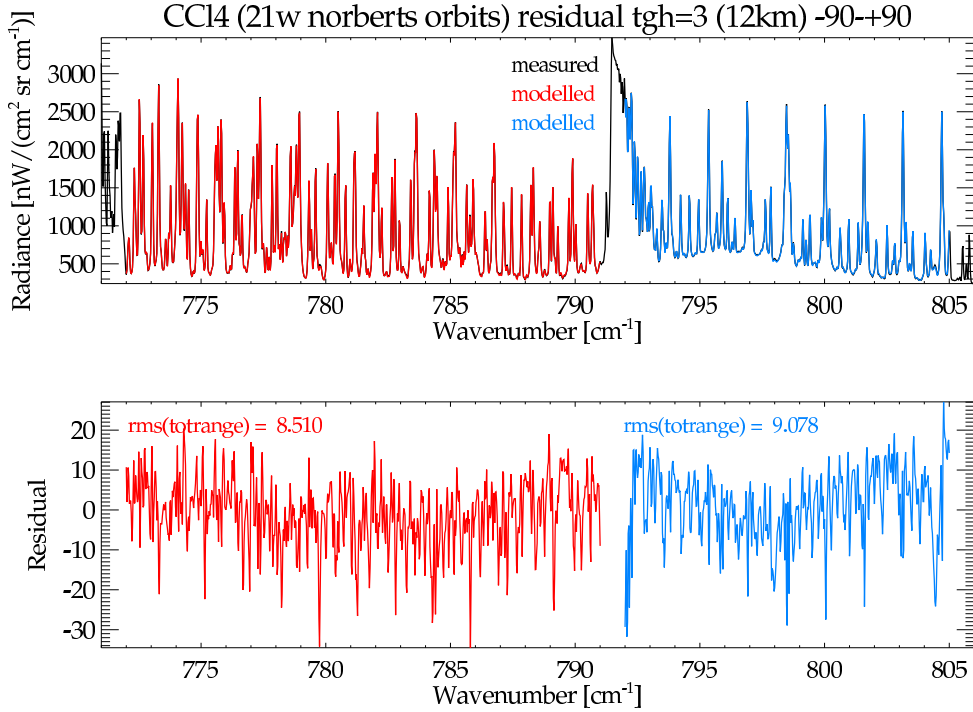


**Figure 1.** Exemplary spectra of MIPAS  $\text{CCl}_4$  at 12 km during the FR period (September 2003). Top panel: spectra; bottom panel: residuals.

able, fitting their concentrations jointly with that of  $\text{CCl}_4$  reduces the fit residuals significantly. This is attributed to spectroscopic inconsistencies of the interferers' spectroscopic data between the spectral region where these were retrieved and the spectral region where  $\text{CCl}_4$  is analyzed. Also fitted were a background continuum accounting for spectral contributions from aerosols and a radiance offset which is constant for all tangent altitudes (Table 1).

These retrieval settings lead to spectral fits as displayed in Fig. 1 and Fig. 2, where an example for the FR period and the RR period are shown, respectively. The measured spectra are plotted in black (not discernible from the best fit modelled in the fitting window), while the red and the blue lines represent the modelled spectra of the regions from  $772.0 - 791.0 \text{ cm}^{-1}$  and  $792.0 - 805.0 \text{ cm}^{-1}$ , respectively. Some periodic residuals are visible in both the FR and the RR period. These result from less than perfectly fitted  $\text{CO}_2$ , but as will be shown in Sec. 5, are only of minor relevance for the accuracy of the retrieved  $\text{CCl}_4$ .

### 3.1 Information cross-talk with PAN

The signature of PAN is particularly prominent in the spectral region of  $\text{CCl}_4$  and can thus be retrieved during the same retrieval step. Actually, jointly fitting PAN is very important for the  $\text{CCl}_4$  retrieval. Since PAN was already retrieved from MIPAS spectra before (Glatthor et al., 2007), it is of obvious interest to investigate the PAN results from the  $\text{CCl}_4$ -PAN joint retrieval in comparison with those from the original PAN retrieval. In there  $\text{CCl}_4$  was fitted alongside PAN but the retrieval was not yet optimized for  $\text{CCl}_4$ . We find slightly higher volume mixing ratios of PAN throughout most of the altitude-latitude cross-section (Fig. 3). As a consequence, areas showing unphysical mixing ratios below zero in the original retrievals (left panel of Fig. 3) are now slightly positive or very close to zero. This suggests that jointly fit PAN from the retrieval optimized for  $\text{CCl}_4$  might be more accurate than PAN retrieved using the old  $\text{CCl}_4$  distributions.

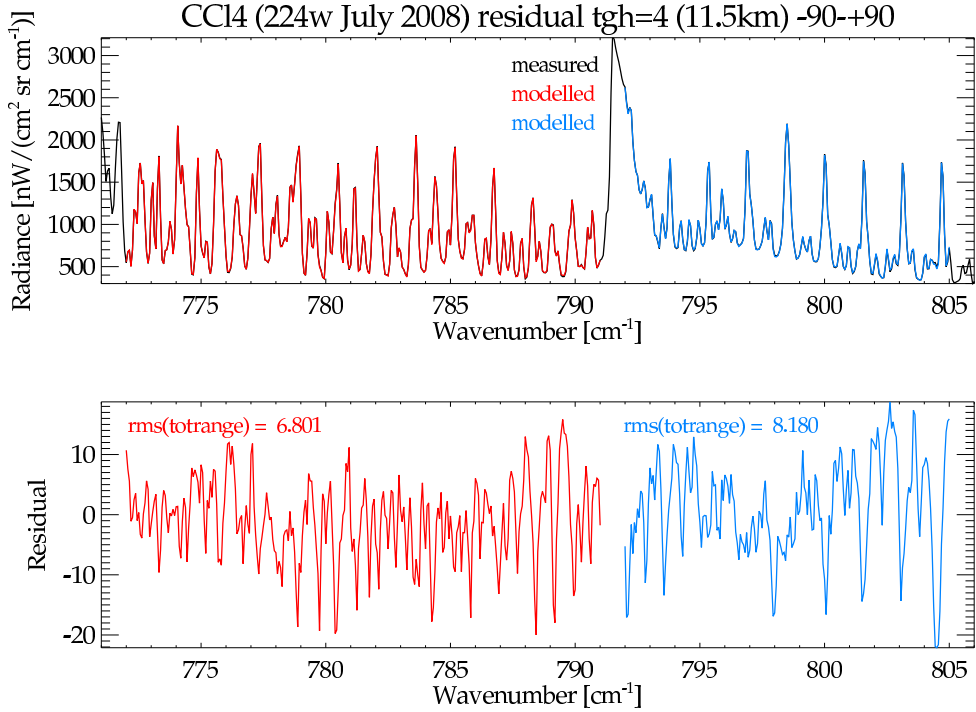


**Figure 2.** Exemplary spectra of MIPAS  $\text{CCl}_4$  at 11.5 km during the RR period (July 2008). Top panel: spectra; bottom panel: residuals.

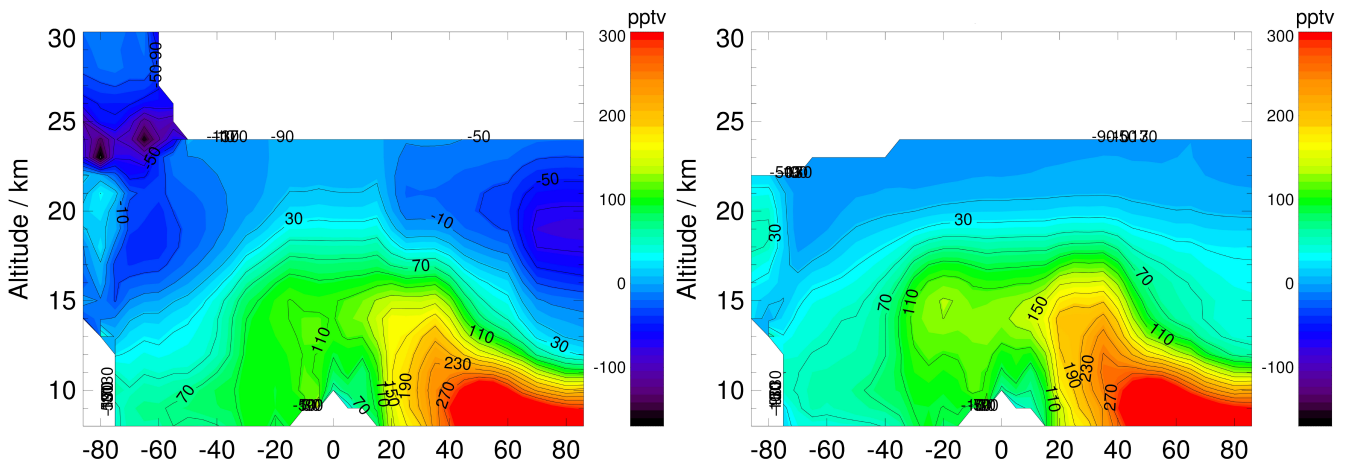


**Figure 3.** PAN altitude/latitude cross-sections (July 2008) from a separate retrieval using the old  $\text{CCl}_4$  distributions (left) and resulting from a joint retrieval with  $\text{CCl}_4$  (right).

**Table 1.** Retrieval details on the spectroscopic region, species imported from preceding retrieval steps and variables fitted jointly during the retrieval process. Brackets denote mixing ratios.

Spectral regions	Imported from preceding retrieval steps	Jointly fitted variables
772.0 - 791.0 $\text{cm}^{-1}$	Shift( $z_{\text{tangent}}$ )	[PAN](z)
792.0 - 805.0 $\text{cm}^{-1}$	T(z)	[ $\text{CH}_3\text{CCl}_3$ ](z)
	$T_{\text{grad}}(z)$	[HCFC-22](z)
	[ $\text{HNO}_3$ ](z)	[ $\text{O}_3$ ](z)
	[ $\text{ClO}$ ](z)	[ $\text{H}_2\text{O}$ ](z)
	[CFC-11](z)	[ $\text{C}_2\text{H}_2$ ](z)
	[ $\text{C}_2\text{H}_6$ ](z)	[COF <sub>2</sub> ](z)
	[HCN](z)	Continuum(z)
	[ $\text{ClONO}_2$ ](z)	offset
	[ $\text{HNO}_4$ ](z)	

225  
230  
235  
240  
245

$\text{CCl}_4$  distributions of July 2008. The upper panel shows what stratospheric  $\text{CCl}_4$  distributions retrieved with the original spectroscopic dataset as presented in HITRAN 2000 (Nemtchinov and Varanasi, 2003) look like. The lower panel shows the same cross-section, but using the new spectroscopic dataset by Harrison et al. (2017) for an otherwise identical retrieval setup. While the qualitative and morphological features of the distribution are very similar, lower volume mixing ratios of  $\text{CCl}_4$  result when the new spectroscopic dataset is used. Comparing these with reported values of ground based measurements as presented in SPARC (2016) indicates that the updated spectroscopic data lead to results which, in the tropopause region, agree better with tropospheric measurements. Tropospheric volume mixing ratios are reported to be at approximately 95 pptv which is very close to what MIPAS Envisat presents around the tropical tropopause and at mid-latitudes of the northern hemisphere when using the new spectroscopic dataset. In contrast, using HITRAN 2000 sometimes results in volume mixing ratios above 100 pptv in the same region. Thus, we consider the new spectroscopic dataset more adequate for the retrieval of  $\text{CCl}_4$ .

### 190 3.2 Line mixing

Since the spectral region where  $\text{CCl}_4$  is retrievable contains a  $\text{CO}_2$  Q-branch, the retrieval is set up to account for line mixing (Funke et al., 1998). This was done by using the Rosenkranz approximation (Rosenkranz, 1975). Tests were also performed using the computationally more demanding direct diagonalisation, but this approach was not found to 195 noticeably change the results of the retrieval. This is possibly the case because the microwindows were carefully selected to omit major spectral signatures of the  $\text{CO}_2$  Q-branch and because the effect of line mixing is generally smaller at stratospheric pressure levels. However, it was still necessary 200 to omit parts of the  $\text{CO}_2$  Q-branch. Fig. 4 and Fig. 5 show spectra where the full spectral region was fitted. In Fig. 4, line mixing was not considered and thus a large peak in the residual is visible close to 791.0  $\text{cm}^{-1}$ . In Fig. 5, the Rosenkranz 205 approximation was used to account for line mixing. Even though the residual is considerably smaller than without line mixing taken into account - as would be expected - peaks significantly larger than for the remainder of the window are 210 still visible between 791.0 and 792.0  $\text{cm}^{-1}$ . Although inclusion of line mixing significantly reduces the residuals in the  $\text{CO}_2$  branch, the residuals are still unacceptably large there. With the Rosenkranz approximation, however, the spectral 215 region excluded from the fit could be narrowed to 791.0 to 792.0  $\text{cm}^{-1}$  from 790.5 to 792.5  $\text{cm}^{-1}$ .

## 4 Results

### 4.1 Distributions

Fig. 7, the lower panel of Fig. 6 and Fig. 8 give an overview of the latitudinal and altitude distribution of  $\text{CCl}_4$  of different time periods. All of the altitude-latitude cross-sections show the expected pattern of  $\text{CCl}_4$  with a rapid decrease with increasing altitude in the stratosphere, as the gas is photolyzed there. In addition, highest volume mixing ratios appear at the equator where  $\text{CCl}_4$ , along with many other trace gases, enters the stratosphere due to the upward transport associated with the Brewer-Dobson circulation. During January 2010, March 2011 and particularly April 2011, subsidence of higher stratospheric air results in reduced mixing ratios over the North pole. In Spring 2011, an unusually stable northern polar vortex resulted in severe ozone depletion and particularly strong subsidence (Manney et al., 2011; Sinnhuber et al., 2011) which is reflected by the observations shown here. In general, MIPAS Envisat shows higher volume mixing ratios in the lower stratosphere during the FR period, which fits well with the overall decline in  $\text{CCl}_4$  abundance in the atmosphere due to its restriction under the Montreal Protocol. This impression is also supported by the lower panel in Fig. 6, which shows lower overall volume mixing ratios than MIPAS sees during the FR period, but which are still slightly higher than during 2010 and 2011. All cross-sections show a maximum in the  $\text{CCl}_4$  volume mixing ratios around the tropical tropopause connected with values of similar magnitude at lower altitudes of northern extratropical regions. This pattern was also seen in HCFC-22 (Chirkov et al., 2016) and

### 265 3.3 New $\text{CCl}_4$ Spectroscopic Data

During the ongoing development of the MIPAS Envisat  $\text{CCl}_4$  retrieval, a new  $\text{CCl}_4$  spectroscopic dataset was published by Harrison et al. (2017). Fig. 6 shows the influence of these 270 spectroscopic data on an altitude-latitude cross-section of

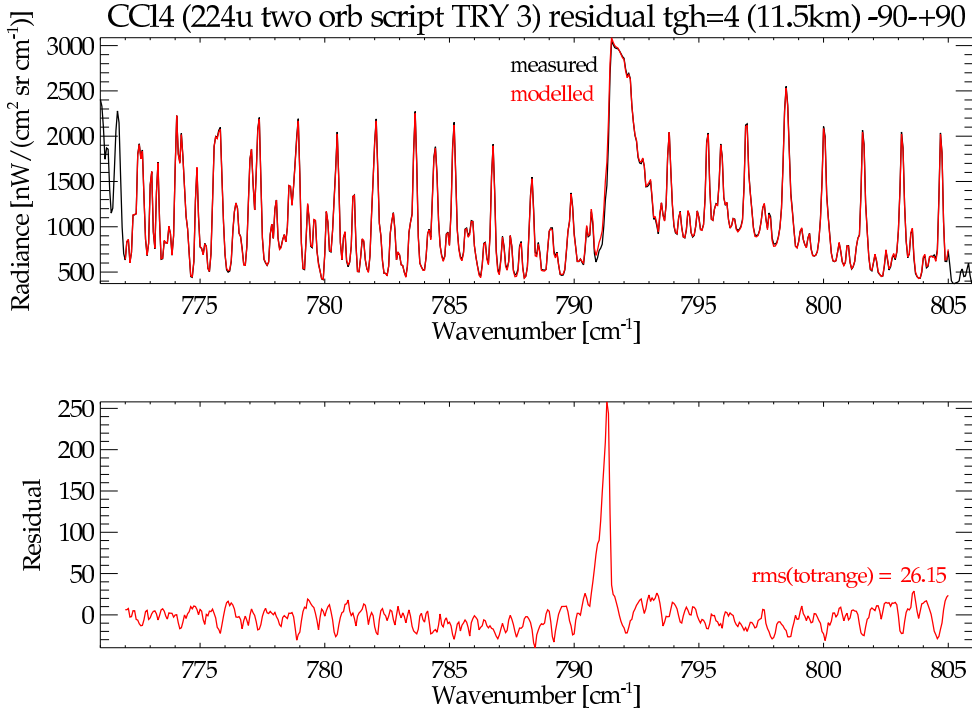


**Figure 4.** Impact of the  $\text{CO}_2$  Q-branch at 11.5 km altitude without considering line mixing. Top panel: spectra; bottom panel: residuals. Black: measured spectrum, hardly discernible because overplotted by modelled spectra.

could be linked to the Asian monsoon. Calculations with the 290 Chemical Lagrangian Model of the Stratosphere (CLaMS) by Vogel et al. (2016) show that there indeed exists a mechanism which can produce local maxima in the upper troposphere in 2D distributions of source gases. So, the monsoon might offer an explanation for the patterns seen in  $\text{CCl}_4$  295 around these atmospheric regions as well.

#### 4.2 Altitude Resolution

280 The vertical resolution of the  $\text{CCl}_4$  profiles is very similar for the FR and the RR period. From about 2.5-3 km at the lower end of the profiles, it degrades to approximately 5 km 285 at  $\sim 25$  km and  $\sim 7$  km at  $\sim 30$  km, calculated as the full width at half maximum of the row of the averaging kernel matrix (Rodgers, 2000). The degrees of freedom are usually around 3.5 for the FR period and close to 4.0 for the RR period (Fig. 9). This is presumably attributed to the finer 300 vertical sampling during the RR period with 27 tangent altitudes compared to 17 tangent altitudes during the FR

period. The signal decreases rapidly with altitude, as the volume mixing ratios of  $\text{CCl}_4$  do. Above 30 km, hardly any  $\text{CCl}_4$  information is available in the MIPAS spectra. Slightly below 20 km, the averaging kernels show negative side wiggles which are more pronounced during the FR period (left panel) than the RR period (right panel).

#### 4.3 Error Budget

Tables 2 and 3 list the error budgets for mid latitudes during the FR and RR period between 10 and 40 km. Examples for other latitudes can be found in the appendix (Tables A1 and A6). For legibility reasons, the errors are only given every 5 km, although the retrieval grid is 1 km. Errors due to elevation uncertainties of the line of sight and uncertainties of several contributing species are given. All profiles show a strong increase in the relative errors at and above 30 km. During the FR period, the absolute total errors are fairly similar below this altitude, while large differences can occur from 20 km

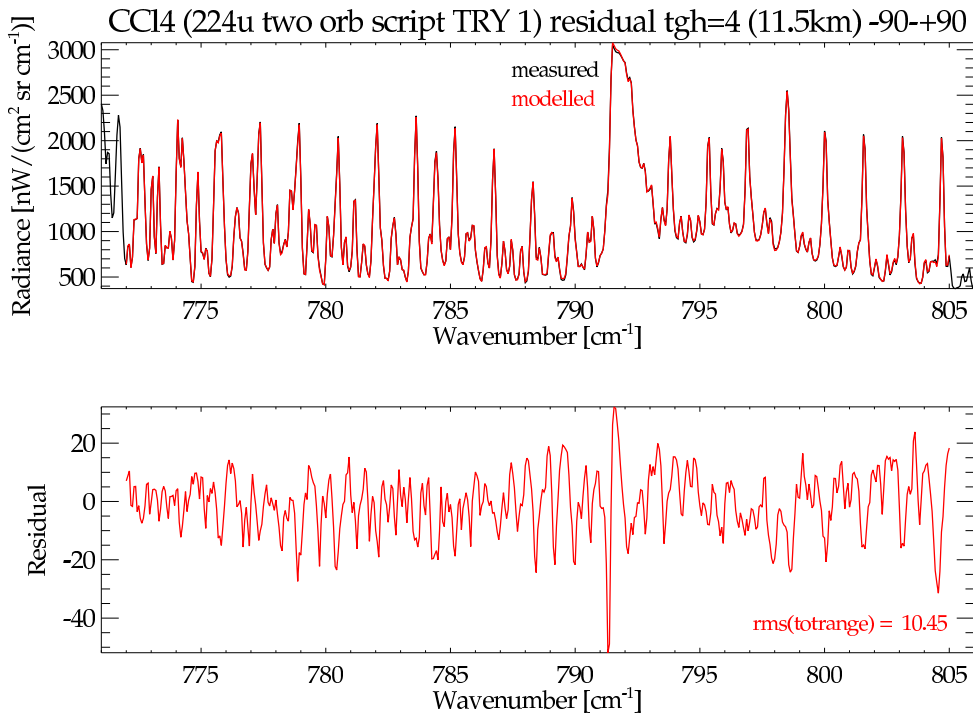


**Figure 5.** Impact of the  $\text{CO}_2$  Q-branch at 11.5 km altitude taking line mixing it into account (right). Top panel: spectra; bottom panel: residuals. Black: measured spectrum, hardly discernible because overplotted by modelled spectra. Note the different scale of the residual axis compared to Fig. 4.

**Table 2.** Error estimates for a mid-latitude profile during the FR period. Errors are given in pptv (relative errors in %).

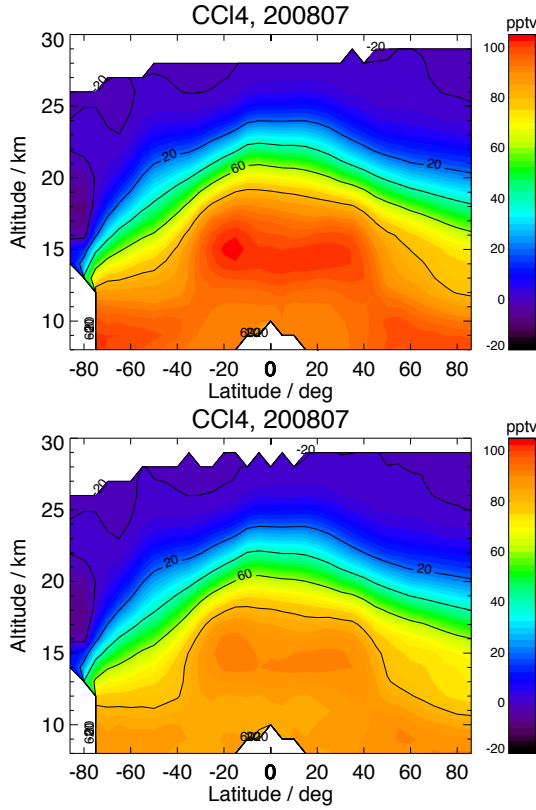
Altitude	total error	noise	total parameter	Gain	LOS	$\text{HNO}_4$	Shift	ILS	Temperature	$\text{ClONO}_2$
40	0.0 ( 69.4)	0.0 ( 57.2)	0.0 ( 38.8)	0.0 ( 24.5)	0.0 ( 22.5)	0.0 ( 18.2)	0.0 ( 1.7)	0.0 ( 9.2)	0.0 ( 6.3)	0.0 ( 5.5)
35	0.0 ( 68.4)	0.0 ( 56.7)	0.0 ( 39.1)	0.0 ( 23.5)	0.0 ( 21.5)	0.0 ( 18.4)	0.0 ( 1.7)	0.0 ( 9.0)	0.0 ( 6.3)	0.0 ( 5.7)
30	0.2 ( 71.0)	0.2 ( 64.3)	0.1 ( 33.8)	0.1 ( 20.3)	0.1 ( 17.9)	0.1 ( 20.3)	0.0 ( 1.8)	0.0 ( 3.0)	0.0 ( 5.1)	0.0 ( 5.1)
25	2.3 ( 480.8)	2.2 ( 459.9)	0.7 ( 144.2)	0.4 ( 79.4)	0.0 ( 3.8)	0.6 ( 115.0)	0.0 ( 10.0)	0.0 ( 0.7)	0.1 ( 23.0)	0.1 ( 17.3)
20	2.9 ( 5.3)	2.4 ( 4.4)	1.6 ( 2.9)	0.0 ( 0.1)	1.5 ( 2.8)	0.1 ( 0.3)	0.0 ( 0.0)	0.7 ( 1.2)	0.1 ( 0.2)	0.1 ( 0.2)
15	5.0 ( 4.9)	2.1 ( 2.1)	4.5 ( 4.5)	0.7 ( 0.7)	4.0 ( 4.0)	0.1 ( 0.1)	0.1 ( 0.1)	2.0 ( 2.0)	0.1 ( 0.1)	0.1 ( 0.1)
10	2.7 ( 3.1)	2.5 ( 2.8)	0.9 ( 1.0)	0.2 ( 0.2)	0.2 ( 0.3)	0.3 ( 0.3)	0.1 ( 0.1)	0.4 ( 0.4)	0.5 ( 0.6)	0.1 ( 0.1)

upwards. Absolute errors are close to 3 pptv between 10 and 25 km, and around 5 to 6 pptv at 15 km where larger volume mixing ratios appear for all atmospheric situations except the polar summer one where the errors stay close to 3 pptv. The largest error component is measurement noise (third column), while at 15 km significant parameter errors have to be considered, in particular the elevation uncertainties of the

line of sight (LOS), and instrument line shape (ILS). Beyond this, uncertainties of  $\text{HNO}_4$  and  $\text{ClONO}_2$  profiles, frequency calibration (shift) and temperature contribute to the total error. The decrease of retrieval noise towards higher altitudes is explained by the coarser altitude resolution at higher altitudes. For the RR period, the patterns look slightly different. There is no peak in the total error around 15 km, but the total

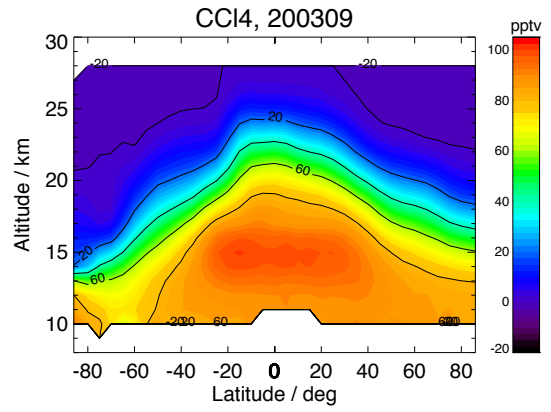
**Table 3.** Error estimates for a mid-latitude profile during the RR period. Errors are given in pptv (relative errors in %).

Altitude	total error	noise	total parameter	Gain	LOS	$\text{HNO}_4$	Shift	ILS	Temperature	$\text{ClONO}_2$
40	0.0 (214.1)	0.0 (127.1)	0.0 (173.9)	0.0 (73.6)	0.0 (147.2)	0.0 (24.8)	0.0 (2.5)	0.0 (24.8)	0.0 (24.1)	0.0 (13.4)
35	0.0 (211.3)	0.0 (128.1)	0.0 (172.9)	0.0 (70.4)	0.0 (147.3)	0.0 (25.0)	0.0 (2.6)	0.0 (24.3)	0.0 (23.7)	0.0 (13.4)
30	0.2 (141.2)	0.1 (123.6)	0.1 (61.8)	0.0 (15.9)	0.1 (47.7)	0.0 (24.7)	0.0 (2.8)	0.0 (22.1)	0.0 (2.8)	0.0 (11.5)
25	2.4 (187.3)	2.2 (171.7)	0.9 (67.1)	0.2 (14.0)	0.4 (30.4)	0.4 (33.6)	0.1 (4.8)	0.6 (44.5)	0.0 (0.0)	0.2 (16.4)
20	3.5 (15.0)	2.6 (11.1)	2.4 (10.3)	0.1 (0.4)	2.3 (9.9)	0.1 (0.4)	0.1 (0.3)	0.1 (0.5)	0.1 (0.2)	0.0 (0.1)
15	3.3 (6.1)	2.0 (3.7)	2.6 (4.8)	0.5 (1.0)	2.5 (4.6)	0.1 (0.3)	0.0 (0.1)	0.1 (0.2)	0.1 (0.1)	0.0 (0.0)
10	5.7 (6.1)	4.3 (4.6)	3.7 (4.0)	1.1 (1.2)	3.5 (3.8)	0.2 (0.2)	0.0 (0.0)	0.4 (0.4)	0.4 (0.4)	0.1 (0.1)

**Figure 6.** Altitude-latitude cross-section of July 2008, using the spectroscopic dataset by Nemtchinov and Varanasi (2003) (top) and using the new spectroscopic data by Harrison et al. (2017).  
340

error is either rather constant at lower altitudes or decreases with altitude. Contributions to the error budget are, however, 345 similar to the FR period.

325 Fig. 10 compares the estimated total error with the deviation of the profiles in a quiescent atmosphere. This comparison was created in a similar way as in Eckert et al. (2016, Sec. 6). Up to 18 km altitude, the sample standard deviation of MIPAS Envisat results is only slightly larger than the estimated error. Thus, these profiles suggest that the estimated error can 350 explain most of the variability in the  $\text{CCl}_4$  profiles up to ap-

**Figure 7.** Altitude-latitude cross-sections of MIPAS  $\text{CCl}_4$  for the FR period (September 2003).

proximately 18 km. Correspondingly, the error estimate can be considered realistic from the bottom of the profile up to this altitude.

#### 335 4.4 Trends

Fig. 11 shows an altitude-latitude cross-section of MIPAS Envisat  $\text{CCl}_4$  trends. These trends were estimated by the same method as described by Eckert et al. (2014), which is based on the method by von Clarman et al. (2010). In addition to the setup used by Eckert et al. (2014), the El-Niño-Southern Oscillation (ENSO) was also taken into account. The data set used for trend calculation covers the entire MIPAS Envisat measurement period from July 2002 to April 2012. The distribution of the trends agrees well with the trends estimated by Valeri et al. (2017), who calculated trends from MIPAS Envisat V7 data they formerly retrieved and displayed them on a pressure-latitude grid. The most likely cause of differences between their and our trend estimates are the underlying MIPAS spectra. We use MIPAS V5 spectra which were found to be subject to an instrument drift due to detector aging (Eckert et al., 2014). Valeri et al. (2017) use version 7 spectra where an attempt was made to tackle the problem of detector aging during the level-1

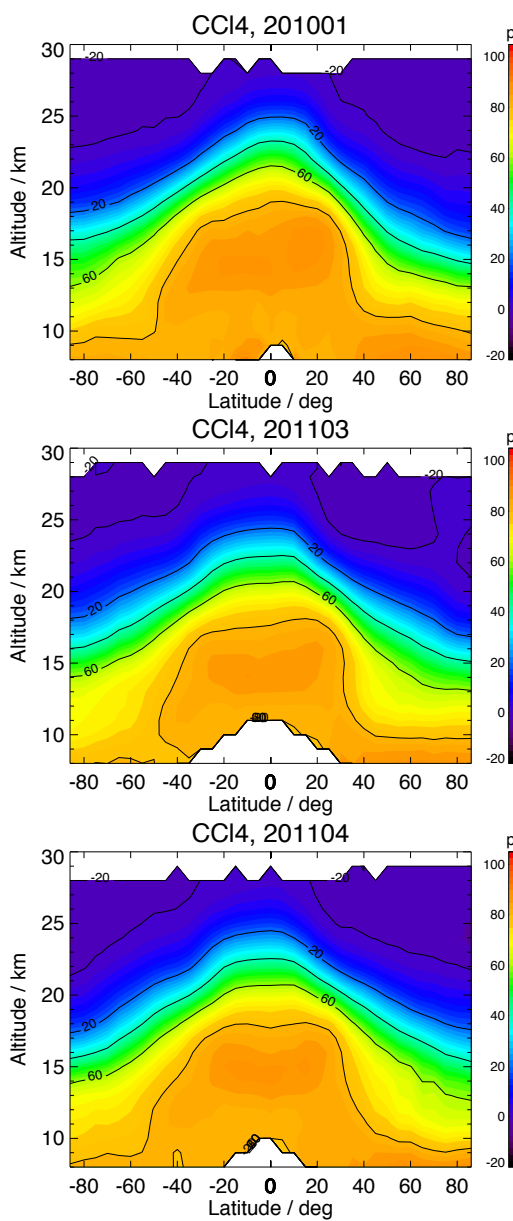


**Figure 8.** Altitude-latitude cross-sections of MIPAS  $\text{CCl}_4$  for the RR period. Top to bottom: July 2008, January 2010 and March and April 2011.

processing. However, Hubert et al. (2016) show that there is still a drift problem in the version 7 MIPAS temperatures. Since these temperature drifts are expected to propagate onto the retrieved  $\text{CCl}_4$  mixing ratios, it is not clear if version 5 or version 7 is more adequate for trend analysis. In spite of these differences and technical differences in the level-2 data processing, the trends inferred by Valeri et al. (2017) and ours show important common features. In both data sets a hemispheric asymmetry is found, with positive trends in

the Southern hemisphere around 25 km (however, the region is larger in our data set) and negative trends in the Northern hemisphere in almost the whole altitude range. Also the average magnitudes of the inferred trends agree reasonably well between both data sets.

## 5 Comparisons

### 5.1 Historical comparisons

#### 5.1.1 ATMOS

The ATMOS (Atmospheric Trace Molecule Spectroscopy) instrument measured in solar occultation covering the spectral region from 600 to 4700  $\text{cm}^{-1}$  with a spectral resolution of 0.01  $\text{cm}^{-1}$ . ATMOS took measurements in 1985, 1992, 1993 and 1994. The ATMOS profiles shown in Fig. 12 were extracted directly from Zander et al. (1996, Fig. 1).  $\text{CCl}_4$  volume mixing ratio profiles in the subtropics (20–35°N; thin dashed lines) and at midlatitudes (35–49°N; thin full lines) are presented there. Measurements were taken from 3 to 12 November in 1994 during the ATLAS-3 shuttle mission. We adopted depicting midlatitude profiles as solid lines and subtropic profiles as dashed lines in Fig. 12 of this manuscript. To compare the ATMOS profiles with MIPAS Envisat, we used MIPAS Envisat data of all years from 3 to 12 November and calculated an arithmetic mean for both latitude bands (subtropics and midlatitudes). In Fig. 12, MIPAS Envisat profiles are shown in blue, while the ATMOS profiles are shown in orange. The ATMOS profiles show higher volume mixing ratios than those of MIPAS Envisat, because they were measured shortly after  $\text{CCl}_4$  emissions were restricted and, thus, volume mixing ratios used to be higher in the atmosphere. However, the general shapes of the ATMOS profiles agree well with those of MIPAS Envisat. Both, MIPAS Envisat and ATMOS, show  $\text{CCl}_4$  mixing ratios which quickly decrease with altitude. The slopes of decline are similar above  $\sim 20$  km. Largest differences are visible at the lower end of the midlatitude profiles. ATMOS  $\text{CCl}_4$  mixing ratios also agree well with Liang et al. (2016, Fig. 2) where a time series of  $\text{CCl}_4$  surface mixing ratios over several decades is shown. Volume mixing ratios at the lower end of the profiles are noticeably higher than 100 pptv, which is in very good agreement with peak values of  $\text{CCl}_4$  shown in Liang et al. (2016, Fig. 2) for the time around and shortly after 1990. Taking the temporal development of the surface mixing ratios into account, ATMOS and MIPAS Envisat measurements provide a coherent picture.

#### 5.1.2 MIPAS-B

The first balloon-borne version of the MIPAS instrument was developed prior to the satellite instrument in the late 1980's and early 1990's at the Institute of Meteorology and Climate Research (IMK) in Karlsruhe (Fischer and Oelhaf,

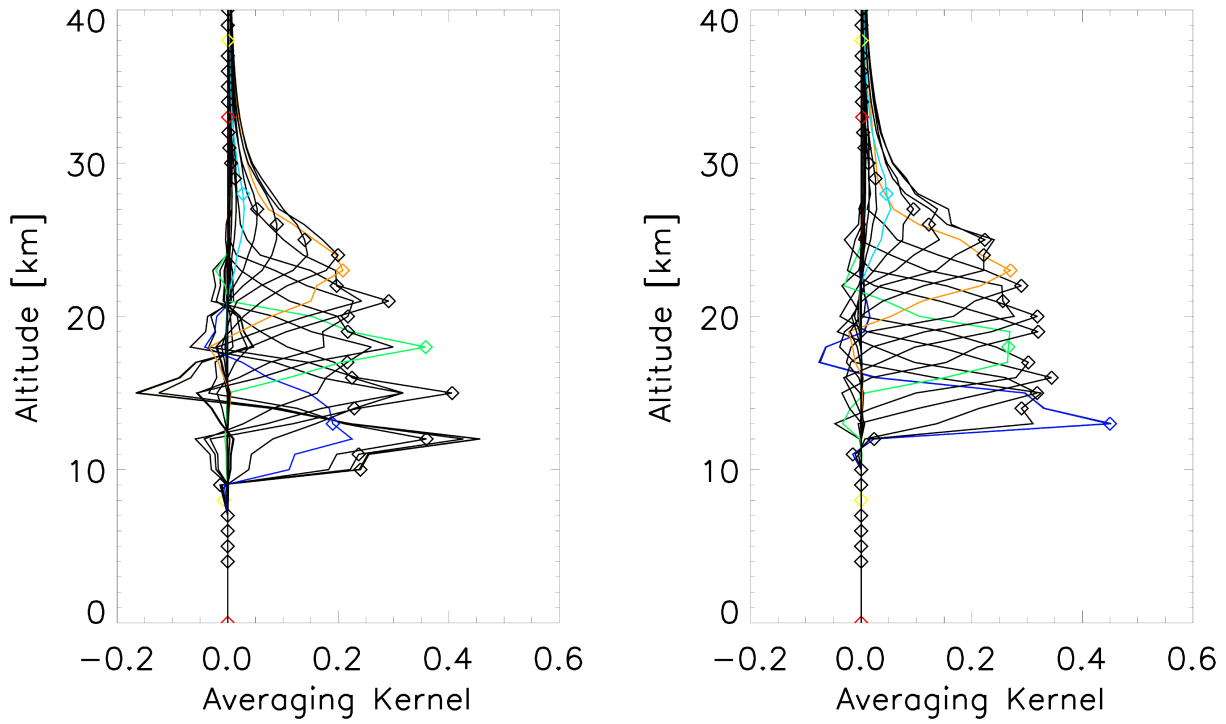


**Figure 9.** Rows of exemplary Averaging Kernels of MIPAS  $\text{CCl}_4$ . Left: FR period (September 2003). Right: RR period (July 2008).

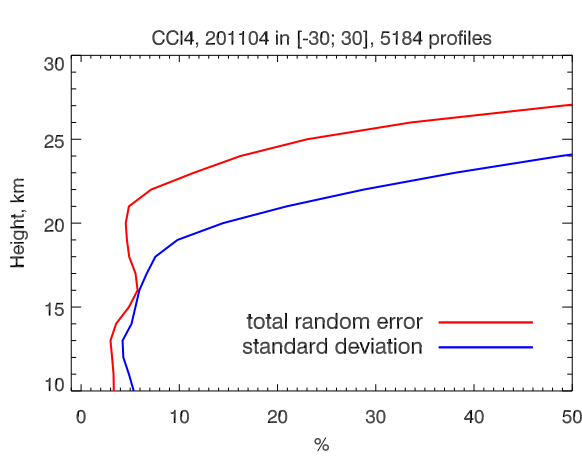


**Figure 10.** Comparison of the estimated total error with the standard deviation of several MIPAS profiles for a quiescent atmospheric situation (equator). Red: total error budget, blue: standard deviation.

1996). Measurements with this instrument have been taken since 1989 (von Clarmann et al., 1993) and first profiles of  $\text{CCl}_4$  were derived from a flight at Kiruna, Sweden, on 14 March 1992 (von Clarmann et al., 1995). Due to the strong

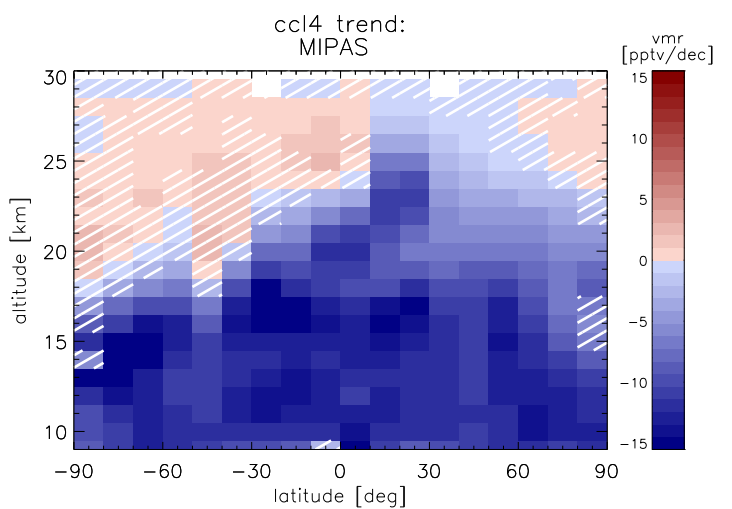


**Figure 11.** Altitude-latitude cross-sections of MIPAS  $\text{CCl}_4$  trends covering the entire measurement period from July 2002 to April 2012. Red colours indicate increasing  $\text{CCl}_4$  volume mixing ratios. Blue colours indicate declining  $\text{CCl}_4$  concentrations. Hatching shows where no statistically significant trends could be calculated at two sigma confidence level.

decrease of  $\text{CCl}_4$  with altitude, a clear signal of the gas could

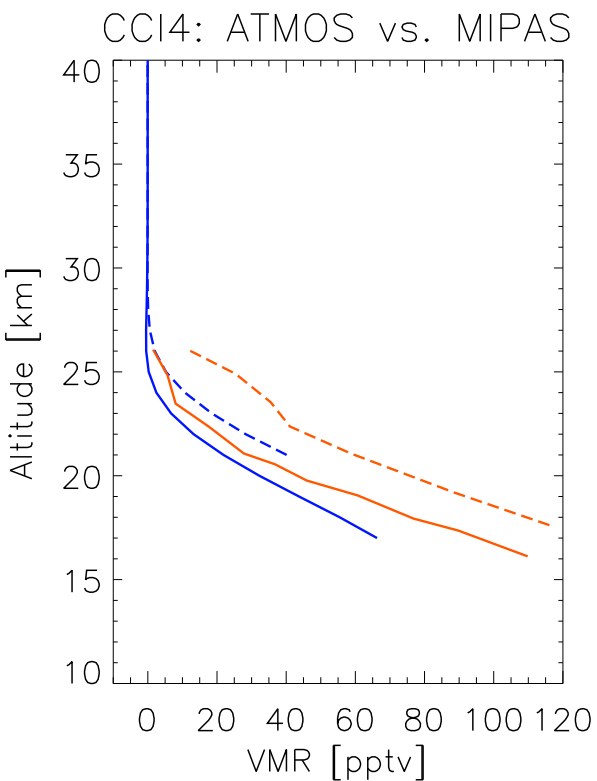


**Figure 12.** Qualitative comparison of profiles from ATMOS (orange) taken during the ATLAS-3 mission (as shown in Zander et al. (1996, Fig. 1)) and climatological means of MIPAS (blue) during 3-12 November of each year. Solid lines refer to midlatitude measurements ( $35\text{--}49^\circ\text{N}$ ). Dashed lines indicate subtropical measurements ( $20\text{--}35^\circ\text{N}$ ).

not be identified at tangent altitudes of 14.5 km and above. Thus, only the spectrum at 11.3 km was analyzed and the total amount of  $\text{CCl}_4$  was estimated by scaling the vertical profile and using information on the shape as measured in polar winter conditions before. This leads to an estimated concentration of approximately 110 pptv at 11.3 km, which is slightly higher than the peak surface values in the long time series of  $\text{CCl}_4$  shown in Liang et al. (2016). Ground based measurements shown in there support favouring the MIPAS Envisat  $\text{CCl}_4$  retrieval with the new spectroscopic dataset, since respective results agree better with measurements shown in Liang et al. (2016). MIPAS-B results overestimate the ground based measurements slightly providing a consistent picture when taking differences in the volume mixing ratios into account which result from the old versus the new spectroscopic dataset.

## 5.2 Comparisons with collocated measurements

All collocated measurements were analyzed using spectroscopic data of Nemtchinov and Varanasi (2003), which are included in the HITRAN 2000 database (Rothman et al., 2003). Thus, in order to allow for a meaningful comparison and not to mask possible other differences, a dedicated MIPAS Envisat comparison dataset was generated which is based on these spectroscopic data as well.

### 5.2.1 ACE-FTS

The Atmospheric Chemistry Experiment Fourier Transform Spectrometer ACE-FTS is one of two instruments aboard the Canadian Satellite SCISAT-1. On 12 August 2003, it was launched into a  $74^\circ$  orbit at 650 km to ensure a focus on higher latitudes. It covers the globe from  $85^\circ\text{S}$  to  $85^\circ\text{N}$ . Since ACE-FTS is an occultation instrument, it takes measurements during 15 sunrises and 15 sunsets a day within two latitude bands. The vertical scan range covers altitudes from the middle troposphere up to 150 km. Wavelengths between  $750\text{ cm}^{-1}$  and  $4400\text{ cm}^{-1}$  ( $13.3\text{ }\mu\text{m}$  and  $2.3\text{ }\mu\text{m}$ ) can be detected with a spectral resolution of  $0.02\text{ cm}^{-1}$ . The vertical sampling depends on the altitude as well as the beta angle. The latter is the angle between the orbit track and the path from the instrument to the sun. The sampling ranges from  $\sim 1$  km between 10 km and 20 km to  $\sim 2\text{--}3.5$  km around 35 km and declines to 5-6 km at the upper end of the vertical range. The field of view covers 3-4 km, which is approximately similar to the vertical resolution of the instrument. Comparisons in this study were made using version 3.5 of the ACE-FTS data. The  $\text{CCl}_4$  retrieval is performed between  $787.5\text{ cm}^{-1}$  and  $805.5\text{ cm}^{-1}$  at altitudes from 7 km to 25 km (Allen et al., 2009).

For the comparison with ACE-FTS (Fig. 13), coincident profiles within 2 hours time difference and no further than  $5^\circ$  latitude and  $10^\circ$  longitude away were used. Profiles at latitudes higher than  $60^\circ\text{S}$  were omitted. Between the lower end and  $\sim 16$  km the agreement is always close to 10 %, with slightly larger differences below 10 km than between 10 and 15 km. Above 15 km, the mean profiles deviate more strongly and exceed relative differences of 50 % above 19 km (Fig. 13d)). However, differences above 19 km are not as apparent in the absolute comparison (Fig. 13a)). The volume mixing ratio difference stays within similar values up to near 25 km. Since  $\text{CCl}_4$  decreases rapidly with altitude, this difference is far more pronounced in relative terms. MIPAS shows slightly lower volume mixing ratios than ACE-FTS, in general. Part of this might be attributed to PAN not being accounted for in the ACE-FTS v3.5 retrieval (Harrison et al., 2017). With PAN missing from the forward model calculations, the retrieval increases  $\text{CCl}_4$  to compensate. Preliminary ACE-FTS version 4 results indicate that retrieved  $\text{CCl}_4$  will skew lower when PAN is included. However, Harrison et al. (2017) do not investigate the magnitude of the

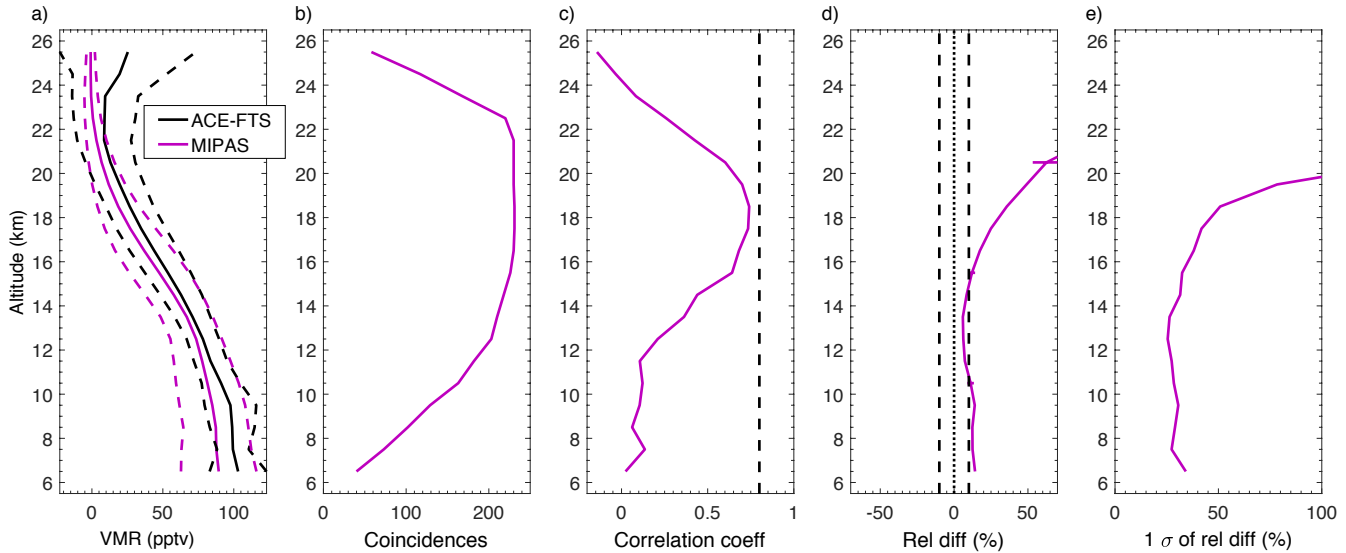


**Figure 13.** Comparison of MIPAS Envisat and version 3.5 ACE-FTS  $\text{CCl}_4$ . a) Mean profiles of all coincident profiles (black: ACE-FTS, magenta: MIPAS). Dashed lines show the standard deviations of the mean profiles. b) Number of coincident points per altitude. c) Correlation coefficient of the mean profiles. d) Relative differences of the mean profiles. e) One standard deviation of the relative differences of the mean profiles.

485 effect of including PAN versus not including it. Other items changed in the retrieval e.g. the microwindow set and new cross sections, so it is not clear how much of the decrease in  $\text{CCl}_4$  can be attributed to the inclusion of PAN as an interferer in the ACE-FTS retrieval. Nevertheless, the agree- 490 515

520 within the 10 % range for the differences up to above 15 km.

### 5.2.2 MIPAS-B2

525 MIPAS-B2 is the follow-up of MIPAS-B (Friedl-Vallon et al., 2004) which was lost in 1992. MIPAS-B and MIPAS-B2 measurements add up to more than 20 flights to date. MIPAS-B2 covers the spectral range from  $750\text{ cm}^{-1}$  to  $2500\text{ cm}^{-1}$  ( $13.3\text{ }\mu\text{m}$  and  $4\text{ }\mu\text{m}$ ) and vertical ranges up to the floating altitude of typically around 30-40 km. The vertical sampling is approximately 1.5 km. The spectral region used for the MIPAS-B2 retrieval ranges from  $786.0$  to  $806.0\text{ cm}^{-1}$ . MIPAS-B2 and MIPAS Envisat 530 use the same retrieval strategy and forward model to derive vertical profiles.

535 Fig. 14 and Fig. 15 show  $\text{CCl}_4$  measurements from a single flight of MIPAS-B2 each, compared with collocated measurements of MIPAS Envisat along diabatic 2-day backward and forward trajectories. These trajectories were calculated at Free University of Berlin (Naujokat and Grunow, 2003) and are based on European Centre for Medium-Range Weather Forecasts (ECMWF)  $1.25^\circ \times 1.25^\circ$  analyses. The

trajectories start at different altitudes at the respective geolocation of the balloon measurement. Coincidence criteria for this comparison were 1 h and 500 km within the temporal and spacial range of the balloon location. Fig. 14 shows a comparison with the MIPAS-B2 flight on 24 January 2010. The comparison with the MIPAS Envisat mean profile (red line), which was calculated from the ensemble of all collocated MIPAS Envisat measurements (red squares), agrees with the MIPAS-B2 measurement (black line) within 5 pptv for most of the altitude range. The MIPAS-B2 measurement lies well within the spread of all collocated MIPAS Envisat profiles. The difference (middle panel) is always close to the total combined error, which includes all error estimates except the spectroscopy error. The latter has not been included because a MIPAS Envisat retrieval setup was used for this comparison which is based on the same spectroscopic data as the MIPAS-B2 retrieval. The right panel shows the relative error, which stays well within 5 % up to 17 km. Only between 16 and 18 km, the relative difference noticeably exceeds the combined error of the instruments.

The comparison of the MIPAS-B2 flight on 31 March 2011 (Fig. 15) with MIPAS Envisat presents even better agreement. The difference between the two profiles never exceeds 5 pptv (middle panel) and stays within or close to the combined error of the instruments throughout the whole altitude range. Larger deviations in the relative differences only occur above 18 km, where the combined error of

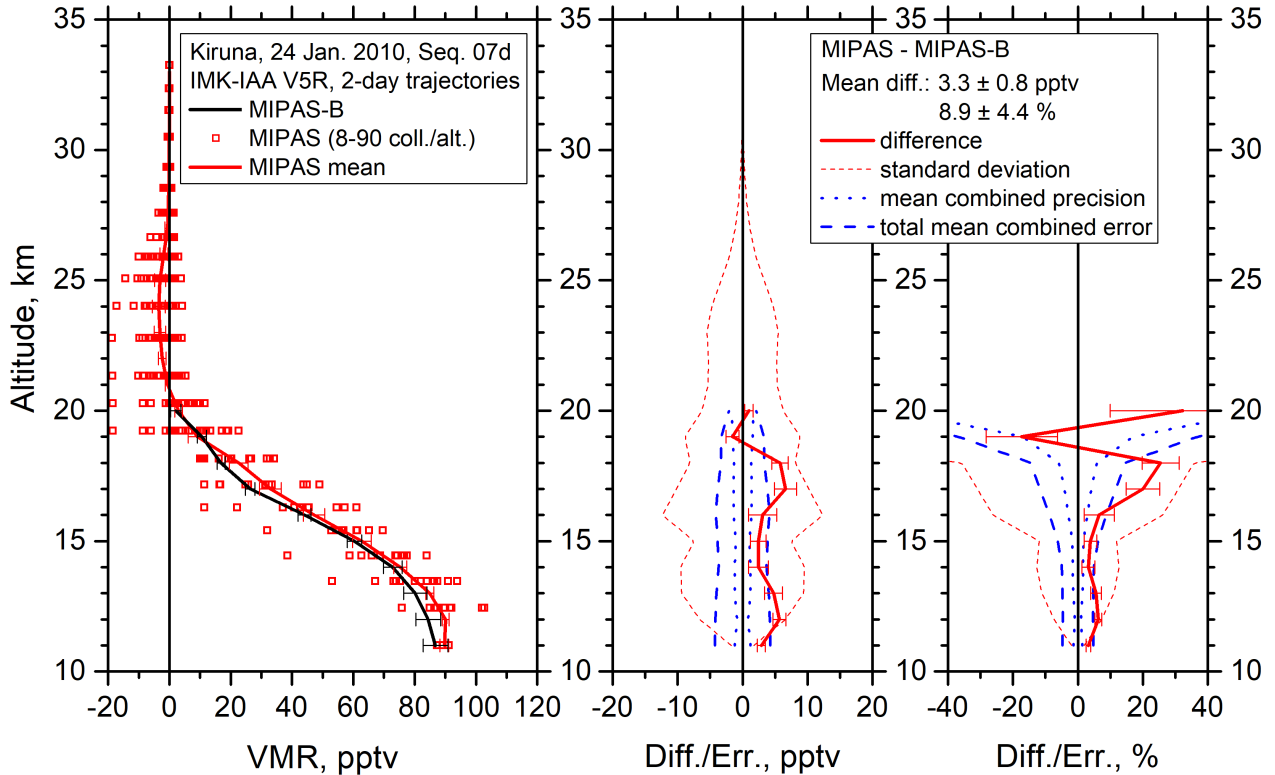


**Figure 14.** Comparison of MIPAS Envisat and MIPAS-B2  $\text{CCl}_4$  for the MIPAS-B2 flight on 24 January 2010 over Kiruna, Sweden. Left: Mean profile of all coincident profiles (black line: MIPAS-B2, red line: MIPAS mean, red squares: coincident MIPAS measurements). Middle: absolute total error budget without consideration of the spectroscopy error. Right: relative error budget - red continuous line: difference between the mean profiles; red dotted line: standard deviation; blue dotted line: mean combined precision; blue dashed line: total mean combined error.

the instruments also increases rapidly, because of small volume mixing ratios of  $\text{CCl}_4$ . Overall, the comparisons with MIPAS-B2 show excellent agreement between the two instruments. This suggests that the MIPAS Envisat  $\text{CCl}_4$  error estimate are realistic and that the residuals in the  $\text{CO}_2$  lines mentioned in Sec. 3.2 have no major impact on the  $\text{CCl}_4$  retrieval. This is also supported by Fig. 10, at least up to about 18 km, since the standard deviation of the profiles can be explained by the MIPAS Envisat error estimates to a large extent.

### 5.2.3 Cryosampler

The Cryosampler whose measurements are used here was developed at Forschungszentrum Jülich (Germany) in the early 1980s (Schmidt et al., 1987) and is a balloon-borne instrument. It collects whole air samples which are then frozen dur-

ing the flight and analyzed using gas chromatography after the flight. In this analysis, a flight performed on 1 April 2011 by University of Frankfurt (Fig. 16 black circles) is compared to collocated MIPAS Envisat profiles that lie within 1000 km and 24 h of the Cryosampler profile. The MIPAS Envisat profiles used for the comparison are those retrieved with the new spectroscopic dataset (continuous blue line: closest MIPAS profile, red line: MIPAS mean profile, blue-greyish lines: all collocated MIPAS profiles). In addition, the closest profile produced with the old spectroscopic dataset is shown (dashed blue line). The only difference between the blue line and the dashed blue line are the different spectroscopic datasets. It is clearly visible that the closest MIPAS profile produced with the new spectroscopic data comes closer to the Cryosampler measurements, even though these still show slightly lower volume mixing ratios of  $\text{CCl}_4$ . A similar pattern of two outliers (second and forth lowest Cryosampler measurements)

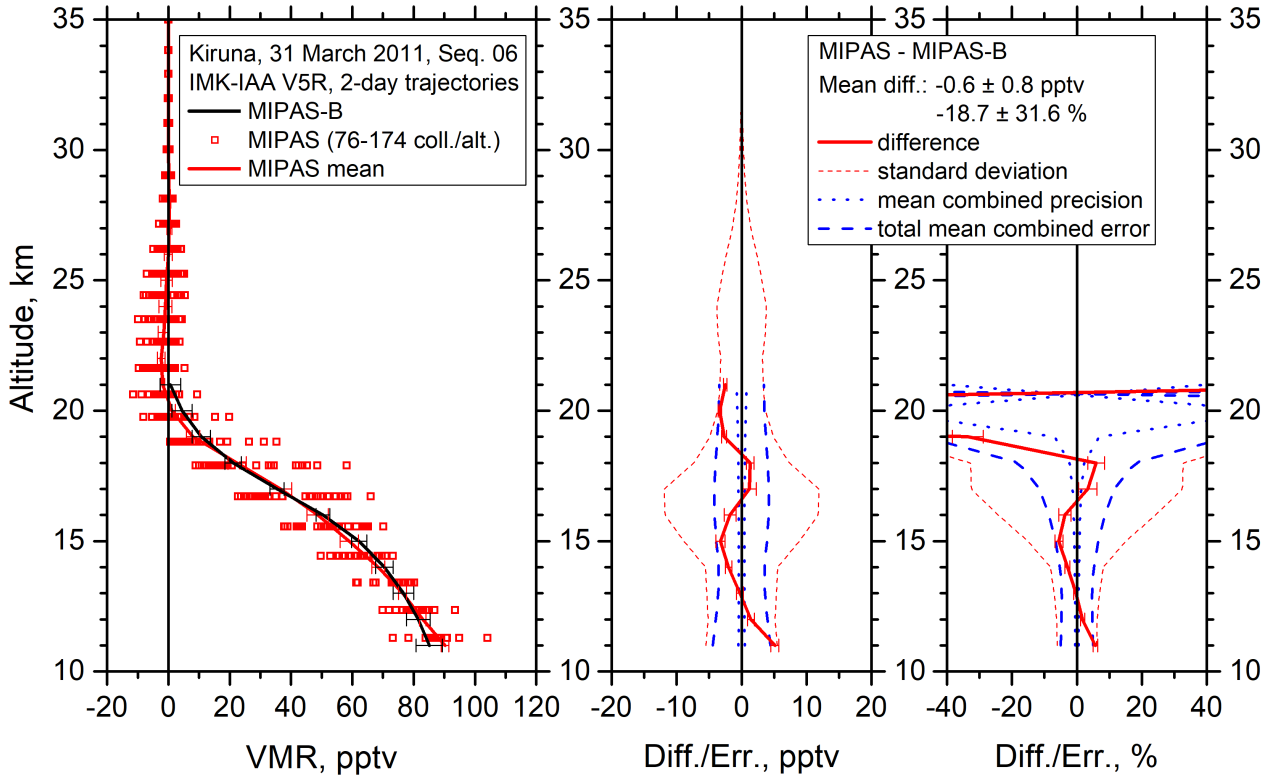


**Figure 15.** Comparison of MIPAS Envisat and MIPAS-B2  $\text{CCl}_4$  for the MIPAS-B2 flight on 31 March 2011 over Kiruna, Sweden. Left: Mean profile of all coincident profiles (black line: MIPAS-B2, red line: MIPAS mean, red squares: coincident MIPAS measurements). Middle: absolute total error budget without consideration of the spectroscopy error. Right: relative error budget - red continuous line: difference between the mean profiles; red dotted line: standard deviation; blue dotted line: mean combined precision; blue dashed line: total mean combined error.

were also seen in a comparison of Cryosampler and MIPAS measurements of CFC-11 and CFC-12 (Eckert et al., 2016), even though the second lowest outlier is not as obvious for the CFCs. However, this might be an indication that Cryosampler captured fine structures (like laminae) produced by the unique atmospheric situation in spring 2011 (Manney et al., 2011; Sinnhuber et al., 2011), that MIPAS Envisat cannot resolve due to its coarser vertical resolution. All other Cryosampler measurements lie within the spread of the collocated MIPAS Envisat profiles. Taking this into account, the overall agreement of MIPAS and Cryosampler is good and Fig. 16 supports the assumption that the retrieval is improved by the usage of the new spectroscopic dataset.

## 6 Conclusions

Vertical profiles of  $\text{CCl}_4$  were retrieved from MIPAS Envisat limb emission spectra considering various interfering trace gases and with PAN playing a particularly important role. Using line-mixing in the forward model made it possible to narrow the spectral region that had to be omitted due to large residuals and thus to include additional information useful for the retrieval of  $\text{CCl}_4$ , even though parts of the  $\text{CO}_2$  Q-branch had still to be excluded. Introducing a new spectroscopic dataset (Harrison et al., 2017) resulted in lower volume mixing ratios of  $\text{CCl}_4$  which agree better with other results, e.g. tropospheric values shown in Liang et al. (2016) and Cryosampler measurements. The expected atmospheric distribution patterns are clearly visible in altitude-latitude cross-sections. These show higher volume mixing ratios of  $\text{CCl}_4$  in the tropics and at lower altitudes which quickly decrease above the tropopause due to photolysis. They also

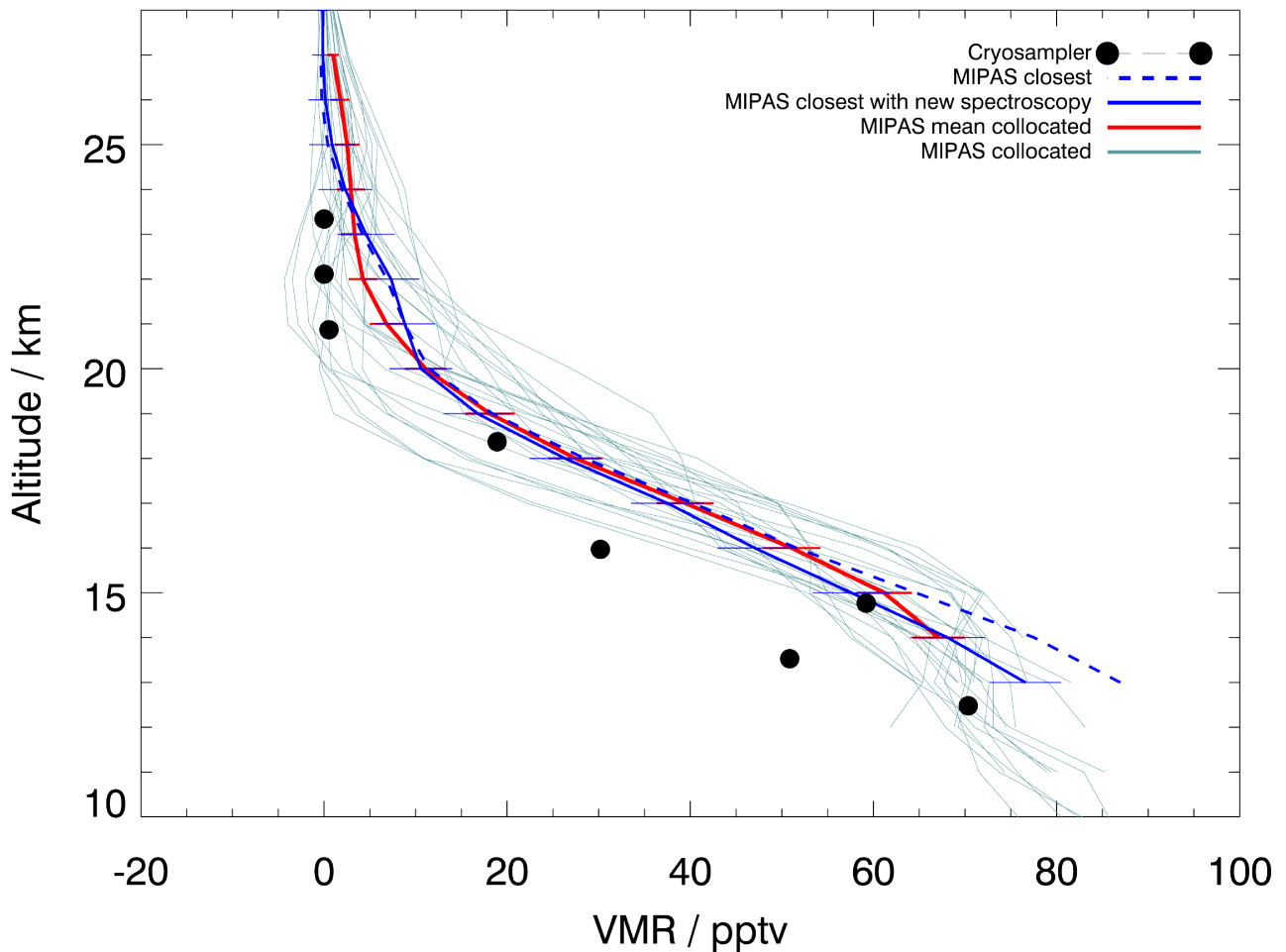


**Figure 16.** Comparison of MIPAS Envisat and cryosampler  $\text{CCl}_4$ . The cryosampler measurement taken on 1 April 2011. The continuous and dashed blue lines are the respective closest MIPAS Envisat profiles with the new and the old spectroscopic dataset.

decrease with increasing latitude and thus follow the Brewer-Dobson circulation. A maximum in the tropics connected with higher values of  $\text{CCl}_4$  below the northern extra-tropical tropopause is a feature also seen in HCFC-22 (Chirkov et al., 2016) where it was associated with the uplift in the Asian monsoon, so  $\text{CCl}_4$  distributions in this region might have a similar explanation. Trends of the entire measurement period from July 2002 to April 2012 show good agreement with trends estimated by Valeri et al. (2017). Comparisons with ACE-FTS and MIPAS-B2 show very good agreement and historical measurements of MIPAS-B2 and ATMOS are coherent with MIPAS Envisat  $\text{CCl}_4$  results using the new spectroscopic data. MIPAS profiles retrieved using the new spectroscopic dataset agree well with Cryosampler and deviations between the measurements can be explained reasonably. The latter comparison also suggests that the new spectroscopic dataset improves the MIPAS Envisat  $\text{CCl}_4$  retrieval. The MIPAS Envisat estimated error can explain most of the variabil-

ity of a set of profiles measured during quiescent atmospheric conditions up to 18 km, so the error estimate seems to be realistic. This is also supported by the comparison of MIPAS Envisat and MIPAS-B2 where the differences between the measurements stay mostly within the combined error of the instruments. Putting differences resulting from different spectral resolutions aside, also the comparison with the Cryosampler profile suggests to favour the spectroscopic dataset introduced by Harrison et al. (2017) over the dataset used before.

*Acknowledgements.* The retrievals of IMK/IAA were partly performed on the HP XC4000 of the Scientific Supercomputing Center (SSC) Karlsruhe under project grant MIPAS. IMK data analysis was supported by DLR under contract number 50EE0901. MIPAS level 1B data were provided by ESA. We acknowledge support by Deutsche Forschungsgemeinschaft and Open Access Publishing Fund of Karlsruhe Institute of Technology. This work was supported

by the DFG project for the 'Consideration of lifetimes of tracers for the determination of stratospheric age spectra and the Brewer-Dobson Circulation (COLIBRI)'. The Atmospheric Chemistry Experiment (ACE), also known as SCISAT, is a Canadian-led mission mainly supported by the Canadian Space Agency and the Natural Sciences and Engineering Research Council of Canada. Balloon flights and data analysis of MIPAS-B data used here were supported by the European Space Agency (ESA), the German Aerospace Center (DLR), CNRS (Centre National de la Recherche Scientifique), and CNES (Centre National d'Etudes Spatiales).

**Appendix A: Error Estimates**

**Table A1.** Error estimates for an equatorial profile during the FR period. Errors are given in pptv (relative errors in %).

Altitude	total error	noise	total parameter	Gain	LOS	$\text{HNO}_4$	Shift	ILS	Temperature	$\text{ClONO}_2$
40	0.0 ( 210.6)	0.0 ( 178.7)	0.0 ( 114.8)	0.0 ( 70.2)	0.0 ( 45.3)	0.0 ( 55.5)	0.0 ( 6.0)	0.0 ( 37.6)	0.0 ( 30.0)	0.0 ( 17.2)
35	0.0 ( 214.1)	0.0 ( 183.5)	0.0 ( 116.2)	0.0 ( 67.3)	0.0 ( 45.3)	0.0 ( 55.7)	0.0 ( 6.0)	0.0 ( 37.3)	0.0 ( 30.0)	0.0 ( 17.1)
30	0.2 ( 195.8)	0.2 ( 177.1)	0.1 ( 85.8)	0.1 ( 51.3)	0.0 ( 23.3)	0.1 ( 54.1)	0.0 ( 5.2)	0.0 ( 17.7)	0.0 ( 23.3)	0.0 ( 14.0)
25	2.3 ( 30.4)	2.2 ( 29.0)	0.9 ( 11.9)	0.4 ( 4.8)	0.5 ( 7.1)	0.5 ( 7.1)	0.1 ( 0.8)	0.2 ( 2.6)	0.2 ( 2.8)	0.1 ( 1.3)
20	2.8 ( 3.8)	2.5 ( 3.4)	1.3 ( 1.8)	0.2 ( 0.2)	0.8 ( 1.2)	0.1 ( 0.2)	0.0 ( 0.0)	0.9 ( 1.2)	0.3 ( 0.4)	0.1 ( 0.2)
15	5.3 ( 5.5)	2.2 ( 2.3)	4.9 ( 5.1)	0.9 ( 1.0)	4.2 ( 4.4)	0.2 ( 0.2)	0.1 ( 0.1)	2.3 ( 2.4)	0.4 ( 0.4)	0.1 ( 0.1)
10	2.8 ( 3.2)	2.6 ( 2.9)	1.0 ( 1.1)	0.2 ( 0.2)	0.1 ( 0.1)	0.2 ( 0.2)	0.1 ( 0.1)	0.3 ( 0.4)	0.8 ( 0.9)	0.1 ( 0.1)

**Table A2.** Error estimates for a polar summer profile during the FR period. Errors are given in pptv (relative errors in %).

Altitude	total error	noise	total parameter	Gain	LOS	$\text{HNO}_4$	Shift	ILS	Temperature	$\text{ClONO}_2$
40	0.0 ( 95.1)	0.0 ( 64.2)	0.0 ( 69.4)	0.0 ( 38.5)	0.0 ( 46.2)	0.0 ( 19.8)	0.0 ( 1.4)	0.0 ( 19.0)	0.0 ( 11.3)	0.0 ( 5.1)
35	0.0 ( 93.7)	0.0 ( 64.1)	0.0 ( 69.0)	0.0 ( 39.4)	0.0 ( 46.8)	0.0 ( 19.7)	0.0 ( 1.4)	0.0 ( 19.0)	0.0 ( 11.3)	0.0 ( 5.2)
30	0.2 ( 117.2)	0.2 ( 87.9)	0.1 ( 73.2)	0.1 ( 39.5)	0.1 ( 53.7)	0.1 ( 26.4)	0.0 ( 1.8)	0.0 ( 11.2)	0.0 ( 11.2)	0.0 ( 5.9)
25	2.5 ( 212.9)	2.2 ( 187.4)	1.2 ( 102.2)	0.5 ( 43.4)	0.9 ( 73.3)	0.6 ( 51.1)	0.1 ( 4.4)	0.1 ( 8.2)	0.1 ( 11.1)	0.1 ( 8.5)
20	2.4 ( 42.2)	2.1 ( 36.9)	1.2 ( 21.1)	0.1 ( 1.7)	1.2 ( 21.1)	0.2 ( 4.0)	0.0 ( 0.6)	0.0 ( 0.4)	0.1 ( 1.5)	0.0 ( 0.7)
15	2.8 ( 4.7)	1.7 ( 2.9)	2.3 ( 3.9)	0.1 ( 0.2)	2.2 ( 3.7)	0.2 ( 0.4)	0.1 ( 0.1)	0.5 ( 0.9)	0.2 ( 0.3)	0.1 ( 0.1)
10	3.0 ( 3.7)	2.3 ( 2.8)	2.0 ( 2.4)	0.1 ( 0.1)	1.4 ( 1.7)	0.1 ( 0.1)	0.1 ( 0.1)	1.2 ( 1.5)	0.3 ( 0.3)	0.0 ( 0.0)

**Table A3.** Error estimates for a polar winter profile during the FR period. Errors are given in pptv (relative errors in %).

Altitude	total error	noise	total parameter	Gain	LOS	$\text{HNO}_4$	Shift	ILS	Temperature	$\text{ClONO}_2$
40	0.0 ( 45.8)	0.0 ( 34.7)	0.0 ( 30.5)	0.0 ( 16.7)	0.0 ( 20.8)	0.0 ( 9.3)	0.0 ( 0.9)	0.0 ( 7.4)	0.0 ( 5.8)	0.0 ( 4.4)
35	0.0 ( 46.6)	0.0 ( 34.6)	0.0 ( 29.3)	0.0 ( 16.0)	0.0 ( 20.0)	0.0 ( 9.3)	0.0 ( 0.9)	0.0 ( 7.3)	0.0 ( 5.9)	0.0 ( 4.4)
30	0.2 ( 47.8)	0.2 ( 40.7)	0.1 ( 26.3)	0.0 ( 11.7)	0.1 ( 19.4)	0.0 ( 10.5)	0.0 ( 0.7)	0.0 ( 1.8)	0.0 ( 4.1)	0.0 ( 4.1)
25	2.4 ( 58.5)	2.2 ( 53.6)	1.1 ( 26.8)	0.4 ( 8.8)	0.8 ( 19.7)	0.6 ( 13.6)	0.0 ( 0.4)	0.1 ( 2.4)	0.1 ( 2.9)	0.2 ( 5.1)
20	2.8 ( 22.8)	2.7 ( 22.0)	0.9 ( 7.3)	0.0 ( 0.4)	0.8 ( 6.8)	0.3 ( 2.4)	0.1 ( 0.4)	0.0 ( 0.1)	0.0 ( 0.1)	0.1 ( 1.0)
15	4.4 ( 7.7)	1.8 ( 3.1)	4.0 ( 7.0)	0.0 ( 0.1)	3.9 ( 6.8)	0.2 ( 0.4)	0.0 ( 0.0)	0.9 ( 1.6)	0.1 ( 0.1)	0.0 ( 0.1)
10	2.7 ( 3.1)	2.5 ( 2.9)	0.9 ( 1.0)	0.2 ( 0.2)	0.5 ( 0.6)	0.1 ( 0.1)	0.1 ( 0.1)	0.1 ( 0.1)	0.5 ( 0.6)	0.1 ( 0.1)

**Table A4.** Error estimates for an equatorial profile during the RR period. Errors are given in pptv (relative errors in %).

Altitude	total error	noise	total parameter	Gain	LOS	$\text{HNO}_4$	Shift	ILS	Temperature	$\text{ClONO}_2$
40	0.0 ( 3058.9)	0.0 ( 2867.7)	0.0 ( 879.4)	0.0 ( 172.1)	0.0 ( 124.3)	0.0 ( 726.5)	0.0 ( 47.8)	0.0 ( 372.8)	0.0 ( 18.2)	0.0 ( 210.3)
35	0.0 ( 18560.0)	0.0 ( 17998.0)	0.0 ( 5511.9)	0.0 ( 899.9)	0.0 ( 4443.2)	0.0 ( 303.7)	0.0 ( 2531.0)	0.0 ( 146.2)	0.0 ( 1293.6)	
30	0.2 ( 73.5)	0.2 ( 60.7)	0.1 ( 41.6)	0.0 ( 13.1)	0.1 ( 19.5)	0.0 ( 14.1)	0.0 ( 2.0)	0.1 ( 31.3)	0.0 ( 3.5)	0.0 ( 3.5)
25	2.6 ( 19.9)	2.0 ( 15.3)	1.6 ( 12.2)	0.4 ( 3.2)	1.2 ( 9.2)	0.3 ( 2.4)	0.1 ( 0.5)	0.9 ( 6.9)	0.1 ( 0.6)	0.1 ( 0.5)
20	3.3 ( 5.5)	2.4 ( 4.0)	2.2 ( 3.7)	0.6 ( 1.0)	2.1 ( 3.5)	0.1 ( 0.1)	0.1 ( 0.1)	0.3 ( 0.5)	0.1 ( 0.2)	0.0 ( 0.1)
15	6.2 ( 7.3)	5.1 ( 6.0)	3.6 ( 4.3)	1.0 ( 1.2)	3.4 ( 4.0)	0.4 ( 0.5)	0.0 ( 0.0)	0.0 ( 0.0)	0.5 ( 0.6)	0.0 ( 0.0)
10	6.2 ( 7.3)	4.9 ( 5.8)	3.7 ( 4.4)	1.1 ( 1.3)	3.5 ( 4.1)	0.4 ( 0.5)	0.0 ( 0.0)	0.1 ( 0.1)	0.5 ( 0.6)	0.0 ( 0.1)

**Table A5.** Error estimates for a polar summer profile during the RR period. Errors are given in pptv (relative errors in %).

Altitude	total error	noise	total parameter	Gain	LOS	$\text{HNO}_4$	Shift	ILS	Temperature	$\text{ClONO}_2$
40	0.0 ( 336.8)	0.0 ( 307.1)	0.0 ( 158.5)	0.0 ( 96.1)	0.0 ( 56.5)	0.0 ( 73.3)	0.0 ( 2.2)	0.0 ( 70.3)	0.0 ( 2.7)	0.0 ( 12.9)
35	0.0 ( 333.4)	0.0 ( 296.4)	0.0 ( 148.2)	0.0 ( 92.6)	0.0 ( 55.6)	0.0 ( 72.2)	0.0 ( 2.0)	0.0 ( 67.6)	0.0 ( 2.7)	0.0 ( 13.0)
30	0.2 ( 299.3)	0.2 ( 273.3)	0.1 ( 123.6)	0.1 ( 80.7)	0.0 ( 52.1)	0.1 ( 69.0)	0.0 ( 0.4)	0.0 ( 27.3)	0.0 ( 3.1)	0.0 ( 7.5)
25	2.2 ( 72.1)	2.1 ( 68.9)	0.6 ( 19.3)	0.3 ( 10.2)	0.1 ( 2.9)	0.5 ( 15.7)	0.0 ( 0.6)	0.0 ( 1.0)	0.0 ( 0.5)	0.1 ( 1.9)
20	3.0 ( 16.2)	2.2 ( 11.9)	2.0 ( 10.8)	0.0 ( 0.1)	2.0 ( 10.8)	0.1 ( 0.4)	0.1 ( 0.5)	0.4 ( 2.3)	0.0 ( 0.2)	0.0 ( 0.1)
15	2.8 ( 3.9)	2.2 ( 3.1)	1.8 ( 2.5)	0.2 ( 0.3)	1.6 ( 2.3)	0.1 ( 0.2)	0.0 ( 0.0)	0.8 ( 1.2)	0.0 ( 0.1)	0.0 ( 0.0)
10	3.0 ( 3.6)	1.8 ( 2.2)	2.5 ( 3.0)	0.2 ( 0.3)	2.2 ( 2.6)	0.0 ( 0.1)	0.1 ( 0.2)	1.0 ( 1.2)	0.1 ( 0.1)	0.0 ( 0.0)

**Table A6.** Error estimates for a polar winter profile during the RR period. Errors are given in pptv (relative errors in %).

Altitude	total error	noise	total parameter	Gain	LOS	$\text{HNO}_4$	Shift	ILS	Temperature	$\text{ClONO}_2$
40	0.0 ( 632.5)	0.0 ( 367.3)	0.0 ( 510.1)	0.0 ( 204.0)	0.0 ( 448.9)	0.0 ( 67.3)	0.0 ( 9.8)	0.0 ( 24.5)	0.0 ( 61.2)	0.0 ( 36.7)
35	0.0 ( 608.6)	0.0 ( 342.4)	0.0 ( 494.5)	0.0 ( 190.2)	0.0 ( 437.4)	0.0 ( 66.6)	0.0 ( 9.5)	0.0 ( 22.8)	0.0 ( 60.9)	0.0 ( 36.1)
30	0.2 ( 369.8)	0.1 ( 228.9)	0.2 ( 281.8)	0.1 ( 112.7)	0.1 ( 264.1)	0.0 ( 42.3)	0.0 ( 6.0)	0.0 ( 2.5)	0.0 ( 33.5)	0.0 ( 22.9)
25	2.9 ( 308.3)	2.2 ( 233.9)	1.8 ( 191.3)	0.7 ( 76.5)	1.6 ( 170.1)	0.4 ( 41.5)	0.1 ( 6.1)	0.2 ( 26.6)	0.2 ( 20.2)	0.2 ( 23.4)
20	2.9 ( 46.0)	2.7 ( 42.8)	1.1 ( 17.4)	0.1 ( 1.4)	1.0 ( 15.9)	0.2 ( 2.5)	0.1 ( 1.2)	0.3 ( 4.6)	0.1 ( 0.9)	0.1 ( 1.3)
15	3.4 ( 5.1)	2.3 ( 3.4)	2.5 ( 3.7)	0.3 ( 0.5)	2.4 ( 3.6)	0.1 ( 0.2)	0.0 ( 0.1)	0.5 ( 0.7)	0.1 ( 0.1)	0.0 ( 0.0)
10	2.2 ( 2.6)	1.5 ( 1.8)	1.6 ( 1.9)	0.0 ( 0.0)	1.4 ( 1.7)	0.1 ( 0.1)	0.0 ( 0.0)	0.7 ( 0.9)	0.2 ( 0.2)	0.0 ( 0.0)

## References

- Allen, N. D. C., Bernath, P. F., Boone, C. D., Chipperfield, M. P., Fu, D., Manney, G. L., Oram, D. E., Toon, G. C., and Weisenstein, D. K.: Global carbon tetrachloride distributions obtained from the Atmospheric Chemistry Experiment (ACE), *Atmospheric Chemistry and Physics*, 9, 7449–7459, doi:10.5194/acp-9-7449-2009, <http://www.atmos-chem-phys.net/9/7449/2009/>, 2009.
- Chirkov, M., Stiller, G. P., Laeng, A., Kellmann, S., von Clar-705  
mann, T., Boone, C., Elkins, J. W., Engel, A., Glatthor, N., Grabowski, U., Harth, C. M., Kiefer, M., Kolonjari, F., Krummel, P. B., Linden, A., Lunder, C. R., Miller, B. R., Montzka, S. A., Mühle, J., O'Doherty, S., Orphal, J., Prinn, R. G., Toon, G., Vollmer, M. K., Walker, K. A., Weiss, R. F., Wiegele, 710  
A., and Young, D.: Global HCFC-22 measurements with MIPAS: retrieval, validation, global distribution and its evolution over 2005–2012, *Atmos. Chem. Phys.*, 16, 3345–3368, doi:10.5194/acp-16-3345-2016, 2016.
- Eckert, E., von Clarmann, T., Kiefer, M., Stiller, G. P., Lossow, 715  
S., Glatthor, N., Degenstein, D. A., Froidevaux, L., Godin-Beckmann, S., Leblanc, T., McDermid, S., Pastel, M., Steinbrecht, W., Swart, D. P. J., Walker, K. A., and Bernath, P. F.: Drift-corrected trends and periodic variations in MIPAS 720  
IMK/IAA ozone measurements, *Atmos. Chem. Phys.*, 14, 2571–2589, doi:10.5194/acp-14-2571-2014, 2014.
- Eckert, E., Laeng, A., Lossow, S., Kellmann, S., Stiller, G., von Clar-725  
mann, T., Glatthor, N., Höpfner, M., Kiefer, M., Oelhaf, H., Orphal, J., Funke, B., Grabowski, U., Haenel, F., Linden, A., Wetzel, G., Woiwode, W., Bernath, P. F., Boone, C., Dut-730  
ton, G. S., Elkins, J. W., Engel, A., Gille, J. C., Kolonjari, F., Sugita, T., Toon, G. C., and Walker, K. A.: MIPAS IMK/IAA CFC-11 ( $\text{CCl}_3\text{F}$ ) and CFC-12 ( $\text{CCl}_2\text{F}_2$ ) measurements: accuracy, precision and long-term stability, *Atmospheric Measurement Techniques*, 9, 3355–3389, doi:10.5194/amt-9-3355-2016, 735  
<http://www.atmos-meas-tech.net/9/3355/2016/>, 2016.
- Fischer, H. and Oelhaf, H.: Remote sensing of vertical profiles of atmospheric trace constituents with MIPAS limb-emission spectrometers, *Appl. Opt.*, 35, 2787–2796, 1996.
- Fischer, H., Birk, M., Blom, C., Carli, B., Carlotti, M., von Clar-740  
mann, T., Delbouille, L., Dudhia, A., Ehhalt, D., Endemann, M., Flaud, J. M., Gessner, R., Kleinert, A., Koopman, R., Langen, J., López-Puertas, M., Mosner, P., Nett, H., Oelhaf, H., Perron, G., Remedios, J., Ridolfi, M., Stiller, G., and Zander, R.: MIPAS: an instrument for atmospheric and climate research, *Atmospheric Chemistry & Physics*, 8, 2151–2188, 2008.
- Friedl-Vallon, F., Maucher, G., Kleinert, A., Lengel, A., Keim, C., Oelhaf, H., Fischer, H., Seefeldner, M., and Trieschmann, O.: Design and characterisation of the balloon-borne Michelson Interferometer for Passive Atmospheric Sounding (MIPAS-B2), 745  
*Appl. Opt.*, 43, 3335–3355, 2004.
- Funke, B., Stiller, G. P., von Clarmann, T., Echle, G., and Fischer, H.:  $\text{CO}_2$  Line Mixing in MIPAS Limb Emission Spectra and its Influence on Retrieval of Atmospheric Parameters, *J. Quant. Spectrosc. Radiat. Transfer*, 59, 215–230, 1998.
- Glatthor, N., von Clarmann, T., Fischer, H., Funke, B., Grabowski, U., Höpfner, M., Kellmann, S., Linden, A., Milz, M., Steck, T., and Stiller, G. P.: Global peroxyacetyl nitrate (PAN) retrieval in 750  
the upper troposphere from limb emission spectra of the Michel-son Interferometer for Passive Atmospheric Sounding MIPAS, *Atmos. Chem. Phys.*, 7, 2775–2787, 2007.
- Harrison, J. J., Boone, C. D., and Bernath, P. F.: New and improved infra-red absorption cross sections and ACE-FTS retrievals of carbon tetrachloride ( $\text{CCl}_4$ ), *Journal of Quantitative Spectroscopy and Radiative Transfer*, 186, 139 – 149, doi:<http://dx.doi.org/10.1016/j.jqsrt.2016.04.025>, <http://www.sciencedirect.com/science/article/pii/S002240731630108X>, satellite Remote Sensing and Spectroscopy: Joint ACE-Odin Meeting, October 2015, 2017.
- Hubert, D., Keppens, A., Granville, J., and Lambert, J.-C.: Multi-TASTE Phase F Validation Report / Comparison of MIPAS ML2PP 7.03 products to sonde and lidar, TN-BIRA-IASB-MultiTASTE-Phase-F-MIPAS-ML2PP7-Iss1-RevB, BIRA-IASB, Brussels, Belgium, 2016.
- IPCC: Contribution of Working Group I to the Fifth Assessment Report of the Intergovernmental Panel on Climate Change, in: *Climate Change 2013: The Physical Science Basis*, edited by Stocker, T., Qin, D., Plattner, G.-K., Tignor, M., Allen, S., Boschung, J., Nauels, A., Xia, Y., Bex, V., and Midgley, P., Cambridge University Press, Cambridge, UK and New York, NY, USA, 33–115 pp, 2013.
- Liang, Q., Newman, P., and S., R.: SPARC Report on the Mystery of Carbon tetrachloride, SPARC Report No. 7, WCRP-13, SPARC, 2016.
- Manney, G. L., Santee, M. L., Rex, M., Livesey, N. J., Pitts, M. C., Veefkind, P., Nash, E. R., Wohltmann, I., Lehmann, R., Froidevaux, L., Poole, L. R., Schoeberl, M. R., Haffner, D. P., Davies, J., Dorokhov, V., Johnson, H. G. B., Kivi, R., Kyrö, E., Larsen, N., Levelt, P. F., Makshtas, A., McElroy, C. T., Nakajima, H., Parrondo, M. C., Tarasick, D. W., von der Gathen, P., Walker, K. A., and Zinoviev, N. S.: Unprecedented Arctic ozone loss in 2011, *Nature*, 478, 469–475, doi:10.1038/nature10556, 2011.
- Naujokat, B. and Grunow, K.: The stratospheric arctic winter 2002/03: balloon flight planning by trajectory calculations, in: *European Rocket and Balloon Programmes and Related Research*, edited by Warmbein, B., vol. 530 of *ESA Special Publication*, pp. 421–425, 2003.
- Nemtchinov, V. and Varanasi, P.: Thermal infrared absorption cross-sections of  $\{\text{CCl}_4\}$  needed for atmospheric remote sensing, *Journal of Quantitative Spectroscopy and Radiative Transfer*, 82, 473 – 481, doi:[http://dx.doi.org/10.1016/S0022-4073\(03\)00171-7](http://dx.doi.org/10.1016/S0022-4073(03)00171-7), <http://www.sciencedirect.com/science/article/pii/S0022407303001717>, the {HITRAN} Molecular Spectroscopic Database: Edition of 2000 Including Updates of 2001., 2003.
- Norton, H. and Beer, R.: New apodizing functions for Fourier spectrometry, *J. Opt. Soc. Am.*, 66, 259–264, (Errata *J. Opt. Soc. Am.*, 67, 419, 1977), 1976.
- Rodgers, C. D.: *Inverse Methods for Atmospheric Sounding: Theory and Practice*, vol. 2 of *Series on Atmospheric, Oceanic and Planetary Physics*, F. W. Taylor, ed., World Scientific, Singapore, New Jersey, London, Hong Kong, 2000.
- Rosenkranz, P. W.: Shape of the 5 mm Oxygen Band in the Atmosphere, *IEEE Transactions on Antennas and Propagation*, AP-23, 498–506, 1975.
- Rothman, L. S., Barbe, A., Benner, D. C., Brown, L. R., Camy-Peyret, C., Carleer, M. R., Chance, K., Clerbaux, C., Dana, V., Devi, V. M., Fayt, A., Flaud, J.-M., Gamche, R. R., Goldman, A., Jacquemart, D., Jucks, K. W., Lafferty, W. J., Mandin, J.-Y., 760  
A.,

- 765 Massie, S. T., Nemchinov, V., Newham, D. A., Perrin, A., Rinsland, C. P., Schroeder, J., Smith, K. M., Smith, M. A. H., Tang, K., Toth, R. A., Vander Auwera, J., Varanasi, P., and Yoshino, K.: The HITRAN molecular spectroscopic database: edition of 2000 including updates through 2001, *J. Quant. Spectrosc. Radiat. Transfer*, 82, 5–44, doi:10.1016/S0022-4073(03)00146-8, 2003.
- 770 Schmidt, U., Kulessa, G., Klein, E., Roeth, E.-P., and Fabian, P.: 825 intercomparison of balloon-borne cryogenic whole air samplers during the MAP/GLOBUS 1983 campaign, *Planetary and Space Science*, 35, 647–656, doi:10.1016/0032-0633(87)90131-0, 1987.
- 775 Sinnhuber, B.-M., Stiller, G., Ruhnke, R., von Clarmann, T., Kell- 830 mann, S., and Aschmann, J.: Arctic winter 2010/2011 at the brink of an ozone hole, *Geophys. Res. Lett.*, 38, L24814, doi:10.1029/2011GL049784, 2011.
- 780 SPARC: SPARC Report on the Mystery of Carbon tetrachloride, Liang, Q. and Newman, P.A. and Reimann, S. (Eds.), 2016.
- 785 Stiller, G. P., ed.: The Karlsruhe Optimized and Precise Radiative Transfer Algorithm (KOPRA), vol. FZKA 6487 of *Wissenschaftliche Berichte*, Forschungszentrum Karlsruhe, Karlsruhe, 2000.
- 790 Valeri, M., Barbara, F., Boone, C., Ceccherini, S., Gai, M., Maucher, G., Raspollini, P., Ridolfi, M., Sgheri, L., Wetzel, G., and Zoppetti, N.:  $\text{CCl}_4$  distribution derived from MIPAS ESA V7 data: validation, trend and lifetime estimation, *Atmospheric Chemistry and Physics Discussions*, 2017, 1–31, doi:10.5194/acp-2016-1163, <http://www.atmos-chem-phys-discuss.net/acp-2016-1163/>, 2017.
- 795 Vogel, B., Günther, G., Müller, R., Groß, J.-U., Afchine, A., Bozem, H., Hoor, P., Krämer, M., Müller, S., Riese, M., Rolf, C., Spelten, N., Stiller, G. P., UngermaNN, J., and Zahn, A.: Long-range transport pathways of tropospheric source gases originating in Asia into the northern lower stratosphere during the Asian monsoon season 2012, *Atmospheric Chemistry and Physics*, 16, 15 301–15 325, doi:10.5194/acp-16-15301-2016, <http://www.atmos-chem-phys.net/16/15301/2016/>, 2016.
- 800 von Clarmann, T., Oelhaf, H., and Fischer, H.: Retrieval of atmospheric  $\text{O}_3$ ,  $\text{HNO}_3$ , CFC-11, and CFC-12 profiles from MIPAS-B–89 limb emission spectra, *Appl. Opt.*, 32, 6808–6817, 1993.
- 805 von Clarmann, T., Linden, A., Oelhaf, H., Fischer, H., Friedl-Vallon, F., Piesch, C., Seefeldner, M., Völker, W., Bauer, R., Engel, A., and Schmidt, U.: Determination of the stratospheric organic chlorine budget in the spring arctic vortex from MIPAS B limb emission spectra and air sampling experiments, *J. Geophys. Res.*, 100, 13,979–13,997, 1995.
- 810 von Clarmann, T., Glatthor, N., Grabowski, U., Höpfner, M., Kellmann, S., Kiefer, M., Linden, A., Mengistu Tsidu, G., Milz, M., Steck, T., Stiller, G. P., Wang, D. Y., Fischer, H., Funke, B., Gil-López, S., and López-Puertas, M.: Retrieval of temperature and tangent altitude pointing from limb emission spectra recorded from space by the Michelson Interferometer for Passive Atmospheric Sounding (MIPAS), *J. Geophys. Res.*, 108, 4736, doi:10.1029/2003JD003602, 2003.
- 815 von Clarmann, T., Höpfner, M., Kellmann, S., Linden, A., Chauhan, S., Funke, B., Grabowski, U., Glatthor, N., Kiefer, M., Schieferdecker, T., Stiller, G. P., and Versick, S.: Retrieval of temperature,  $\text{H}_2\text{O}$ ,  $\text{O}_3$ ,  $\text{HNO}_3$ ,  $\text{CH}_4$ ,  $\text{N}_2\text{O}$ ,  $\text{ClONO}_2$  and  $\text{ClO}$  from MIPAS reduced resolution nominal mode limb emission measurements, *Atmos. Meas. Techn.*, 2, 159–175, 2009.
- 820 von Clarmann, T., Stiller, G., Grabowski, U., Eckert, E., and Orphal, J.: Technical Note: Trend estimation from irregularly sampled, correlated data, *Atmos. Chem. Phys.*, 10, 6737–6747, 2010.
- 825 World Meteorological Organization (WMO): Scientific Assessment of Ozone Depletion: 2014, Global Ozone Research and Monitoring Project – Report No. 55, 416 pp., Geneva, Switzerland, 2014.
- Zander, R., Mahieu, E., Gunson, M. R., Abrams, M. C., Chang, A. Y., Abbas, M. M., Aelig, C., Engel, A., Goldman, A., Irion, F. W., Kämpfer, N., Michelson, H. A., Newchurch, M. J., Rinsland, C. P., Salawitch, R. J., Stiller, G. P., and Toon, G. C.: The 1994 northern midlatitude budget of stratospheric chlorine derived from ATMOS/ATLAS-3 observations, *Geophys. Res. Lett.*, 23, 2357–2360, 1996.

# MIPAS IMK/IAA Carbon Tetrachloride (CCl<sub>4</sub>) Retrieval and first Comparison with other Instruments

Ellen E. Eckert<sup>1</sup>, Thomas T. von Clarmann<sup>1</sup>, Alexandra A. Laeng<sup>1</sup>, Gabriele G. P. Stiller<sup>1</sup>, Bernd B. Funke<sup>1</sup>, Norbert N. Glatthor<sup>1</sup>, Udo U. Grabowski<sup>1</sup>, Sylvia S. Kellmann<sup>1</sup>, Michael M. Kiefer<sup>1</sup>, Andrea A. Linden<sup>1</sup>, Gerald A. Babenhausenheide<sup>1</sup>, G. Wetzel<sup>1</sup>, Christopher C. Boone<sup>2</sup>, Andreas A. Engel<sup>3</sup>, Jeremy J. J. Harrison<sup>4,5,6</sup>, Patrick P. E. Sheese<sup>7</sup>, Kaley K. A. Walker<sup>2,7</sup>, and Peter P. F. Bernath<sup>2,8</sup>

<sup>1</sup>Karlsruhe Institute of Technology, Institute of Meteorology and Climate Research, Karlsruhe, Germany

<sup>2</sup>Department of Chemistry, University of Waterloo, Waterloo, Ontario, Canada

<sup>3</sup>Institut für Atmosphäre und Umwelt, J. W. Goethe Universität, Frankfurt, Germany

<sup>4</sup>Department of Physics, University of Leicester, University Road, Leicester LE1 7RH, United Kingdom

<sup>5</sup>National Centre for Earth Observation, University of Leicester, University Road, Leicester LE1 7RH, United Kingdom

<sup>6</sup>Leicester Institute for Space and Earth Observation, University of Leicester, University Road, Leicester LE1 7RH, United Kingdom

<sup>7</sup>Department of Physics, University of Toronto, Toronto, Ontario, Canada

<sup>8</sup>Department of Chemistry and Biochemistry, Old Dominion University, Norfolk, VA 23529-0126, USA

Correspondence to: E. Eckert (ellen.eckert@kit.edu)

**Abstract.** MIPAS thermal limb emission measurements were used to derive vertically resolved profiles of carbon tetrachloride (CCl<sub>4</sub>). Level-1b data versions MIPAS/5.02 to MIPAS/5.06 were converted into volume mixing ratio profiles using the level-2 processor developed at Karlsruhe Institute of Technology (KIT) Institute of Meteorology and Climate Research (IMK) and Consejo Superior de Investigaciones Científicas (CSIC), Instituto de Astrofísica de Andalucía (IAA). Consideration of peroxyacetyl nitrate (PAN) as interfering species, which is jointly retrieved, and CO<sub>2</sub> line mixing ~~was found to be is~~ crucial for reliable retrievals. Parts of the CO<sub>2</sub> Q-branch region that overlap with the CCl<sub>4</sub> signature were omitted, since large residuals were still found even though line mixing was considered in the forward model. However, the omitted spectral region could be narrowed ~~considerably noticeably~~ when line mixing was accounted for. A new CCl<sub>4</sub> spectroscopic dataset leads to slightly smaller CCl<sub>4</sub> volume mixing ratios. In general, latitude-altitude cross-section show the expected CCl<sub>4</sub> features with highest values of around 90 pptv at altitudes at and below the tropical tropopause and values decreasing with altitude and latitude due to stratospheric decomposition. Other patterns, such as subsidence in the polar vortex during winter and early spring, are also visible in the distributions. The decline in CCl<sub>4</sub> abundance during the MIPAS Envisat mea-

surement period (July 2002 to April 2012) is clearly reflected in the ~~retrieved distributions~~ altitude-latitude cross-section of trends estimated from the entire retrieved data set.

## 1 Introduction

Carbon tetrachloride (CCl<sub>4</sub>) is an anthropogenically produced halogen yielding trace gas and partly responsible for stratospheric ozone depletion. It is also a potent greenhouse gas with a 100-year global warming potential of 1730 (IPCC, 2013; World Meteorological Organization (WMO), 2014). CCl<sub>4</sub> was commonly used in fire extinguishers, as a precursor to refrigerants and in dry cleaning prior to ~~1987~~ 1990, when it was restricted within the framework of the London Amendment to the Montreal Protocol. Its abundances in the atmosphere increased steadily from the first part of the 20th century. Emissions declined significantly after ~~1987~~ 1990, as well as the amount of CCl<sub>4</sub> in the atmosphere with a few years delay~~~~~. 2007-2012 bottom-up emissions of 1 to 4 kilotonnes/year were assessed by combining country-by-country reports to the United Nations Environmental Programme (UNEP) (Liang et al., 2016). This bottom-up estimate differs considerably from the 57(±17) kilotonnes/year top-down emissions which were ~~reported evaluated~~ in 2014

(World Meteorological Organization (WMO), 2014) using atmospheric measurements and lifetime estimates. Even when possible  $\text{CCl}_4$  precursors and unreported inadvertent emissions are accounted for, the gap between reported bottom-up and estimated top-down  $\text{CCl}_4$  emissions cannot be closed, as bottom-up emissions still only add up to 25 kilotonnes/year (SPARC, 2016). Besides a sink in the atmosphere,  $\text{CCl}_4$  is decomposed in the ocean and the soil with different lifetimes for each sink. Reassessment of the different lifetime estimates, which are essential for an adequate top-down assessment of emissions, leads to lower emissions of  $\sim 40(\pm 15)$  kilotonnes/year. While the gap between bottom-up and top-down emissions is considerably now smaller after reassessments, the discrepancy is still not solved entirely. Measurements Previous measurements of stratospheric  $\text{CCl}_4$ , besides those of MIPAS Envisat, have also been performed by the Atmospheric Chemistry Experiment Fourier Transform Spectrometer (ACE-FTS), a Cryosampler instrument employed at Frankfurt University and the balloon borne version of MIPAS (MIPAS-B2). The first version of the balloon borne MIPAS instrument (MIPAS-B) and ATMOS (Atmospheric Trace Molecule Spectroscopy) also measured  $\text{CCl}_4$ , but not during the MIPAS Envisat measurement period (Zander et al., 1987; von Clarmann et al., 1995) (Zander et al., 1996; von Clarmann et al., 1995). Additional measurements, especially vertically well resolved ones with global coverage such as satellite measurements from MIPAS, can help to improve the understanding of the atmospheric  $\text{CCl}_4$  budget and stratospheric lifetime estimate. Furthermore, as a tracer with relatively short stratospheric lifetimes,  $\text{CCl}_4$  measurements can improve the understanding of changes in Brewer-Dobson circulation by further constraining the lower boundary, e.g. processes around the tropopause.

In this study, we present the retrieval of  $\text{CCl}_4$  distributions from MIPAS limb emission spectra. First, we characterize the MIPAS instrument (Sec. 2), followed by a detailed description of the retrieval and the specific issues that had to be dealt with to derive  $\text{CCl}_4$  concentration (Sec. 3). We then compare the results of the MIPAS Envisat  $\text{CCl}_4$  retrieval with those of ACE-FTS and those of the second balloon-borne MIPAS instrument (MIPAS-B2) and those of Cryosampler measurements (Sec. 5) and summarize the results in the conclusions (Sec. 6).

## 2 MIPAS

The Michelson Interferometer for Passive Atmospheric Sounding (MIPAS) was one of the instruments aboard the European Environmental Satellite (Envisat). It was launched into a sun-synchronous orbit at an altitude of approximately 800 km on 1 March 2002. On 8 April 2012, all communication with the satellite was lost ending an observation period of more than 10 years. Envisat orbited the earth 14.4 times

a day crossing the equator at 10:00 and 22:00 local time. MIPAS measured infrared emissions between  $685\text{ cm}^{-1}$  and  $2410\text{ cm}^{-1}$  ( $14.6$  and  $4.15\mu\text{m}$ ) (Fischer et al., 2008), which allows for day and night time measurements with global coverage. The initial spectral resolution of the instrument was  $0.025\text{ cm}^{-1}$  ( $0.0483\text{ cm}^{-1}$  after a "Norton-Beer strong" apodization (Norton and Beer, 1976)). An instrument failure in March 2004 led to an observation gap until January 2005 when the instrument was successfully restarted. The first period (June 2002 to March 2004) is referred to as full spectral resolution (FR) period, while the period from January 2005 to April 2012 is referred to as reduced spectral resolution (RR) period. Due to a problem with one of the interferometer slides, MIPAS could only be operated with a spectral resolution of  $0.0625\text{ cm}^{-1}$  ( $0.121\text{ cm}^{-1}$  apodized) from January 2005 on. In this study, only measurements from the instrument's "nominal operation mode" are used. In this mode, the number of tangent altitudes increased from 17 during the FR period to 27 during the RR period. The vertical coverage ranges from 6 km to around 68 km during the FR period and up to around 70 km during the RR period, respectively. MIPAS initially took around 1000 measurements per day. In 2005, operation was resumed at reduced duty cycle. By the end of 2007, MIPAS was back at full duty cycle which amounts to approximately 1300 RR measurements per day. The horizontal sampling changed from 510 km during the FR period to 410 km during the RR period.

The temperature and various atmospheric trace gases are retrieved from level-1b data using a retrieval processor developed at the Institute of Meteorology and Climate Research at the Karlsruhe Institute of Technology (KIT) in close cooperation with the Instituto de Astrofísica de Andalucía (CSIC) in Granada, Spain. Results shown in this publication are based on a selected set of retrievals from September 2003 (FR period), July 2008, January 2010 and March and April 2011 (RR period) cover both the FR and the RR period.

## 3 Retrieval

The MIPAS Envisat retrieval is based on a non-linear least squares approach and employs a first-order Tikhonov-type regularization (von Clarmann et al., 2003, 2009). The radiative transfer is modelled using the Karlsruhe Optimized and Precise Radiative Transfer Algorithm (KOPRA) model (Stiller, 2000).

The spectral regions used for the retrieval of  $\text{CCl}_4$  are  $772.0 - 791.0\text{ cm}^{-1}$  and  $792.0 - 805.0\text{ cm}^{-1}$ . The gap from  $791.0$  to  $792.0\text{ cm}^{-1}$  is necessary, since even when accounting for line mixing, strong effects from the  $\text{CO}_2$  Q-branch still occurred in the residuals (Fig. ??, right plot). Several results from previous steps in the retrieval chain were used to derive  $\text{CCl}_4$  (Table 1) including the spectral shift ( $z_{\text{tangent}}$ ), the temperature ( $T$ ), the horizontal temperature gradient ( $T_{\text{grad}}$ ) and mixing ratio profiles of  $\text{HNO}_3$ ,  $\text{ClO}$ ,  $\text{CFC-11}$ ,  $\text{C}_2\text{H}_6$ ,

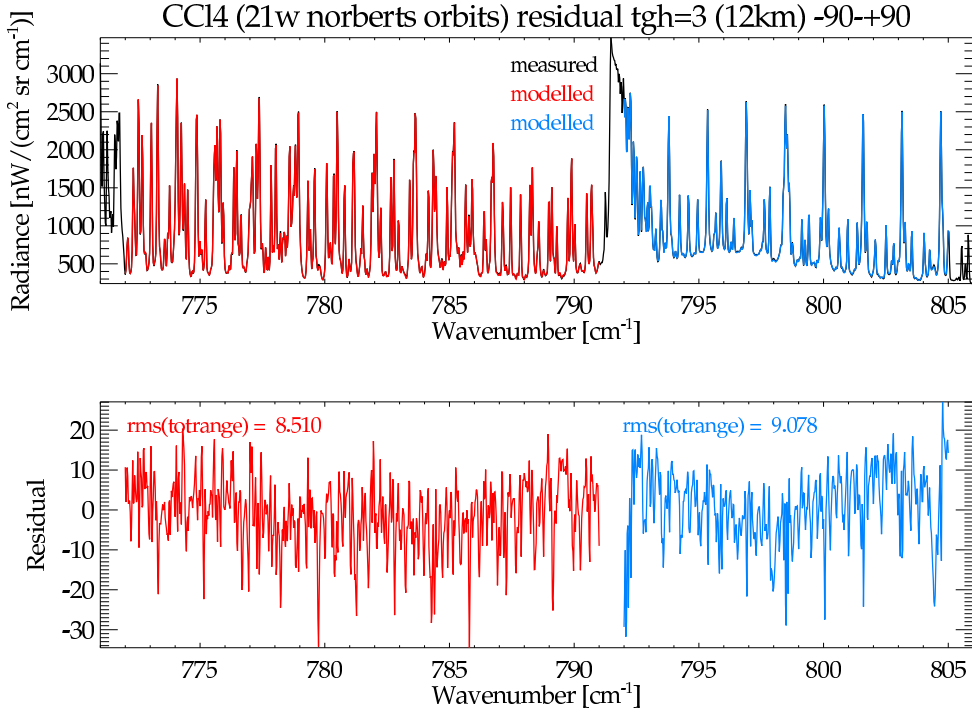


**Figure 1.** Exemplary spectra of MIPAS  $\text{CCl}_4$  at 12 km and 11.5 km, respectively. **Left:** during the FR period (September 2003). **Right:** RR period (July 2008). Top panel: spectra; bottom panel: residuals.

HCN,  $\text{ClONO}_2$  and  $\text{HNO}_4$ .

In addition, several species were found to improve the retrieval whenever their mixing ratio profiles were fitted alongside  $\text{CCl}_4$ . These are peroxyacetyl nitrate (PAN),  $\text{CH}_3\text{CCl}_3$ , HCFC-22,  $\text{O}_3$ ,  $\text{H}_2\text{O}$ ,  $\text{C}_2\text{H}_2$  and  $\text{COF}_2$ . Although for most of these species results from preceding retrieval steps are available, fitting their concentrations jointly with that of  $\text{CCl}_4$  reduces the fit residuals significantly. This is attributed to spectroscopic inconsistencies of the interferers' spectroscopic data between the spectral region where these were retrieved and the spectral region where  $\text{CCl}_4$  is analyzed. Also fitted were a background continuum accounting for spectral contributions from aerosols and a radiance offset which is constant for all tangent altitudes (Table 1).

These specifications retrieval settings lead to spectral fits as displayed in Fig. 22 and Fig. 2, where an example for the FR period (left) and the RR period (right) are shown. The measured spectra are plotted in black (not discernible from the best fitting fit modelled in the fitting

window), while the red and the blue lines represent the modelled spectra of the regions from 772.0 - 791.0  $\text{cm}^{-1}$  and 792.0 - 805.0  $\text{cm}^{-1}$ , respectively. Some periodic residuals are visible in both the FR and the RR period. These result from less than perfectly fitted  $\text{CO}_2$ , but as will be shown in Sec. 5, are only of minor relevance for the accuracy of the retrieved  $\text{CCl}_4$ .

### 3.1 Information cross-talk with PAN

The signature of PAN is particularly prominent in the spectral region of  $\text{CCl}_4$  and can thus be retrieved during the same retrieval step. Actually, jointly fitting PAN improves is very important for the  $\text{CCl}_4$  retrieval. Since PAN was already retrieved from MIPAS spectra before (Glatthor et al., 2007), it is of obvious interest to investigate the PAN results from the  $\text{CCl}_4$ -PAN joint retrieval in comparison with those from the original PAN retrieval. In there  $\text{CCl}_4$  was fitted alongside PAN but the retrieval was not yet optimized for  $\text{CCl}_4$ . We find slightly higher volume mixing ratios of PAN

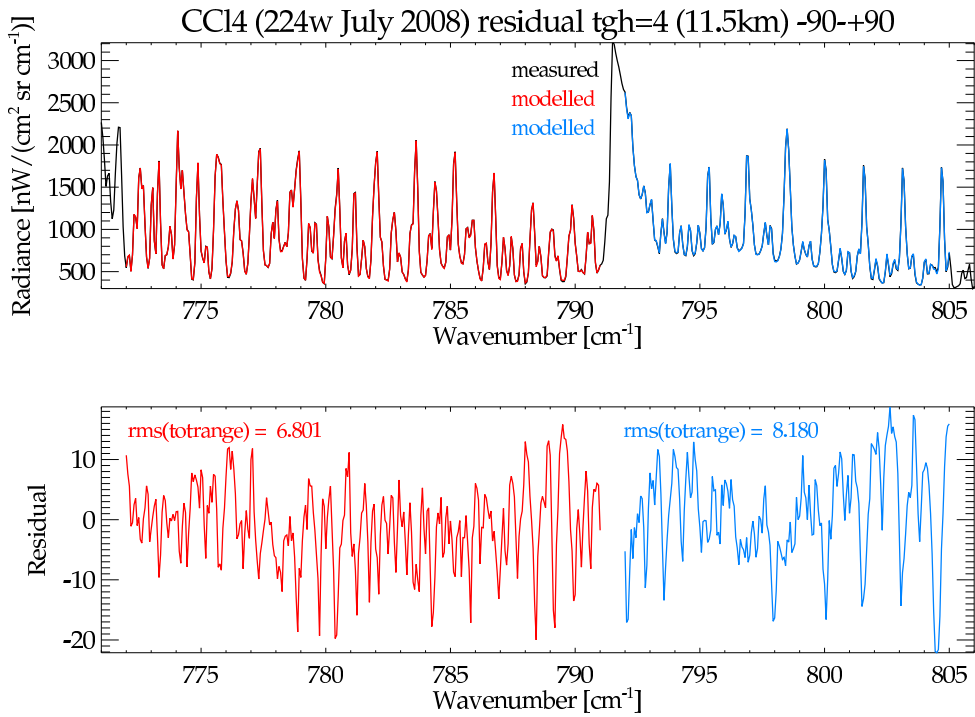


**Figure 2.** Exemplary spectra of MIPAS  $\text{CCl}_4$  at 11.5 km during the RR period (July 2008). Top panel: spectra; bottom panel: residuals.

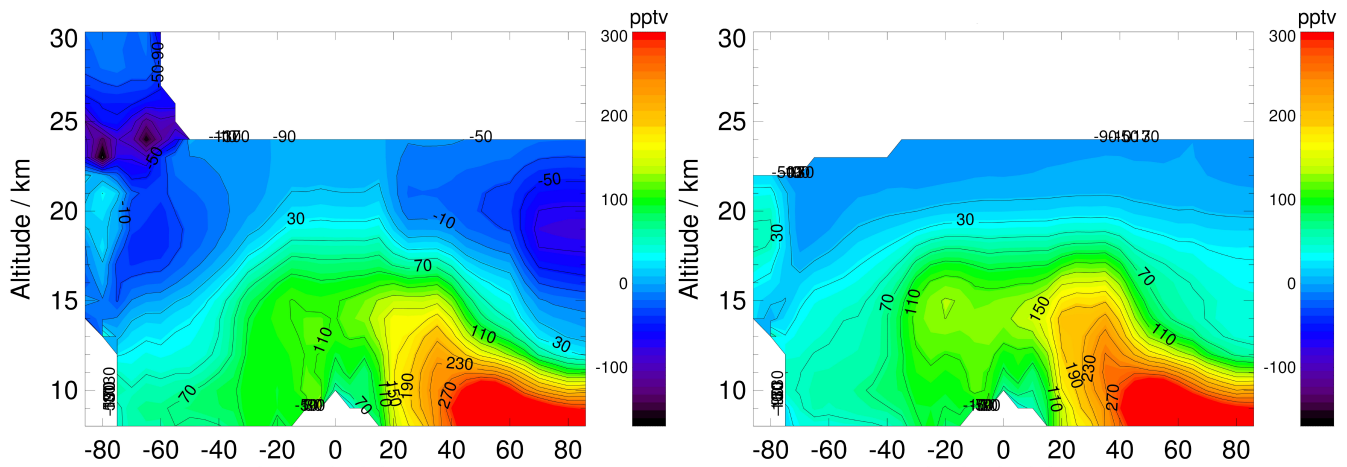


**Figure 3.** PAN altitude/latitude cross-sections (July 2008) from a separate retrieval using climatological the old  $\text{CCl}_4$  distributions (left) and resulting from a joint retrieval with  $\text{CCl}_4$  (right). **Black: measured spectrum, hardly discernible because overplotted by modelled spectra.**

**Table 1.** Retrieval details on the spectroscopic region, species imported from preceding retrieval steps and variables fitted jointly during the retrieval process. Brackets denote mixing ratios.

Spectral regions	Imported from preceding retrieval steps	Jointly fitted variables
772.0 - $\text{790.5}$ $\text{791.0}$ $\text{cm}^{-1}$	Shift( $z_{\text{tangent}}$ )	[PAN](z)
$\text{793.5}$ $\text{792.0}$ - 805.0 $\text{cm}^{-1}$	T(z)	[ $\text{CH}_3\text{CCl}_3$ ](z)
	$T_{\text{grad}}(z)$ [ $\text{HNO}_3$ ](z) [ $\text{ClO}$ ](z) [ $\text{CFC-11}$ ](z) [ $\text{C}_2\text{H}_6$ ](z) [ $\text{HCN}$ ](z) [ $\text{ClONO}_2$ ](z) [ $\text{HNO}_4$ ](z)	[HCFC-22](z) [ $\text{O}_3$ ](z) [ $\text{H}_2\text{O}$ ](z) [ $\text{C}_2\text{H}_2$ ](z) [ $\text{COF}_2$ ](z) Continuum(z) offset

throughout most of the altitude-latitude cross-section (Fig. 3). As a consequence, areas showing unphysical mixing ratios below zero ~~white areas in extratropical regions above  $\sim 15$  km in the original retrievals~~ (left panel of Fig. 3) ~~in the original retrievals~~ are now slightly positive or very close to zero. This suggests that ~~PAN results from the joint fits jointly fit PAN from the retrieval optimized for  $\text{CCl}_4$~~  might be more accurate than ~~the PAN retrieved using climatological the old  $\text{CCl}_4$  profiles~~ distributions.

### 3.2 Line mixing

Since the spectral region where  $\text{CCl}_4$  is retrievable contains a  $\text{CO}_2$  Q-branch, the retrieval is ~~setup set up~~ to account for line mixing (Funke et al., 1998). This was done by using the Rosenkranz approximation (Rosenkranz, 1975). Tests were also performed using the computationally more demanding direct diagonalisation, but this approach was not found to noticeably change the results of the retrieval. This is possibly the case because the microwindows were carefully selected to omit major spectral signatures of the  $\text{CO}_2$  Q-branch and because the effect of line mixing is generally smaller at stratospheric pressure levels. However, it was still necessary to omit parts of the  $\text{CO}_2$  Q-branch. Fig. ?? shows a spectrum ~~4 and Fig. 5 show spectra~~ where the full spectral region was fitted. ~~On the left~~ ~~In Fig. 4~~, line mixing was not considered and thus a large peak in the residual is visible close to  $791.0 \text{ cm}^{-1}$ . ~~On the right~~ ~~In Fig. 5~~, the Rosenkranz approximation was used to account for line mixing. Even though the residual is considerably smaller than without line mixing taken into account - as would be expected - peaks significantly larger than for the remainder of the window are

still visible between  $791.0$  and  $792.0 \text{ cm}^{-1}$ . Although inclusion of line mixing significantly reduces the residuals in the  $\text{CO}_2$  branch, the residuals are still unacceptably large there. With the Rosenkranz approximation, however, the spectral region excluded from the fit could be narrowed to  $791.0$  to  $792.0 \text{ cm}^{-1}$  ~~from  $790.5$  to  $792.5 \text{ cm}^{-1}$~~ .

### 3.3 New $\text{CCl}_4$ Spectroscopic Data

During the ongoing development of the MIPAS Envisat  $\text{CCl}_4$  retrieval, a new  $\text{CCl}_4$  spectroscopic dataset was published by Harrison et al. (2017). Fig. 6 shows the influence of these spectroscopic data on an altitude-latitude cross-section of  $\text{CCl}_4$  distributions of July 2008. The upper panel shows what ~~the~~ stratospheric  $\text{CCl}_4$  distribution distributions retrieved with the original spectroscopic dataset as presented in HITRAN 2000 (Nemtchinov and Varanasi, 2003) ~~looks~~ like. The lower panel shows the same cross-section, but using the new spectroscopic dataset by Harrison et al. (2017) for an otherwise identical retrieval setup. While the qualitative and morphological features of the distribution are very similar, lower volume mixing ratios of  $\text{CCl}_4$  result when the new spectroscopic ~~data are dataset is~~ used. Comparing these with reported values of ground based measurements as presented in SPARC (2016) indicates that the updated spectroscopic data ~~produces lead to~~ results which, in the tropopause region, agree better with tropospheric measurements. Tropospheric volume mixing ratios are reported to be at approximately 95 pptv which is very close to what MIPAS Envisat presents around the tropical tropopause and at mid-latitudes of the northern hemisphere when using the new spectroscopic dataset. In contrast, using HITRAN 2000 sometimes results in volume mixing ratios above 100 pptv in the same region. Thus, we consider the new spectroscopic dataset more adequate for the retrieval of  $\text{CCl}_4$ .

## 4 Results

### 4.1 Distributions

Fig. 7, the lower panel of Fig. 6 and Fig. 8 give an overview of the latitudinal and altitude distribution of  $\text{CCl}_4$  ~~of different time periods~~. All of the altitude-latitude cross-sections show the expected pattern of  $\text{CCl}_4$  with a rapid decrease with increasing altitude in the stratosphere, as the gas is photolyzed there. In addition, highest volume mixing ratios appear at the equator where  $\text{CCl}_4$ , along with many other trace gases, enters the stratosphere due to the upward transport associated with the Brewer-Dobson circulation. During January 2010, March 2011 and particularly April 2011, subsidence of higher stratospheric air results in reduced mixing ratios over the North pole. In Spring 2011, an unusually stable northern polar vortex resulted in severe ozone depletion and particularly strong subsidence (Manney et al., 2011; Sinnhuber et al., 2011) which is reflected by the observations

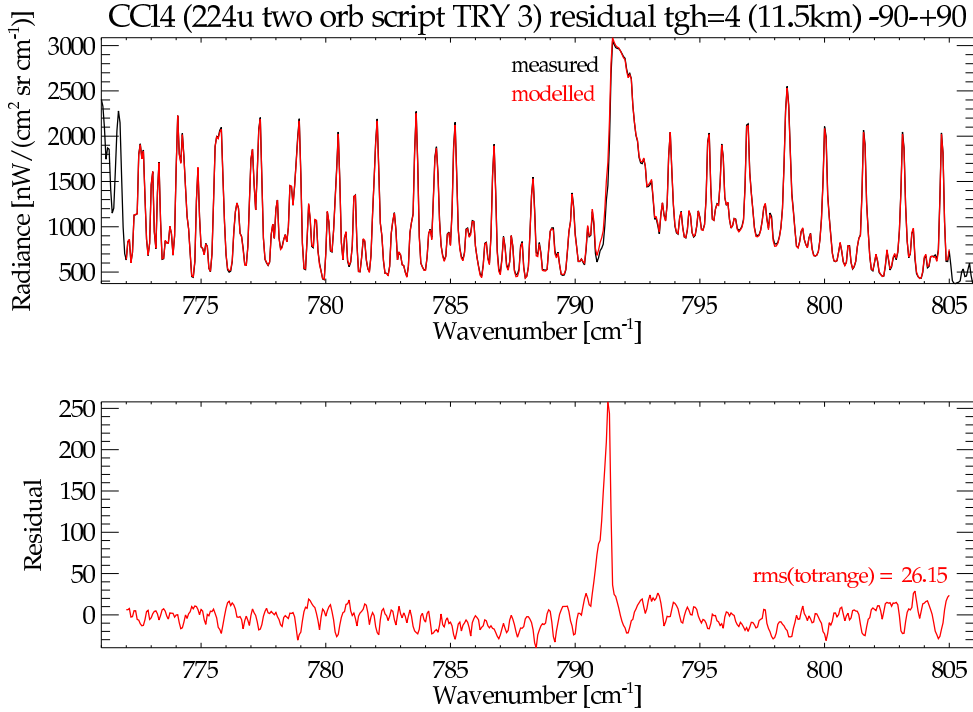


**Figure 4.** Impact of the  $\text{CO}_2$  Q-branch at 11.5 km altitude without considering line mixing (left) and with taking it into account (right). Top panels: spectra; bottom panels: residuals. Note the different scale of the residual axis. Black: measured spectrum, hardly discernible because overplotted by modelled spectra.

shown here. In general, MIPAS Envisat shows higher volume mixing ratios in the lower stratosphere during the FR period, which fits well with the overall decline in  $\text{CCl}_4$  abundance in the atmosphere due to its restriction under the Montreal Protocol. This impression is also supported by the lower panel in Fig. 6, which shows lower overall volume mixing ratios than MIPAS sees during the FR period, but which are still slightly higher than during 2010 and 2011. All cross-sections show a maximum in the  $\text{CCl}_4$  volume mixing ratios around the tropical tropopause connected with values of similar magnitude at lower altitudes of northern extratropical regions. This pattern was also seen in HCFC-22 (Chirkov et al., 2016) and could be linked to the Asian monsoon. Calculations with the Chemical Lagrangian Model of the Stratosphere (CLaMS) by Vogel et al. (2016) show that there indeed exists a mechanism which can produce local maxima in the upper troposphere in 2D distributions of source gases. So, the mon-

soon might offer an explanation for the patterns seen in  $\text{CCl}_4$  around these atmospheric regions as well.

#### 4.2 Altitude Resolution

The vertical resolution of the  $\text{CCl}_4$  profiles is very similar for the FR and the RR period. From about 2.5–3 km at the lower end of the profiles, it degrades to approximately 5 km at  $\sim 25$  km and  $\sim 7$  km at  $\sim 30$  km, calculated as the full width at half maximum of the row of the averaging kernel matrix (Rodgers, 2000). The degrees of freedom are usually around 3.5 for the FR period and close to 4.0 for the RR period (Fig. 9). This is presumably attributed to the finer vertical sampling during the RR period with 27 tangent altitudes compared to 17 tangent altitudes during the FR period. The signal decreases rapidly with altitude, as the volume mixing ratios of  $\text{CCl}_4$  do. Above 30 km, hardly any  $\text{CCl}_4$  information is available in the MIPAS spectra. Slightly below 20 km, the averaging kernels show negative side

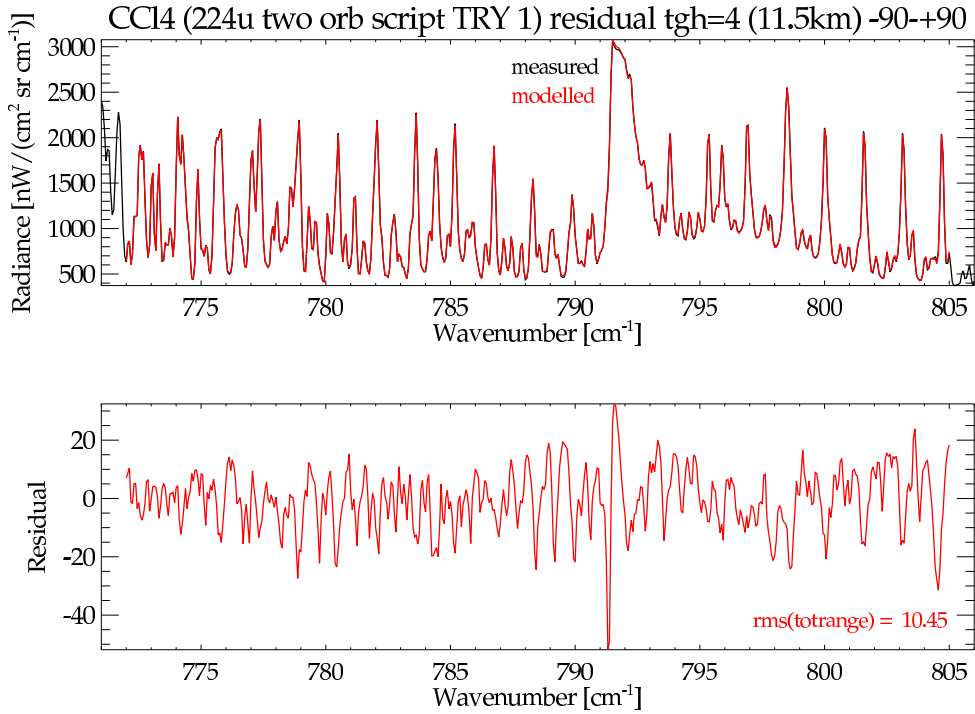


**Figure 5.** Impact of the  $\text{CO}_2$  Q-branch at 11.5 km altitude taking line mixing it into account (right). Top panel: spectra; bottom panel: residuals. Black: measured spectrum, hardly discernible because overplotted by modelled spectra. Note the different scale of the residual axis compared to Fig. 4.

wiggles which are more pronounced during the FR period (left panel) than the RR period (right panel).

305

### 4.3 Error Budget

Tables 2 and 3 list the error budgets for mid latitudes during the FR and RR period between 10 and 40 km. Examples for other latitudes can be found in the appendix (Tables A1 and A6). For legibility reasons, the errors are only given every 5 km, although the retrieval grid is 1 km. Errors due to elevation uncertainties of the line of sight and uncertainties of several contributing species are given. All profiles show a strong increase in the relative errors at and above 30 km. During the FR period, the absolute total errors are fairly similar below this altitude, while large differences can occur from 20 km upwards. Absolute errors are close to 3 pptv between 10 and 25 km, and around 5 to 6 pptv at 15 km where larger volume mixing ratios appear for all atmospheric situations except

the polar summer one where the errors stay close to 3 pptv. The largest error component is measurement noise (third column), while at 15 km significant parameter errors have to be considered, in particular the elevation uncertainties of the line of sight (LOS), and instrument line shape (ILS). Beyond this, uncertainties of  $\text{HNO}_4$  and  $\text{ClONO}_2$  profiles, frequency calibration (shift) and temperature contribute to the total error. The decrease of retrieval noise towards higher altitudes is explained by the coarser altitude resolution at higher altitudes. For the RR period, the patterns look slightly different. There is no peak in the total error around 15 km, but the total error is either rather constant at lower altitudes or decreases with altitude. Contributions to the error budget are, however, similar to the FR period.

Fig. 10 compares the estimated total error with the deviation of the profiles in a quiescent atmosphere. This comparison was created in a similar way as in Eckert et al. (2016, Sec. 6). Up to 18 km altitude, the sample standard deviation of MI-

**Table 2.** Error ~~estimate~~ estimates for a mid-latitude profile during the FR period. Errors are given in pptv (relative errors in %).

Altitude	total error	noise	total parameter	Gain	LOS	$\text{HNO}_4$	Shift	ILS	Temperature	$\text{ClONO}_2$
40	0.0 ( 69.4)	0.0 ( 57.2)	0.0 ( 38.8)	0.0 ( 24.5)	0.0 ( 22.5)	0.0 ( 18.2)	0.0 ( 1.7)	0.0 ( 9.2)	0.0 ( 6.3)	0.0 ( 5.5)
35	0.0 ( 68.4)	0.0 ( 56.7)	0.0 ( 39.1)	0.0 ( 23.5)	0.0 ( 21.5)	0.0 ( 18.4)	0.0 ( 1.7)	0.0 ( 9.0)	0.0 ( 6.3)	0.0 ( 5.7)
30	0.2 ( 71.0)	0.2 ( 64.3)	0.1 ( 33.8)	0.1 ( 20.3)	0.1 ( 17.9)	0.1 ( 20.3)	0.0 ( 1.8)	0.0 ( 3.0)	0.0 ( 5.1)	0.0 ( 5.1)
25	2.3 ( 480.8)	2.2 ( 459.9)	0.7 ( 144.2)	0.4 ( 79.4)	0.0 ( 3.8)	0.6 ( 115.0)	0.0 ( 10.0)	0.0 ( 0.7)	0.1 ( 23.0)	0.1 ( 17.3)
20	2.9 ( 5.3)	2.4 ( 4.4)	1.6 ( 2.9)	0.0 ( 0.1)	1.5 ( 2.8)	0.1 ( 0.3)	0.0 ( 0.0)	0.7 ( 1.2)	0.1 ( 0.2)	0.1 ( 0.2)
15	5.0 ( 4.9)	2.1 ( 2.1)	4.5 ( 4.5)	0.7 ( 0.7)	4.0 ( 4.0)	0.1 ( 0.1)	0.1 ( 0.1)	2.0 ( 2.0)	0.1 ( 0.1)	0.1 ( 0.1)
10	2.7 ( 3.1)	2.5 ( 2.8)	0.9 ( 1.0)	0.2 ( 0.2)	0.2 ( 0.3)	0.3 ( 0.3)	0.1 ( 0.1)	0.4 ( 0.4)	0.5 ( 0.6)	0.1 ( 0.1)

**Table 3.** Error ~~estimate~~ estimates for a mid-latitude profile during the RR period. Errors are given in pptv (relative errors in %).

Altitude	total error	noise	total parameter	Gain	LOS	$\text{HNO}_4$	Shift	ILS	Temperature	$\text{ClONO}_2$
40	0.0 ( 214.1)	0.0 ( 127.1)	0.0 ( 173.9)	0.0 ( 73.6)	0.0 ( 147.2)	0.0 ( 24.8)	0.0 ( 2.5)	0.0 ( 24.8)	0.0 ( 24.1)	0.0 ( 13.4)
35	0.0 ( 211.3)	0.0 ( 128.1)	0.0 ( 172.9)	0.0 ( 70.4)	0.0 ( 147.3)	0.0 ( 25.0)	0.0 ( 2.6)	0.0 ( 24.3)	0.0 ( 23.7)	0.0 ( 13.4)
30	0.2 ( 141.2)	0.1 ( 123.6)	0.1 ( 61.8)	0.0 ( 15.9)	0.1 ( 47.7)	0.0 ( 24.7)	0.0 ( 2.8)	0.0 ( 22.1)	0.0 ( 2.8)	0.0 ( 11.5)
25	2.4 ( 187.3)	2.2 ( 171.7)	0.9 ( 67.1)	0.2 ( 14.0)	0.4 ( 30.4)	0.4 ( 33.6)	0.1 ( 4.8)	0.6 ( 44.5)	0.0 ( 0.0)	0.2 ( 16.4)
20	3.5 ( 15.0)	2.6 ( 11.1)	2.4 ( 10.3)	0.1 ( 0.4)	2.3 ( 9.9)	0.1 ( 0.4)	0.1 ( 0.3)	0.1 ( 0.5)	0.1 ( 0.2)	0.0 ( 0.1)
15	3.3 ( 6.1)	2.0 ( 3.7)	2.6 ( 4.8)	0.5 ( 1.0)	2.5 ( 4.6)	0.1 ( 0.3)	0.0 ( 0.1)	0.1 ( 0.2)	0.1 ( 0.1)	0.0 ( 0.0)
10	5.7 ( 6.1)	4.3 ( 4.6)	3.7 ( 4.0)	1.1 ( 1.2)	3.5 ( 3.8)	0.2 ( 0.2)	0.0 ( 0.0)	0.4 ( 0.4)	0.4 ( 0.4)	0.1 ( 0.1)

PAS Envisat results is only slightly larger than the estimated error. Thus, these profiles suggest that the estimated error can explain most of the variability in the  $\text{CCl}_4$  profiles up to approximately 18 km, ~~which suggests that~~. Correspondingly, the error estimate ~~is~~ can be considered realistic from the bottom of the profile up to this altitude.

#### 4.4 Trends

Fig. 11 shows an altitude-latitude cross-section of MIPAS Envisat  $\text{CCl}_4$  trends. These trends were estimated by the same method as described by Eckert et al. (2014), which is based on the method by von Clarmann et al. (2010). In addition to the setup used by Eckert et al. (2014), the El-Niño-Southern Oscillation (ENSO) was also taken into account. The data set used for trend calculation covers the entire MIPAS Envisat measurement period from July 2002 to April 2012. The distribution of the trends agrees well with the trends estimated by Valeri et al. (2017), who calculated trends from MIPAS Envisat V7 data they formerly retrieved and displayed them on a pressure-latitude grid. The most likely cause of differences between their and our trend estimates are the underlying MIPAS spectra. We use MIPAS V5 spectra which were found to be subject to an instrument drift due to detector aging (Eckert et al., 2014). Valeri et al. (2017) use version 7 spectra where an attempt was made to tackle the problem of detector aging during the level-1 processing. However, Hubert et al. (2016) show that there is still a drift problem in the version 7 MIPAS temperatures. Since these temperature drifts are expected to propagate onto the retrieved  $\text{CCl}_4$  mixing ratios, it is

not clear if version 5 or version 7 is more adequate for trend analysis. In spite of these differences and technical differences in the level-2 data processing, the trends inferred by Valeri et al. (2017) and ours show important common features. In both data sets a hemispheric asymmetry is found, with positive trends in the Southern hemisphere around 25 km (however, the region is larger in our data set) and negative trends in the Northern hemisphere in almost the whole altitude range. Also the average magnitudes of the inferred trends agree reasonably well between both data sets.

## 5 Comparisons

### 5.1 Historical comparisons

#### 5.1.1 ATMOS

The ATMOS (Atmospheric Trace Molecule Spectroscopy) instrument measured in solar occultation covering the spectral region from 600 to 4700  $\text{cm}^{-1}$  with a spectral resolution of 0.01  $\text{cm}^{-1}$ . ~~It took measurements of 12 sunsets between 25.6–32.7°N and 7 sunrises 46.7–49.0°S during the Spacelab 3 (SL3) mission (Farmer and Raper, 1986), e.g. during April and May 1985. A~~ ATMOS took measurements in 1985, 1992, 1993 and 1994. The ATMOS profiles shown in Fig. 12 were extracted directly from Zander et al. (1996, Fig. 1).  $\text{CCl}_4$  volume mixing ratio ~~profile at 30 profiles in the subtropics (20–35°N; thin dashed lines) and at midlatitudes (35–49°N; is presented in Zander et al. (1987) (;~~ thin full lines) are presented there. Measurements were taken from 3 to 12

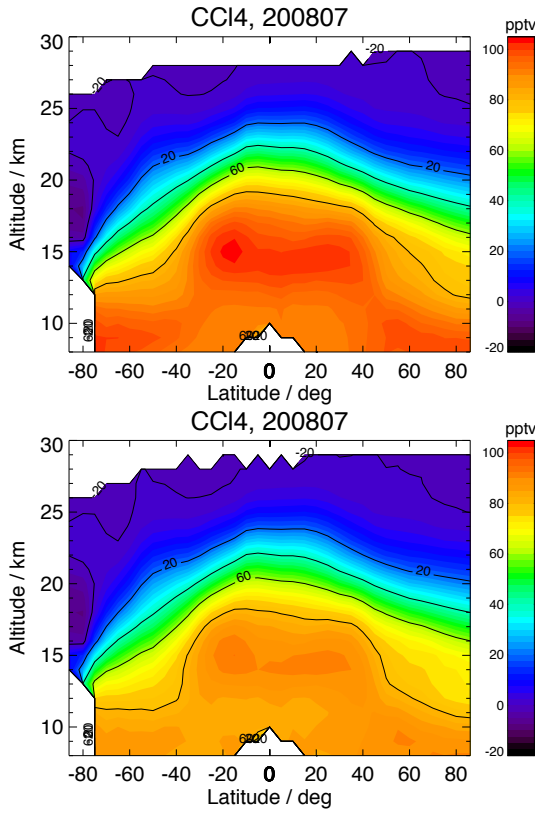


**Figure 6.** Altitude-latitudinal cross-section of July 2008, using the spectroscopic dataset by Nemtchinov and Varanasi (2003) (top) and using the new spectroscopic data by Harrison et al. (2017).

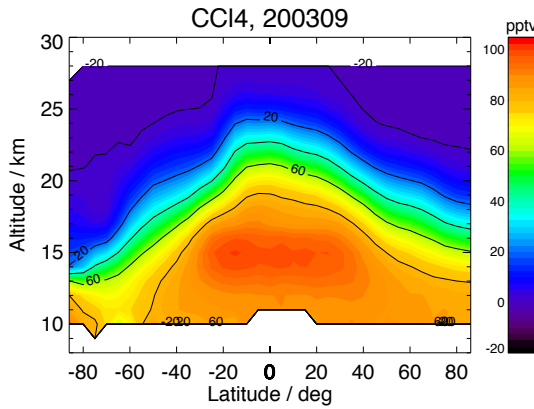


**Figure 7.** Altitude-latitudinal cross-sections of MIPAS  $\text{CCl}_4$  for the FR period (September 2003).

400

November in 1994 during the ATLAS-3 shuttle mission. We adopted depicting midlatitude profiles as solid lines and subtropic profiles as dashed lines in Fig. 16 for which a spectroscopic dataset provided by Massie et al. (1985) was

used. This profile shows 12 of this manuscript. To compare the ATOMS profiles with MIPAS Envisat, we used MIPAS Envisat data of all years from 3 to 12 November and calculated an arithmetic mean for both latitude bands (subtropics and midlatitudes). In Fig. 12, MIPAS Envisat profiles are shown in blue, while the ATOMS profiles are shown in orange. The ATOMS profiles show higher volume mixing ratios than those of MIPAS Envisat, because it was measured before they were measured shortly after  $\text{CCl}_4$

405

410

415

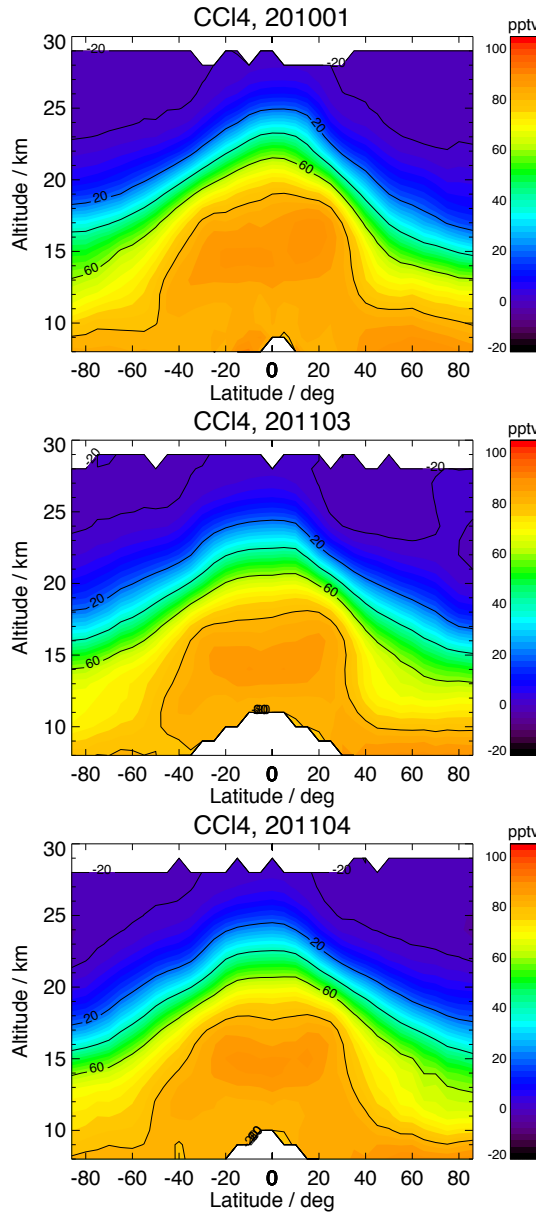


**Figure 8.** Altitude-latitudinal cross-sections of MIPAS  $\text{CCl}_4$  for the RR period. Top to bottom: July 2008, January 2010 and March and April 2011.

420

425

430

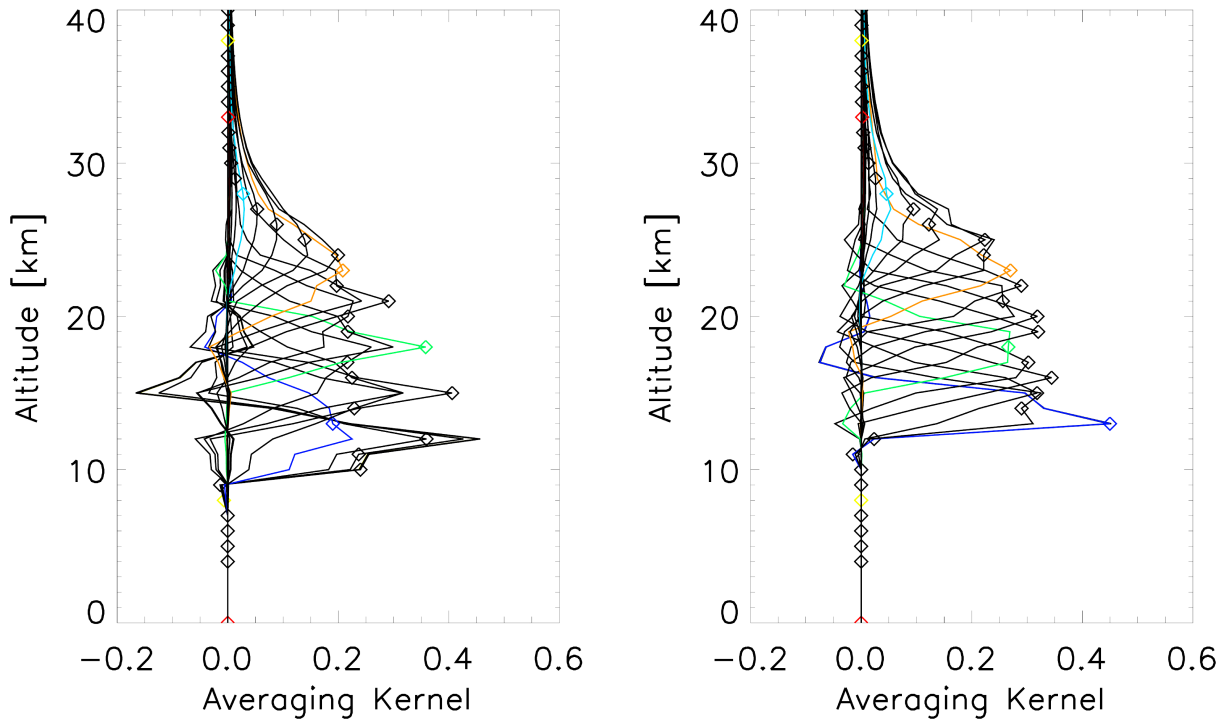


**Figure 9.** Rows of exemplary Averaging Kernels of MIPAS  $\text{CCl}_4$ . Left: FR period (September 2003). Right: RR period (July 2008).

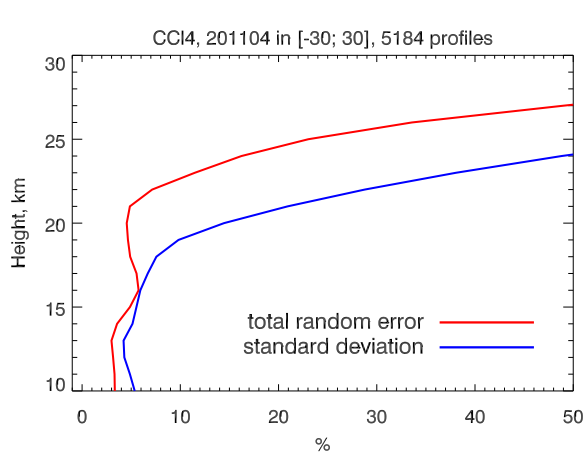


**Figure 10.** Comparison of the estimated total error with the standard deviation of several MIPAS profiles for a quiescent atmospheric situation (equator). Red: total error budget, blue: standard deviation.

emissions were restricted and, thus, volume mixing ratios used to be higher in the atmosphere. However, the general ~~shape-shapes~~ of the ATMOS ~~profile agrees well with that~~ profiles agree well with those of MIPAS Envisat. Both, MI-

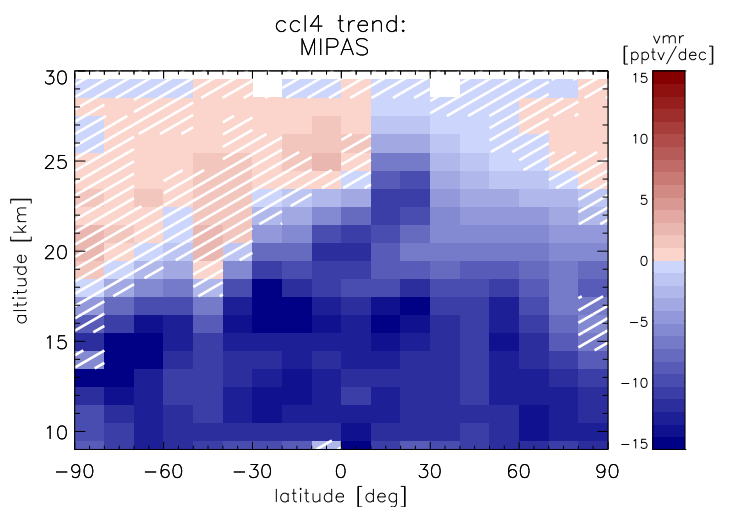


**Figure 11.** Altitude-latitude cross-sections of MIPAS  $\text{CCl}_4$  trends covering the entire measurement period from July 2002 to April 2012. Red colours indicate increasing  $\text{CCl}_4$  volume mixing ratios. Blue colours indicate declining  $\text{CCl}_4$  concentrations. Hatching shows where no statistically significant trends could be calculated at two sigma confidence level.

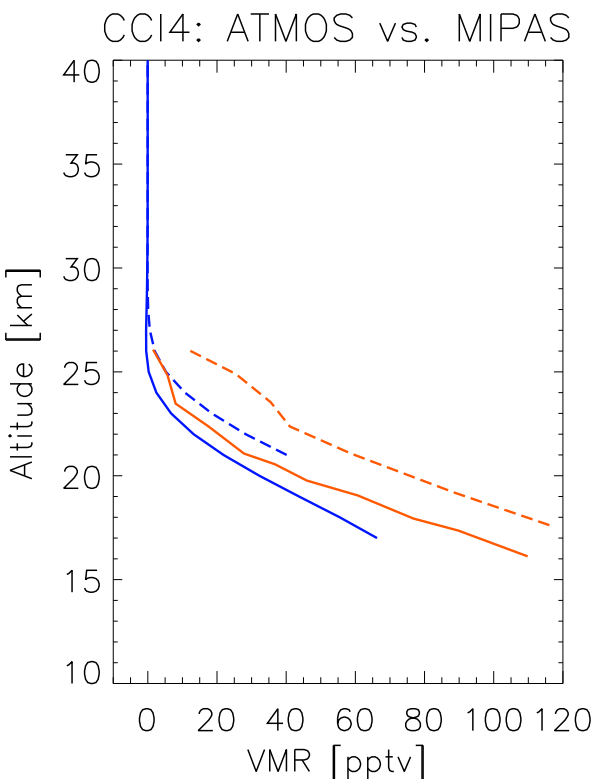


**Figure 12.** Qualitative comparison of profiles from ATMOS (orange) taken during the ATLAS-3 mission (as shown in Zander et al. (1996, Fig. 1)) and climatological means of MIPAS (blue) during 3-12 November of each year. Solid lines refer to midlatitude measurements ( $35\text{--}49^\circ\text{N}$ ). Dashed lines indicate subtropical measurements ( $20\text{--}35^\circ\text{N}$ ).

### 5.1.2 MIPAS-B

The first balloon-borne version of the MIPAS instrument was developed prior to the satellite instrument in the late 1980's and early 1990's at the Institute of Meteorology and Climate Research (IMK) in Karlsruhe (Fischer and Oelhaf, 1996; Friedl-Vallon et al., 2004) (Fischer and Oelhaf, 1996; Friedl-Vallon et al., 2004). Measurements with this instrument have been taken since 1989 (von Clarmann et al., 1993) and first profiles of  $\text{CCl}_4$  were derived from a flight at Kiruna, Sweden, on 14 March 1992 (von Clarmann et al., 1995). Due to the strong decrease of  $\text{CCl}_4$  with altitude, a clear signal of the gas could not be identified at tangent altitudes of 14.5 km and above. Thus, only the spectrum at 11.3 km was analyzed and the total amount of  $\text{CCl}_4$  was estimated by scaling the vertical profile and using information on the shape as measured in polar winter conditions before. This leads to an estimated concentration of approximately 110 pptv at 11.3 km, which is slightly higher than the peak surface values in the long time series of  $\text{CCl}_4$  shown in Liang et al. (2016). Ground based measurements shown there support favouring the MIPAS Envisat  $\text{CCl}_4$  retrieval with the new spectroscopic dataset, since respective results agree better with measurements shown in Liang et al. (2016). MIPAS-B results overestimate the ground based measurements slightly providing a consistent picture when taking differences in the volume mixing ratios into account which result from the old versus the new spectroscopic dataset.

## 5.2 Comparisons with collocated measurements

Since all comparison data for comparisons based on All collocated measurements were retrieved analyzed using spectroscopic data introduced in of Nemtchinov and Varanasi (2003), which are included in the HITRAN 2000 (Nemtchinov and Varanasi, 2003), MIPAS Envisat retrievals based on this spectroscopic dataset were also used for the comparison for reasons of consistency and in order database (Rothman et al., 2003). Thus, in order to allow for a meaningful comparison and not to mask possible other discrepancies differences, a dedicated MIPAS Envisat comparison dataset was generated which is based on these spectroscopic data as well.

### 5.2.1 ACE-FTS

Comparison of MIPAS Envisat and version 3.5 ACE-FTS  $\text{CCl}_4$ . Left: Mean profiles of all coincident profiles (black: ACE-FTS, magenta: MIPAS). Dashed lines show the standard deviations of the mean profiles. Second to the left: Number of coincident points per altitude. Middle: Correlation coefficient of the mean profiles. Second to the right: Relative differences of the mean profiles. Right: One standard deviation of the relative differences of the mean profiles. The Atmospheric Chemistry Experiment Fourier

450

455

460

465

470

475

480

485

490

495

500

505

510

515

520

525

530

535

540

545

550

555

560

565

570

575

580

585

590

595

600

605

610

615

620

625

630

635

640

645

650

655

660

665

670

675

680

685

690

695

700

705

710

715

720

725

730

735

740

745

750

755

760

765

770

775

780

785

790

795

800

805

810

815

820

825

830

835

840

845

850

855

860

865

870

875

880

885

890

895

900

905

910

915

920

925

930

935

940

945

950

955

960

965

970

975

980

985

990

995

1000

1005

1010

1015

1020

1025

1030

1035

1040

1045

1050

1055

1060

1065

1070

1075

1080

1085

1090

1095

1100

1105

1110

1115

1120

1125

1130

1135

1140

1145

1150

1155

1160

1165

1170

1175

1180

1185

1190

1195

1200

1205

1210

1215

1220

1225

1230

1235

1240

1245

1250

1255

1260

1265

1270

1275

1280

1285

1290

1295

1300

1305

1310

1315

1320

1325

1330

1335

1340

1345

1350

1355

1360

1365

1370

1375

1380

1385

1390

1395

1400

1405

1410

1415

1420

1425

1430

1435

1440

1445

1450

1455

1460

1465

1470

1475

1480

1485

1490

1495

1500

1505

1510

1515

1520

1525

1530

1535

1540

1545

1550

1555

1560

1565

1570

1575

1580

1585

1590

1595

1600

1605

1610

1615

1620

1625

1630

1635

1640

1645

1650

1655

1660

1665

1670

1675

1680

1685

1690

1695

1700

1705

1710

1715

1720

1725

1730

1735

1740

1745

1750

1755

1760

1765

1770

1775

1780

1785

1790

1795

1800

1805

1810

1815

1820

1825

1830

1835

1840

1845

1850

1855

1860

1865

1870

1875

1880

1885

1890

1895

1900

1905

1910

1915

1920

1925

1930

1935

1940

1945

1950

1955

1960

1965

1970

1975

1980

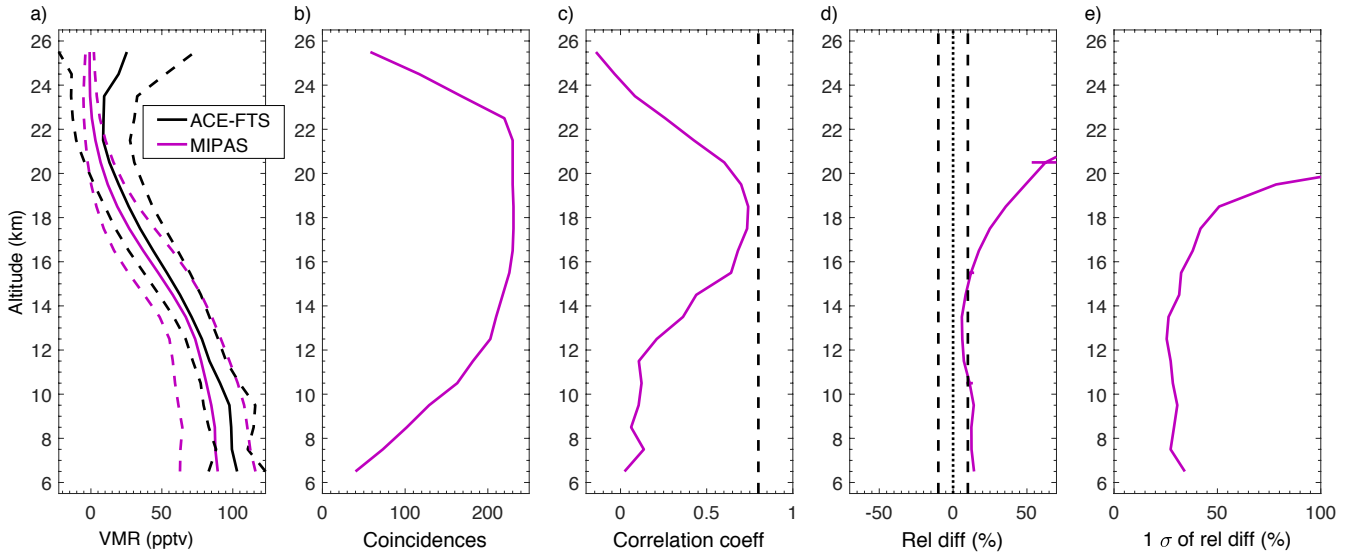


**Figure 13.** Comparison of MIPAS Envisat and version 3.5 ACE-FTS  $\text{CCl}_4$ . a) Mean profiles of all coincident profiles (black: ACE-FTS, magenta: MIPAS). Dashed lines show the standard deviations of the mean profiles. b) Number of coincident points per altitude. c) Correlation coefficient of the mean profiles. d) Relative differences of the mean profiles. e) One standard deviation of the relative differences of the mean profiles.

Transform Spectrometer ACE-FTS is one of two instruments 505 aboard the Canadian Satellite SCISAT-1. On 12 August 2003, it was launched into a  $74^\circ$  orbit at 650 km to ensure a focus on higher latitudes. It covers the globe from  $85^\circ\text{S}$  to 510  $85^\circ\text{N}$ . Since ACE-FTS is an occultation instrument, it takes measurements during 15 sunrises and 15 sunsets a day within two latitude bands. The vertical scan range covers altitudes from the middle troposphere up to 150 km. Wavelengths between  $750\text{ cm}^{-1}$  and  $4400\text{ cm}^{-1}$  ( $13.3\text{ }\mu\text{m}$  and  $2.3\text{ }\mu\text{m}$ ) can be detected with a spectral resolution of  $0.02\text{ cm}^{-1}$ . The vertical sampling depends on the altitude as well as the beta angle. The latter is the angle between the orbit track and the path from the instrument to the sun. The sampling ranges from  $\sim 1$  km between 10 km and 20 km to  $\sim 2\text{--}3.5$  km around 515 35 km and declines to 5–6 km at the upper end of the vertical range. The field of view covers 3–4 km, which is approximately similar to the vertical resolution of the instrument. Comparisons in this study were made using version 3.5 of 520 the ACE-FTS data. The  $\text{CCl}_4$  retrieval is performed between  $787.5\text{ cm}^{-1}$  and  $805.5\text{ cm}^{-1}$  at altitudes from 7 km to 25 km (Allen et al., 2009).

For the comparison with ACE-FTS (Fig. 13), coincident profiles within 2 hours time difference and no further than  $5^\circ$  latitude and  $10^\circ$  longitude away were used. Profiles at 525 latitudes higher than  $60^\circ\text{S}$  were omitted. Between the lower end and  $\sim 16$  km the agreement is always close to 10 %, while with slightly larger differences below 10 km than between 10 and 15 km. Above 15 km, the mean profiles

deviate above this altitude more strongly and exceed relative differences of 50 % above 19 km (second panel to the right Fig. 13d)). However, this difference is differences above 19 km are not as apparent in the absolute comparison (left panel Fig. 13a)). The volume mixing ratio difference stays within similar values up to near 25 km. Since  $\text{CCl}_4$  decreases rapidly with altitude, this difference is far more pronounced in relative terms. MIPAS shows slightly lower volume mixing ratios than ACE-FTS, in general. However, with only a small number of coincident measurements being available, the Part of this might be attributed to PAN not being accounted for in the ACE-FTS v3.5 retrieval (Harrison et al., 2017). With PAN missing from the forward model calculations, the retrieval increases  $\text{CCl}_4$  to compensate. Preliminary ACE-FTS version 4 results indicate that retrieved  $\text{CCl}_4$  will skew lower when PAN is included. However, Harrison et al. (2017) do not investigate the magnitude of the effect of including PAN versus not including it. Other items changed in the retrieval e.g. the microwindow set and new cross sections, so it is not clear how much of the decrease in  $\text{CCl}_4$  can be attributed to the inclusion of PAN as an interferer in the ACE-FTS retrieval. Nevertheless, the agreement between MIPAS Envisat and ACE is very good, staying within the 10 % range for the differences up to above 15 km.

## 5.2.2 MIPAS-B

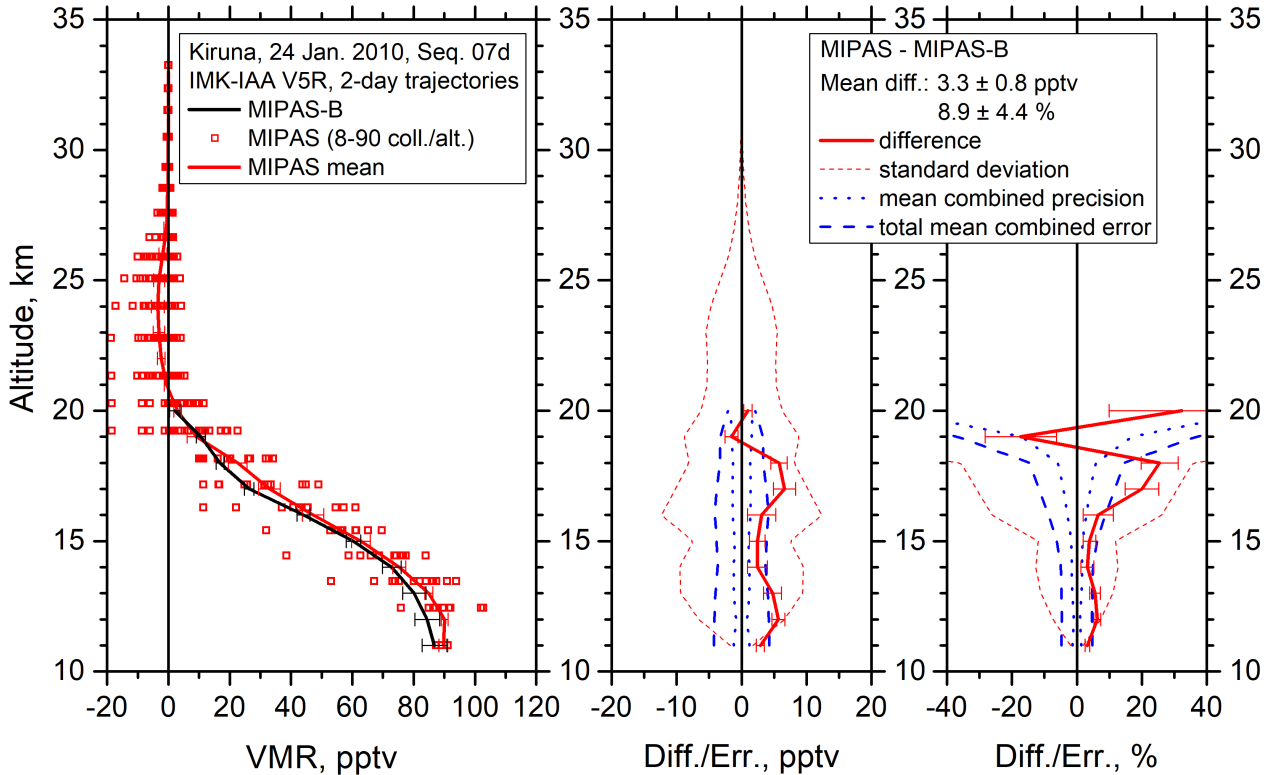


**Figure 14.** Comparison of MIPAS Envisat and MIPAS-B2  $\text{CCl}_4$  for the MIPAS-B2 flight on 24 January 2010 over Kiruna, Sweden. Left: Mean profile of all coincident profiles (black line: MIPAS-B2, red line: MIPAS mean, red squares: coincident MIPAS measurements). Middle: absolute total error budget without consideration of the spectroscopy error. Right: relative error budget - red continuous line: difference between the mean profiles; red dotted line: standard deviation; blue dotted line: mean combined precision; blue dashed line: total mean combined error.

**Comparison of MIPAS Envisat and MIPAS-B2  $\text{CCl}_4$  for the MIPAS-B2 flights on 24 January 2010 and on 31 March 2011 over Kiruna, Sweden. Left: Mean profile of all coincident profiles (black line: MIPAS-B2, red line: MIPAS mean, red squares: coincident MIPAS measurements). Middle: absolute total error budget without consideration of the spectroscopy error. Right: relative error budget.** MIPAS-B2 is the follow-up of MIPAS-B (Friedl-Vallon et al., 2004) which was lost in 1992. MIPAS-B and MIPAS-B2 measurements add up to more than 20 flights to date. MIPAS-B2 covers the spectral range from  $750 \text{ cm}^{-1}$  to  $2500 \text{ cm}^{-1}$  ( $13.3 \mu\text{m}$  and  $4 \mu\text{m}$ ) and vertical ranges up to the floating altitude of typically around 30–40 km. The vertical sampling is approximately 1.5 km. The spectral region used for the MIPAS-B2 retrieval ranges from  $786.0$  to  $806.0 \text{ cm}^{-1}$ . MIPAS-B2 and MIPAS Envisat use the same retrieval strategy and forward model to derive

vertical profiles.

The two panels of Fig. ??-14 and Fig. 15 show  $\text{CCl}_4$  measurements from a single flight of MIPAS-B2 each, compared with collocated measurements of MIPAS Envisat along diabatic 2-day backward and forward trajectories. These trajectories were calculated at Free University of Berlin (Naujokat and Grunow, 2003) and are based on European Centre for Medium-Range Weather Forecasts (ECMWF)  $1.25^\circ \times 1.25^\circ$  analyses. The trajectories start at different altitudes at the respective geolocation of the balloon measurement. Coincidence criteria for this comparison were 1 h and 500 km within the temporal and spacial range of the balloon location. The left panel of Fig. ??-14 shows a comparison with the MIPAS-B2 flight on 24 January 2010. The comparison with the MIPAS Envisat mean profile (red line), which was calculated from the ensemble of all collocated

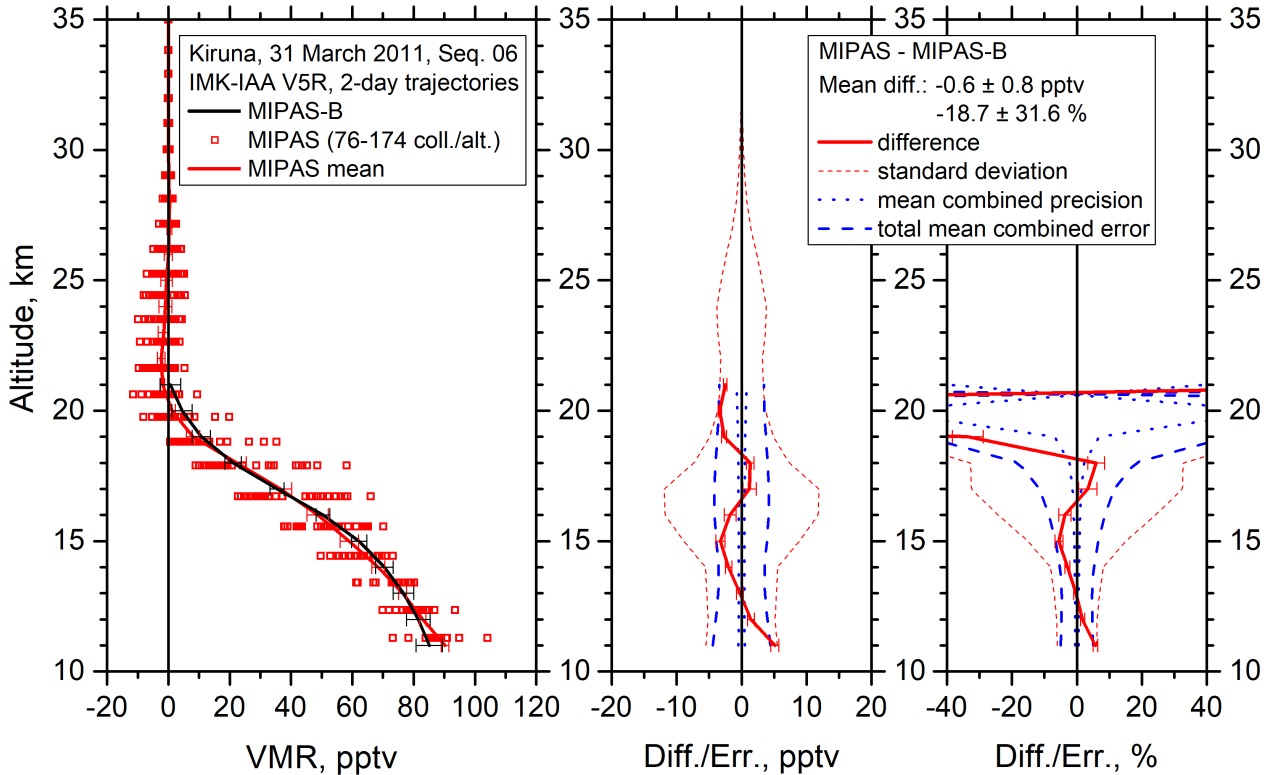


**Figure 15.** Comparison of MIPAS Envisat and MIPAS-B2  $\text{CCl}_4$  for the MIPAS-B2 flight on 31 March 2011 over Kiruna, Sweden. Left: Mean profile of all coincident profiles (black line: MIPAS-B2, red line: MIPAS mean, red squares: coincident MIPAS measurements). Middle: absolute total error budget without consideration of the spectroscopy error. Right: relative error budget - red continuous line: difference between the mean profiles; red dotted line: standard deviation; blue dotted line: mean combined precision; blue dashed line: total mean combined error.

MIPAS Envisat measurements (red squares), agrees with the MIPAS-B2 measurement (black line) within 5 pptv for most of the altitude range. The MIPAS-B2 measurement lies well within the spread of all collocated MIPAS Envisat profiles. The difference (middle panel) is always close to the total combined error, which includes all error estimates except the spectroscopy error. The latter has not been included because a MIPAS Envisat retrieval [setup](#) was used for this comparison which is based on the same spectroscopic data as the MIPAS-B2 retrieval. The right panel shows the relative error, which stays well within 5 % up to 17 km. Only between 16 and 18 km, the relative difference noticeably exceeds the combined error of the instruments.

The comparison of the MIPAS-B2 flight on 31 March 2011 (Fig. [??, right plot 15](#)) with MIPAS Envisat presents even better agreement. The difference between the two profiles never

exceeds 5 pptv (middle panel) and stays within or close to the combined error of the instruments throughout the whole altitude range. Larger deviations in the relative differences only occur above 18 km, where the combined error of the instruments also increases rapidly, because of small volume mixing ratios of  $\text{CCl}_4$ . Overall, the comparisons with MIPAS-B2 show excellent agreement between the two instruments. This suggests that the MIPAS Envisat  $\text{CCl}_4$  error estimate are realistic and that the residuals in the  $\text{CO}_2$  lines mentioned in Sec. 3.2 have no major impact on the  $\text{CCl}_4$  retrieval. This is also supported by Fig. 10, at least up to about 18 km, since the standard deviation of the profiles can be explained by the MIPAS Envisat error estimates to a large extent.

### 5.2.3 Cryosampler

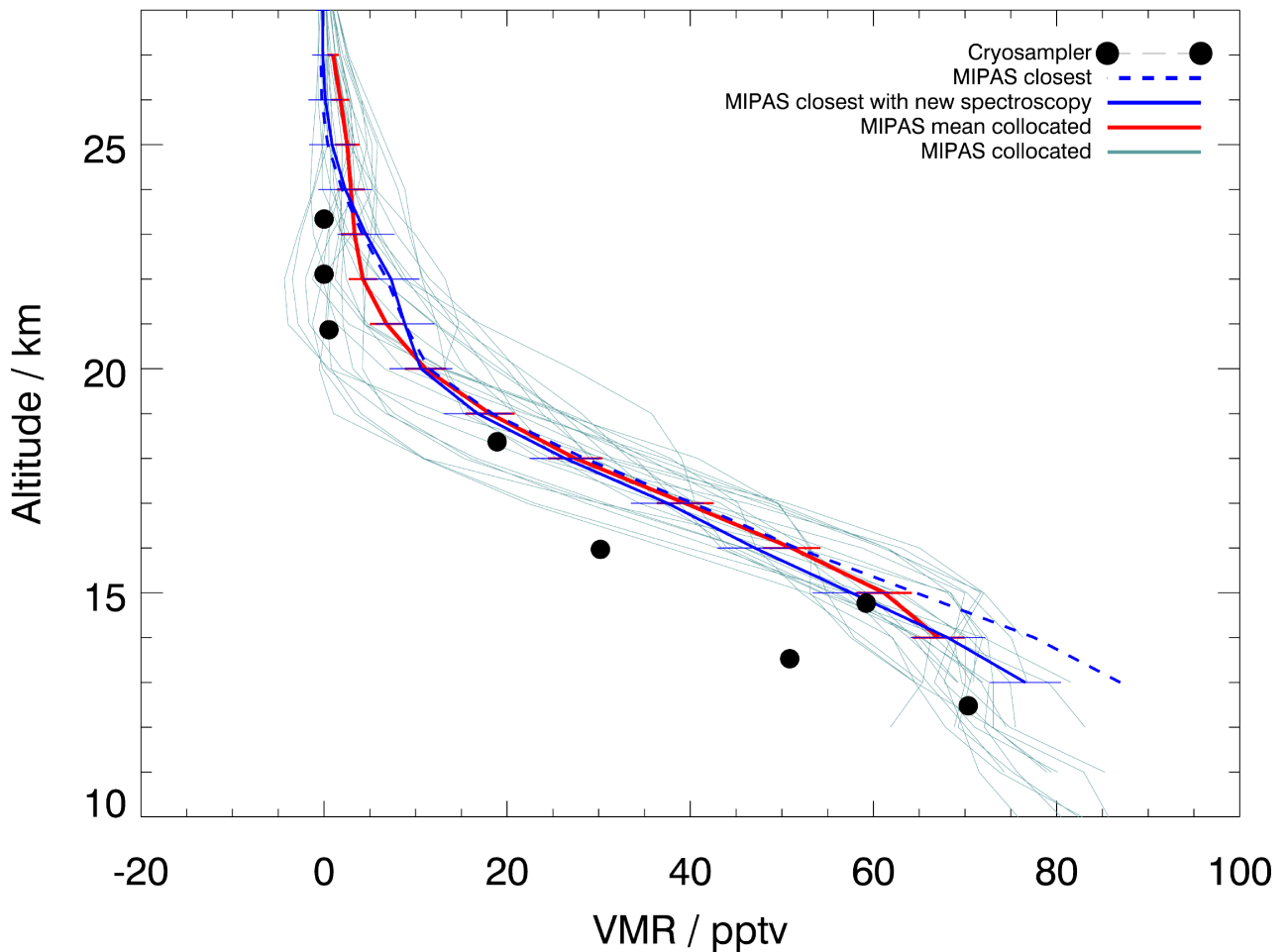


**Figure 16.** Comparison of MIPAS Envisat and cryosampler  $\text{CCl}_4$ . The cryosampler measurement taken on 1 April 2011. The continuous and dashed blue lines are the respective closest MIPAS Envisat profiles with the new and the old spectroscopic dataset.

~~Comparison of MIPAS Envisat and MIPAS B2  $\text{CCl}_4$  for a cryosampler measurement taken on 1 April 2011.~~

<sup>595</sup> ~~The continuous and dashed blue lines are the respective closest MIPAS Envisat profiles with the new and the old spectroscopic dataset.~~ The Cryosampler whose measurements are used here was developed at Forschungszentrum <sup>600</sup> Jülich (Germany) in the early 1980s (Schmidt et al., 1987) <sup>615</sup> and is a balloon-borne instrument. It collects whole air samples which are then frozen during the flight and analyzed using gas chromatography after the flight. In this analysis, a flight performed on 1 April 2011 by University of Frankfurt (Fig. 16 black circles) is compared to collocated MIPAS <sup>620</sup> Envisat profiles that lie within 1000 km and 24 h of the Cryosampler profile. The MIPAS Envisat profiles used for the comparison are those retrieved with the new spectroscopic dataset (continuous blue line: closest MIPAS profile,

<sup>610</sup> red line: MIPAS mean profile, blue-greyish lines: all collocated MIPAS profiles). In addition, the closest profile produced with the old spectroscopic dataset is shown (dashed blue line). The only difference between the blue line and the dashed blue line are the different spectroscopic datasets. It is clearly visible that the closest MIPAS profile produced with the new spectroscopic data comes closer to the Cryosampler measurements, even though these still show slightly lower volume mixing ratios of  $\text{CCl}_4$ . A similar pattern of two outliers (second and forth lowest Cryosampler measurements) were also seen in a comparison of Cryosampler and MIPAS measurements of CFC-11 and CFC-12 (Eckert et al., 2016), even though the second lowest outlier is not as obvious for the CFCs. However, this might be an indication that Cryosampler captured fine structures (like laminae) produced by the unique atmospheric situation in spring 2011

(Manney et al., 2011; Sinnhuber et al., 2011), that MIPAS <sup>680</sup> Envisat cannot resolve due to its coarser vertical resolution. All other Cryosampler measurements lie within the spread of the collocated MIPAS Envisat profiles. Taking this into account, the overall agreement of MIPAS and Cryosampler is good and Fig. 16 supports the assumption that the retrieval <sup>685</sup> is improved by the usage of the new spectroscopic dataset.

## 6 Conclusions

Vertical profiles of  $\text{CCl}_4$  were retrieved from MIPAS Envisat limb emission spectra considering various interfering trace gases and with PAN playing a particularly important role. Using line-mixing in the forward model made it possible to narrow the spectral region that had to be omitted due to large residuals and thus to include additional information useful for the retrieval of  $\text{CCl}_4$ , even though parts of the  $\text{CO}_2$  Q-branch had still to be excluded. Introducing a new spectroscopic dataset (Harrison et al., 2017) resulted in lower volume mixing ratios of  $\text{CCl}_4$  which agree better with other ~~measurements~~ <sup>690</sup> results, e.g. tropospheric values shown in Liang et al. (2016) <sup>695</sup> and Cryosampler measurements. The expected atmospheric distribution patterns are clearly visible in altitude-latitude cross-sections. These show higher volume mixing ratios of  $\text{CCl}_4$  in the tropics and at lower altitudes which quickly decrease above the tropopause due to photolysis. They also decrease with increasing latitude and thus follow the Brewer-Dobson circulation. A maximum in the tropics connected with higher values of  $\text{CCl}_4$  below the northern extra-tropical tropopause is a feature also seen in HCFC-22 (Chirkov et al., 2016) where ~~they were~~ <sup>700</sup> it was associated with the uplift in the Asian monsoon, so  $\text{CCl}_4$  distributions in this region might have a similar explanation. Trends of the entire measurement period from July 2002 to April 2012 show good agreement with trends estimated by Valeri et al. (2017). Comparisons with ACE-FTS and MIPAS-B2 show very good agreement and historical measurements of MIPAS-B2 and ATMOS are coherent with MIPAS Envisat  $\text{CCl}_4$  results using the new spectroscopic data. MIPAS profiles retrieved using the new spectroscopic dataset agree well with Cryosampler and deviations between the measurements can be explained reasonably. The latter comparison also suggests that the new spectroscopic dataset improves the MIPAS Envisat  $\text{CCl}_4$  retrieval. The MIPAS Envisat estimated error can explain most of the variability of ~~the profiles~~ <sup>705</sup> a set of profiles measured during quiescent atmospheric conditions up to 18 km, so the error estimate seems to be realistic. This is also supported by the comparison of MIPAS Envisat and MIPAS-B2 where the differences between the measurements stay mostly within the combined error of the instruments. Putting differences resulting from different special resolutions aside, also the comparison with the Cryosampler profile suggests to favour the spectroscopic dataset introduced by Harrison et al. (2017) over the dataset used before.

*Acknowledgements.* The retrievals of IMK/IAA were partly performed on the HP XC4000 of the Scientific Supercomputing Cen-

ter (SSC) Karlsruhe under project grant MIPAS. IMK data analysis was supported by DLR under contract number 50EE0901. MIPAS level 1B data were provided by ESA. We acknowledge support by Deutsche Forschungsgemeinschaft and Open Access Publishing Fund of Karlsruhe Institute of Technology. This work was supported by the DFG project for the 'Consideration of lifetimes of tracers for the determination of stratospheric age spectra and the Brewer-Dobson Circulation (COLIBRI)'. The Atmospheric Chemistry Experiment (ACE), also known as SCISAT, is a Canadian-led mission mainly supported by the Canadian Space Agency and the Natural Sciences and Engineering Research Council of Canada. Balloon flights and data analysis of MIPAS-B data used here were supported by the European Space Agency (ESA), the German Aerospace Center (DLR), CNRS (Centre National de la Recherche Scientifique), and CNES (Centre National d'Etudes Spatiales).

695 **Appendix A: Error Estimates**

**Table A1.** Error estimates for an equatorial profile during the FR period. Errors are given in pptv (relative errors in %).

Altitude	total error	noise	total parameter	Gain	LOS	$\text{HNO}_4$	Shift	ILS	Temperature	$\text{ClONO}_2$
40	0.0 ( 210.6)	0.0 ( 178.7)	0.0 ( 114.8)	0.0 ( 70.2)	0.0 ( 45.3)	0.0 ( 55.5)	0.0 ( 6.0)	0.0 ( 37.6)	0.0 ( 30.0)	0.0 ( 17.2)
35	0.0 ( 214.1)	0.0 ( 183.5)	0.0 ( 116.2)	0.0 ( 67.3)	0.0 ( 45.3)	0.0 ( 55.7)	0.0 ( 6.0)	0.0 ( 37.3)	0.0 ( 30.0)	0.0 ( 17.1)
30	0.2 ( 195.8)	0.2 ( 177.1)	0.1 ( 85.8)	0.1 ( 51.3)	0.0 ( 23.3)	0.1 ( 54.1)	0.0 ( 5.2)	0.0 ( 17.7)	0.0 ( 23.3)	0.0 ( 14.0)
25	2.3 ( 30.4)	2.2 ( 29.0)	0.9 ( 11.9)	0.4 ( 4.8)	0.5 ( 7.1)	0.5 ( 7.1)	0.1 ( 0.8)	0.2 ( 2.6)	0.2 ( 2.8)	0.1 ( 1.3)
20	2.8 ( 3.8)	2.5 ( 3.4)	1.3 ( 1.8)	0.2 ( 0.2)	0.8 ( 1.2)	0.1 ( 0.2)	0.0 ( 0.0)	0.9 ( 1.2)	0.3 ( 0.4)	0.1 ( 0.2)
15	5.3 ( 5.5)	2.2 ( 2.3)	4.9 ( 5.1)	0.9 ( 1.0)	4.2 ( 4.4)	0.2 ( 0.2)	0.1 ( 0.1)	2.3 ( 2.4)	0.4 ( 0.4)	0.1 ( 0.1)
10	2.8 ( 3.2)	2.6 ( 2.9)	1.0 ( 1.1)	0.2 ( 0.2)	0.1 ( 0.1)	0.2 ( 0.2)	0.1 ( 0.1)	0.3 ( 0.4)	0.8 ( 0.9)	0.1 ( 0.1)

**Table A2.** Error estimates for a polar summer profile during the FR period. Errors are given in pptv (relative errors in %).

Altitude	total error	noise	total parameter	Gain	LOS	$\text{HNO}_4$	Shift	ILS	Temperature	$\text{ClONO}_2$
40	0.0 ( 95.1)	0.0 ( 64.2)	0.0 ( 69.4)	0.0 ( 38.5)	0.0 ( 46.2)	0.0 ( 19.8)	0.0 ( 1.4)	0.0 ( 19.0)	0.0 ( 11.3)	0.0 ( 5.1)
35	0.0 ( 93.7)	0.0 ( 64.1)	0.0 ( 69.0)	0.0 ( 39.4)	0.0 ( 46.8)	0.0 ( 19.7)	0.0 ( 1.4)	0.0 ( 19.0)	0.0 ( 11.3)	0.0 ( 5.2)
30	0.2 ( 117.2)	0.2 ( 87.9)	0.1 ( 73.2)	0.1 ( 39.5)	0.1 ( 53.7)	0.1 ( 26.4)	0.0 ( 1.8)	0.0 ( 11.2)	0.0 ( 11.2)	0.0 ( 5.9)
25	2.5 ( 212.9)	2.2 ( 187.4)	1.2 ( 102.2)	0.5 ( 43.4)	0.9 ( 73.3)	0.6 ( 51.1)	0.1 ( 4.4)	0.1 ( 8.2)	0.1 ( 11.1)	0.1 ( 8.5)
20	2.4 ( 42.2)	2.1 ( 36.9)	1.2 ( 21.1)	0.1 ( 1.7)	1.2 ( 21.1)	0.2 ( 4.0)	0.0 ( 0.6)	0.0 ( 0.4)	0.1 ( 1.5)	0.0 ( 0.7)
15	2.8 ( 4.7)	1.7 ( 2.9)	2.3 ( 3.9)	0.1 ( 0.2)	2.2 ( 3.7)	0.2 ( 0.4)	0.1 ( 0.1)	0.5 ( 0.9)	0.2 ( 0.3)	0.1 ( 0.1)
10	3.0 ( 3.7)	2.3 ( 2.8)	2.0 ( 2.4)	0.1 ( 0.1)	1.4 ( 1.7)	0.1 ( 0.1)	0.1 ( 0.1)	1.2 ( 1.5)	0.3 ( 0.3)	0.0 ( 0.0)

**Table A3.** Error estimates for a polar winter profile during the FR period. Errors are given in pptv (relative errors in %).

Altitude	total error	noise	total parameter	Gain	LOS	$\text{HNO}_4$	Shift	ILS	Temperature	$\text{ClONO}_2$
40	0.0 ( 45.8)	0.0 ( 34.7)	0.0 ( 30.5)	0.0 ( 16.7)	0.0 ( 20.8)	0.0 ( 9.3)	0.0 ( 0.9)	0.0 ( 7.4)	0.0 ( 5.8)	0.0 ( 4.4)
35	0.0 ( 46.6)	0.0 ( 34.6)	0.0 ( 29.3)	0.0 ( 16.0)	0.0 ( 20.0)	0.0 ( 9.3)	0.0 ( 0.9)	0.0 ( 7.3)	0.0 ( 5.9)	0.0 ( 4.4)
30	0.2 ( 47.8)	0.2 ( 40.7)	0.1 ( 26.3)	0.0 ( 11.7)	0.1 ( 19.4)	0.0 ( 10.5)	0.0 ( 0.7)	0.0 ( 1.8)	0.0 ( 4.1)	0.0 ( 4.1)
25	2.4 ( 58.5)	2.2 ( 53.6)	1.1 ( 26.8)	0.4 ( 8.8)	0.8 ( 19.7)	0.6 ( 13.6)	0.0 ( 0.4)	0.1 ( 2.4)	0.1 ( 2.9)	0.2 ( 5.1)
20	2.8 ( 22.8)	2.7 ( 22.0)	0.9 ( 7.3)	0.0 ( 0.4)	0.8 ( 6.8)	0.3 ( 2.4)	0.1 ( 0.4)	0.0 ( 0.1)	0.0 ( 0.1)	0.1 ( 1.0)
15	4.4 ( 7.7)	1.8 ( 3.1)	4.0 ( 7.0)	0.0 ( 0.1)	3.9 ( 6.8)	0.2 ( 0.4)	0.0 ( 0.0)	0.9 ( 1.6)	0.1 ( 0.1)	0.0 ( 0.1)
10	2.7 ( 3.1)	2.5 ( 2.9)	0.9 ( 1.0)	0.2 ( 0.2)	0.5 ( 0.6)	0.1 ( 0.1)	0.1 ( 0.1)	0.1 ( 0.1)	0.5 ( 0.6)	0.1 ( 0.1)

**Table A4.** Error estimates for an equatorial profile during the RR period. Errors are given in pptv (relative errors in %).

Altitude	total error	noise	total parameter	Gain	LOS	$\text{HNO}_4$	Shift	ILS	Temperature	$\text{ClONO}_2$
40	0.0 ( 3058.9)	0.0 ( 2867.7)	0.0 ( 879.4)	0.0 ( 172.1)	0.0 ( 124.3)	0.0 ( 726.5)	0.0 ( 47.8)	0.0 ( 372.8)	0.0 ( 18.2)	0.0 ( 210.3)
35	0.0 ( 18560.0)	0.0 ( 17998.0)	0.0 ( 5511.9)	0.0 ( 899.9)	0.0 ( 4443.2)	0.0 ( 303.7)	0.0 ( 2531.0)	0.0 ( 146.2)	0.0 ( 1293.6)	
30	0.2 ( 73.5)	0.2 ( 60.7)	0.1 ( 41.6)	0.0 ( 13.1)	0.1 ( 19.5)	0.0 ( 14.1)	0.0 ( 2.0)	0.1 ( 31.3)	0.0 ( 3.5)	0.0 ( 3.5)
25	2.6 ( 19.9)	2.0 ( 15.3)	1.6 ( 12.2)	0.4 ( 3.2)	1.2 ( 9.2)	0.3 ( 2.4)	0.1 ( 0.5)	0.9 ( 6.9)	0.1 ( 0.6)	0.1 ( 0.5)
20	3.3 ( 5.5)	2.4 ( 4.0)	2.2 ( 3.7)	0.6 ( 1.0)	2.1 ( 3.5)	0.1 ( 0.1)	0.1 ( 0.1)	0.3 ( 0.5)	0.1 ( 0.2)	0.0 ( 0.1)
15	6.2 ( 7.3)	5.1 ( 6.0)	3.6 ( 4.3)	1.0 ( 1.2)	3.4 ( 4.0)	0.4 ( 0.5)	0.0 ( 0.0)	0.0 ( 0.0)	0.5 ( 0.6)	0.0 ( 0.0)
10	6.2 ( 7.3)	4.9 ( 5.8)	3.7 ( 4.4)	1.1 ( 1.3)	3.5 ( 4.1)	0.4 ( 0.5)	0.0 ( 0.0)	0.1 ( 0.1)	0.5 ( 0.6)	0.0 ( 0.1)

**Table A5.** Error estimates for a polar summer profile during the RR period. Errors are given in pptv (relative errors in %).

Altitude	total error	noise	total parameter	Gain	LOS	$\text{HNO}_4$	Shift	ILS	Temperature	$\text{ClONO}_2$
40	0.0 ( 336.8)	0.0 ( 307.1)	0.0 ( 158.5)	0.0 ( 96.1)	0.0 ( 56.5)	0.0 ( 73.3)	0.0 ( 2.2)	0.0 ( 70.3)	0.0 ( 2.7)	0.0 ( 12.9)
35	0.0 ( 333.4)	0.0 ( 296.4)	0.0 ( 148.2)	0.0 ( 92.6)	0.0 ( 55.6)	0.0 ( 72.2)	0.0 ( 2.0)	0.0 ( 67.6)	0.0 ( 2.7)	0.0 ( 13.0)
30	0.2 ( 299.3)	0.2 ( 273.3)	0.1 ( 123.6)	0.1 ( 80.7)	0.0 ( 52.1)	0.1 ( 69.0)	0.0 ( 0.4)	0.0 ( 27.3)	0.0 ( 3.1)	0.0 ( 7.5)
25	2.2 ( 72.1)	2.1 ( 68.9)	0.6 ( 19.3)	0.3 ( 10.2)	0.1 ( 2.9)	0.5 ( 15.7)	0.0 ( 0.6)	0.0 ( 1.0)	0.0 ( 0.5)	0.1 ( 1.9)
20	3.0 ( 16.2)	2.2 ( 11.9)	2.0 ( 10.8)	0.0 ( 0.1)	2.0 ( 10.8)	0.1 ( 0.4)	0.1 ( 0.5)	0.4 ( 2.3)	0.0 ( 0.2)	0.0 ( 0.1)
15	2.8 ( 3.9)	2.2 ( 3.1)	1.8 ( 2.5)	0.2 ( 0.3)	1.6 ( 2.3)	0.1 ( 0.2)	0.0 ( 0.0)	0.8 ( 1.2)	0.0 ( 0.1)	0.0 ( 0.0)
10	3.0 ( 3.6)	1.8 ( 2.2)	2.5 ( 3.0)	0.2 ( 0.3)	2.2 ( 2.6)	0.0 ( 0.1)	0.1 ( 0.2)	1.0 ( 1.2)	0.1 ( 0.1)	0.0 ( 0.0)

**Table A6.** Error estimates for a polar winter profile during the RR period. Errors are given in pptv (relative errors in %).

Altitude	total error	noise	total parameter	Gain	LOS	$\text{HNO}_4$	Shift	ILS	Temperature	$\text{ClONO}_2$
40	0.0 ( 632.5)	0.0 ( 367.3)	0.0 ( 510.1)	0.0 ( 204.0)	0.0 ( 448.9)	0.0 ( 67.3)	0.0 ( 9.8)	0.0 ( 24.5)	0.0 ( 61.2)	0.0 ( 36.7)
35	0.0 ( 608.6)	0.0 ( 342.4)	0.0 ( 494.5)	0.0 ( 190.2)	0.0 ( 437.4)	0.0 ( 66.6)	0.0 ( 9.5)	0.0 ( 22.8)	0.0 ( 60.9)	0.0 ( 36.1)
30	0.2 ( 369.8)	0.1 ( 228.9)	0.2 ( 281.8)	0.1 ( 112.7)	0.1 ( 264.1)	0.0 ( 42.3)	0.0 ( 6.0)	0.0 ( 2.5)	0.0 ( 33.5)	0.0 ( 22.9)
25	2.9 ( 308.3)	2.2 ( 233.9)	1.8 ( 191.3)	0.7 ( 76.5)	1.6 ( 170.1)	0.4 ( 41.5)	0.1 ( 6.1)	0.2 ( 26.6)	0.2 ( 20.2)	0.2 ( 23.4)
20	2.9 ( 46.0)	2.7 ( 42.8)	1.1 ( 17.4)	0.1 ( 1.4)	1.0 ( 15.9)	0.2 ( 2.5)	0.1 ( 1.2)	0.3 ( 4.6)	0.1 ( 0.9)	0.1 ( 1.3)
15	3.4 ( 5.1)	2.3 ( 3.4)	2.5 ( 3.7)	0.3 ( 0.5)	2.4 ( 3.6)	0.1 ( 0.2)	0.0 ( 0.1)	0.5 ( 0.7)	0.1 ( 0.1)	0.0 ( 0.0)
10	2.2 ( 2.6)	1.5 ( 1.8)	1.6 ( 1.9)	0.0 ( 0.0)	1.4 ( 1.7)	0.1 ( 0.1)	0.0 ( 0.0)	0.7 ( 0.9)	0.2 ( 0.2)	0.0 ( 0.0)

## References

- Allen, N. D. C., Bernath, P. F., Boone, C. D., Chipperfield, M. P., Fu, D., Manney, G. L., Oram, D. E., Toon, G. C., and Weisenstein, D. K.: Global carbon tetrachloride distributions obtained from the Atmospheric Chemistry Experiment (ACE), *Atmospheric Chemistry and Physics*, 9, 7449–7459, doi:10.5194/acp-9-7449-2009, <http://www.atmos-chem-phys.net/9/7449/2009/>, 2009.
- Chirkov, M., Stiller, G. P., Laeng, A., Kellmann, S., von Clarman, T., Boone, C., Elkins, J. W., Engel, A., Glatthor, N., Grabowski, U., Harth, C. M., Kiefer, M., Kolonjari, F., Krummel, P. B., Linden, A., Lunder, C. R., Miller, B. R., Montzka, S. A., Mühle, J., O'Doherty, S., Orphal, J., Prinn, R. G., Toon, G., Vollmer, M. K., Walker, K. A., Weiss, R. F., Wiegele, A., and Young, D.: Global HCFC-22 measurements with MIPAS: retrieval, validation, global distribution and its evolution over 2005–2012, *Atmos. Chem. Phys.*, 16, 3345–3368, doi:10.5194/acp-16-3345-2016, 2016.
- Eckert, E., von Clarman, T., Kiefer, M., Stiller, G. P., Lossow, S., Glatthor, N., Degenstein, D. A., Froidevaux, L., Godin-Beckmann, S., Leblanc, T., McDermid, S., Pastel, M., Steinbrecht, W., Swart, D. P. J., Walker, K. A., and Bernath, P. F.: Drift-corrected trends and periodic variations in MIPAS IMK/IAA ozone measurements, *Atmos. Chem. Phys.*, 14, 2571–2589, doi:10.5194/acp-14-2571-2014, 2014.
- Eckert, E., Laeng, A., Lossow, S., Kellmann, S., Stiller, G., von Clarman, T., Glatthor, N., Höpfner, M., Kiefer, M., Oelhaf, H., Orphal, J., Funke, B., Grabowski, U., Haenel, F., Linden, A., Wetzel, G., Woiwode, W., Bernath, P. F., Boone, C., Dutton, G. S., Elkins, J. W., Engel, A., Gille, J. C., Kolonjari, F., Sugita, T., Toon, G. C., and Walker, K. A.: MIPAS IMK/IAA CFC-11 ( $\text{CCl}_3\text{F}$ ) and CFC-12 ( $\text{CCl}_2\text{F}_2$ ) measurements: accuracy, precision and long-term stability, *Atmospheric Measurement Techniques*, 9, 3355–3389, doi:10.5194/amt-9-3355-2016, <http://www.atmos-meas-tech.net/9/3355/2016/>, 2016.
- Farmer, C. B. and Raper, O. F.: High resolution infrared spectroscopy from space: A preliminary report on the results of the Atmospheric Trace Module Spectroscopy (ATMOS) experiment on Spacelab 3, in: NSDA Conference Proceedings, vol. CP 2429, pp. 42–62, 1986.
- Fischer, H. and Oelhaf, H.: Remote sensing of vertical profiles of atmospheric trace constituents with MIPAS limb-emission spectrometers, *Appl. Opt.*, 35, 2787–2796, 1996.
- Fischer, H., Birk, M., Blom, C., Carli, B., Carlotti, M., von Clarman, T., Delbouille, L., Dudhia, A., Ehhalt, D., Endemann, M., Flaud, J. M., Gessner, R., Kleinert, A., Koopman, R., Langen, J., López-Puertas, M., Mosner, P., Nett, H., Oelhaf, H., Perron, G., Remedios, J., Ridolfi, M., Stiller, G., and Zander, R.: MIPAS: an instrument for atmospheric and climate research, *Atmospheric Chemistry & Physics*, 8, 2151–2188, 2008.
- Friedl-Vallon, F., Maucher, G., Kleinert, A., Lengel, A., Keim, C., Oelhaf, H., Fischer, H., Seefeldner, M., and Trieschmann, O.: Design and characterisation of the balloon-borne Michelson Interferometer for Passive Atmospheric Sounding (MIPAS-B2), *Appl. Opt.*, 43, 3335–3355, 2004.
- Funke, B., Stiller, G. P., von Clarman, T., Echle, G., and Fischer, H.:  $\text{CO}_2$  Line Mixing in MIPAS Limb Emission Spectra and its Influence on Retrieval of Atmospheric Parameters, *J. Quant. Spectrosc. Radiat. Transfer*, 59, 215–230, 1998.
- Glatthor, N., von Clarman, T., Fischer, H., Funke, B., Grabowski, U., Höpfner, M., Kellmann, S., Linden, A., Milz, M., Steck, T., and Stiller, G. P.: Global peroxyacetyl nitrate (PAN) retrieval in the upper troposphere from limb emission spectra of the Michelson Interferometer for Passive Atmospheric Sounding MIPAS, *Atmos. Chem. Phys.*, 7, 2775–2787, 2007.
- Harrison, J. J., Boone, C. D., and Bernath, P. F.: New and improved infra-red absorption cross sections and ACE-FTS retrievals of carbon tetrachloride ( $\text{CCl}_4$ ), *Journal of Quantitative Spectroscopy and Radiative Transfer*, 186, 139 – 149, doi:<http://dx.doi.org/10.1016/j.jqsrt.2016.04.025>, <http://www.sciencedirect.com/science/article/pii/S002240731630108X>, satellite Remote Sensing and Spectroscopy: Joint ACE-Odin Meeting, October 2015, 2017.
- Hubert, D., Keppens, A., Granville, J., and Lambert, J.-C.: Multi-TASTE Phase F Validation Report / Comparison of MIPAS ML2PP 7.03 products to sonde and lidar, TN-BIRA-IASB-MultiTASTE-Phase-F-MIPAS-ML2PP7-Iss1-RevB, BIRA-IASB, Brussels, Belgium, 2016.
- IPCC: Contribution of Working Group I to the Fifth Assessment Report of the Intergovernmental Panel on Climate Change, in: *Climate Change 2013: The Physical Science Basis*, edited by Stocker, T., Qin, D., Plattner, G.-K., Tignor, M., Allen, S., Boschung, J., Nauels, A., Xia, Y., Bex, V., and Midgley, P., Cambridge University Press, Cambridge, UK and New York, NY, USA, 33–115 pp, 2013.
- Liang, Q., Newman, P., and S., R.: SPARC Report on the Mystery of Carbon tetrachloride, SPARC Report No. 7, WCRP-13, SPARC, 2016.
- Manney, G. L., Santee, M. L., Rex, M., Livesey, N. J., Pitts, M. C., Veefkind, P., Nash, E. R., Wohltmann, I., Lehmann, R., Froidevaux, L., Poole, L. R., Schoeberl, M. R., Haffner, D. P., Davies, J., Dorokhov, V., Johnson, H. G. B., Kivi, R., Kyrö, E., Larsen, N., Levelt, P. F., Makshtas, A., McElroy, C. T., Nakajima, H., Parrondo, M. C., Tarasick, D. W., von der Gathen, P., Walker, K. A., and Zinoviev, N. S.: Unprecedented Arctic ozone loss in 2011, *Nature*, 478, 469–475, doi:10.1038/nature10556, 2011.
- Massie, S. T., Goldman, A., Murcay, D. G., and Gille, J. C.: Approximate absorption cross sections of F12, F11,  $\text{C}_1\text{ONO}_2$ ,  $\text{N}_2\text{O}_5$ ,  $\text{HNO}_3$ ,  $\text{CCl}_4$ ,  $\text{CF}_4$ , F21, F113, F114, and  $\text{HNO}_4$ , *Appl. Opt.*, 24, 3426–3427, doi:10.1364/AO.24.003426, <http://ao.osa.org/abstract.cfm?URI=ao-24-21-3426>, 1985.
- Naujokat, B. and Grunow, K.: The stratospheric arctic winter 2002/03: balloon flight planning by trajectory calculations, in: *European Rocket and Balloon Programmes and Related Research*, edited by Warmbein, B., vol. 530 of *ESA Special Publication*, pp. 421–425, 2003.
- Nemtchinov, V. and Varanasi, P.: Thermal infrared absorption cross-sections of  $\{\text{CCl}_4\}$  needed for atmospheric remote sensing, *Journal of Quantitative Spectroscopy and Radiative Transfer*, 82, 473 – 481, doi:[http://dx.doi.org/10.1016/S0022-4073\(03\)00171-7](http://dx.doi.org/10.1016/S0022-4073(03)00171-7), <http://www.sciencedirect.com/science/article/pii/S0022407303001717>, the {HITRAN} Molecular Spectroscopic Database: Edition of 2000 Including Updates of 2001., 2003.
- Norton, H. and Beer, R.: New apodizing functions for Fourier spectrometry, *J. Opt. Soc. Am.*, 66, 259–264, (Errata *J. Opt. Soc. Am.*, 67, 419, 1977), 1976.
- Rodgers, C. D.: Inverse Methods for Atmospheric Sounding: Theory and Practice, vol. 2 of *Series on Atmospheric, Oceanic and*

- 815 *Planetary Physics*, F. W. Taylor, ed., World Scientific, Singapore, New Jersey, London, Hong Kong, 2000.
- Rosenkranz, P. W.: Shape of the 5 mm Oxygen Band in the Atmo- 815 sphere, *IEEE Transactions on Antennas and Propagation*, AP-23, 498–506, 1975.
- Rothman, L. S., Barbe, A., Benner, D. C., Brown, L. R., Camy- 820 Peyret, C., Carleer, M. R., Chance, K., Clerbaux, C., Dana, V., Devi, V. M., Fayt, A., Flaud, J.-M., Gamche, R. R., Goldman, A., 825 Jacquemart, D., Jucks, K. W., Lafferty, W. J., Mandin, J.-Y., Massie, S. T., Nemchinov, V., Newnham, D. A., Perrin, A., Rins- 830 land, C. P., Schroeder, J., Smith, K. M., Smith, M. A. H., Tang, K., Toth, R. A., Vander Auwera, J., Varanasi, P., and Yoshino, K.: The HITRAN molecular spectroscopic database: edition of 835 2000 including updates through 2001, *J. Quant. Spectrosc. Radiat. Transfer*, 82, 5–44, doi:10.1016/S0022-4073(03)00146-8, 2003.
- Schmidt, U., Kulessa, G., Klein, E., Roeth, E.-P., and Fabian, P.: 830 intercomparison of balloon-borne cryogenic whole air samplers 835 during the MAP/GLOBUS 1983 campaign, *Planetary and Space Science*, 35, 647–656, doi:10.1016/0032-0633(87)90131-0, 1987.
- Sinnhuber, B.-M., Stiller, G., Ruhnke, R., von Clarmann, T., Kell- 835 mann, S., and Aschmann, J.: Arctic winter 2010/2011 at the 840 brink of an ozone hole, *Geophys. Res. Lett.*, 38, L24814, doi:10.1029/2011GL049784, 2011.
- SPARC: SPARC Report on the Mystery of Carbon tetrachloride, Liang, Q. and Newman, P.A. and Reimann, S. (Eds.), 2016.
- 840 Stiller, G. P., ed.: The Karlsruhe Optimized and Precise Radiative Transfer Algorithm (KOPRA), vol. FZKA 6487 of *Wissenschaftliche Berichte*, Forschungszentrum Karlsruhe, Karlsruhe, 2000.
- Valeri, M., Barbara, F., Boone, C., Ceccherini, S., Gai, M., 845 Maucher, G., Raspollini, P., Ridolfi, M., Sgheri, L., Wetzel, G., and Zoppetti, N.:  $\text{CCl}_4$  distribution derived from MIPAS ESA V7 data: validation, trend and lifetime estimation, *Atmospheric Chemistry and Physics Discussions*, 2017, 1–31, doi:10.5194/acp-2016-1163, 850 <http://www.atmos-chem-phys-discuss.net/acp-2016-1163/>, 2017.
- Vogel, B., Günther, G., Müller, R., Groß, J.-U., Afchine, A., Bozem, H., Hoor, P., Krämer, M., Müller, S., Riese, M., Rolf, C., Spelten, N., Stiller, G. P., Ungermann, J., and Zahn, A.: 855 Long-range transport pathways of tropospheric source gases originating in Asia into the northern lower stratosphere during the Asian monsoon season 2012, *Atmospheric Chemistry and Physics*, 16, 15 301–15 325, doi:10.5194/acp-16-15301-2016, <http://www.atmos-chem-phys.net/16/15301/2016/>, 2016.
- von Clarmann, T., Oelhaf, H., and Fischer, H.: Retrieval of atmo- 860 spheric  $\text{O}_3$ ,  $\text{HNO}_3$ , CFC-11, and CFC-12 profiles from MIPAS–B–89 limb emission spectra, *Appl. Opt.*, 32, 6808–6817, 1993.
- von Clarmann, T., Linden, A., Oelhaf, H., Fischer, H., Friedl- 865 Vallon, F., Piesch, C., Seefeldner, M., Völker, W., Bauer, R., Engel, A., and Schmidt, U.: Determination of the stratospheric organic chlorine budget in the spring arctic vortex from MIPAS B limb emission spectra and air sampling experiments, *J. Geophys. Res.*, 100, 13,979–13,997, 1995.
- von Clarmann, T., Glatthor, N., Grabowski, U., Höpfner, M., Kell- 870 mann, S., Kiefer, M., Linden, A., Mengistu Tsidu, G., Milz, M., Steck, T., Stiller, G. P., Wang, D. Y., Fischer, H., Funke,
- B., Gil-López, S., and López-Puertas, M.: Retrieval of temperature and tangent altitude pointing from limb emission spectra recorded from space by the Michelson Interferometer for Passive Atmospheric Sounding (MIPAS), *J. Geophys. Res.*, 108, 4736, doi:10.1029/2003JD003602, 2003.
- von Clarmann, T., Höpfner, M., Kellmann, S., Linden, A., Chauhan, S., Funke, B., Grabowski, U., Glatthor, N., Kiefer, M., Schieferdecker, T., Stiller, G. P., and Versick, S.: Retrieval of temperature,  $\text{H}_2\text{O}$ ,  $\text{O}_3$ ,  $\text{HNO}_3$ ,  $\text{CH}_4$ ,  $\text{N}_2\text{O}$ ,  $\text{ClONO}_2$  and  $\text{ClO}$  from MIPAS reduced resolution nominal mode limb emission measurements, *Atmos. Meas. Techn.*, 2, 159–175, 2009.
- von Clarmann, T., Stiller, G., Grabowski, U., Eckert, E., and Orphal, J.: Technical Note: Trend estimation from irregularly sampled, correlated data, *Atmos. Chem. Phys.*, 10, 6737–6747, 2010.
- World Meteorological Organization (WMO): Scientific Assessment of Ozone Depletion: 2014, Global Ozone Research and Monitoring Project – Report No. 55, 416 pp., Geneva, Switzerland, 2014.
- Zander, R., Rinsland, C. P., Farmer, C. B., and Norton, R. H.: Infrared spectroscopic measurements of halogenated source gases in the stratosphere with the ATMOS instrument, *J. Geophys. Res.*, 92, 9836–9850, 1987.
- Zander, R., Mahieu, E., Gunson, M. R., Abrams, M. C., Chang, A. Y., Abbas, M. M., Aelig, C., Engel, A., Goldman, A., Irion, F. W., Kämpfer, N., Michelson, H. A., Newchurch, M. J., Rinsland, C. P., Salawitch, R. J., Stiller, G. P., and Toon, G. C.: The 1994 northern midlatitude budget of stratospheric chlorine derived from ATMOS/ATLAS–3 observations, *Geophys. Res. Lett.*, 23, 2357–2360, 1996.